

**On the Role of Synoptic Disturbances  
in Formation and Maintenance  
of  
Blocking Flows**

**ARAI Miki**

*Division of Ocean and Atmospheric Science,  
Graduate school of Environmental Earth Science,  
Hokkaido University*

**August, 2002**

# Abstract

The role of synoptic disturbances in the formation and maintenance of the blocking flows is investigated using a barotropic quasi-geostrophic  $\beta$ -channel model.

In the first part of this dissertation, effectiveness of the eddy straining mechanism proposed by Shutts (1983) is examined in a quasi-linear framework. The model used here possesses two stationary solutions when the vorticity forcing associated with the analytical modon solution is assumed: one solution referred to as “blocking solution” closely resembles the modon solution while another referred to as “zonal flow solution” is characterized by dominant zonal flows. The infinitesimal transient eddies which mimic synoptic disturbances are generated by a wave-maker forcing located far upstream of the diffuence associated with the basic flow prescribed by stable stationary solutions. The effectiveness of the eddy straining mechanism is examined by comparing the basic flow with the second-order flow induced by the time-averaged potential vorticity (PV) divergence due to imposed eddies.

Although the distribution of the time-averaged PV divergence for the blocking solution is PV north/south, divergence/convergence dipole upstream of the diffuence of the basic flow as suggested by Shutts (1983), the computed second-order flow has a quadruple structure, which tends to shift the blocking dipole downstream but not enforcing the blocking. On the other hand, the second-order flow tends to maintain diffuence associated with the zonal solution. Thus, the effectiveness of eddy straining mechanism depends on the basic flow.

The second-order flow for the blocking solution is also drastically deformed by a small distortion of the PV divergence field due to a small change of the horizontal scale and the meridional position of the imposed eddies relative to the diffluent region. Thus, it is suggested that the effectiveness of eddy straining mechanism also depends on the property of synoptic eddies.

Further verification of the above results is made by examining nonlinear evolutions of the modon solution due to imposed transient eddies. We find again that the eddy straining mechanism is not also effective to maintain the diffuence associated with the modon solution against the Ekman friction.

In the second part, we examine the formation and the maintenance mechanism of the blocking flows when there is low-frequency variations which are considered to be an important agent to the blocking formation in recent studies (Nakamura et al. 1997, Cash and Lee 2000). For

this aim, we use the  $\beta$ -channel barotropic model with an isolated topography. This model has stationary solutions and periodic solutions with dominant zonal wavenumber 4 components for  $h=900$  m in the range of  $10 \text{ m/s} \leq U \leq 20 \text{ m/s}$ , where  $U$  is the uniform zonal wind speed. Several time integrations are performed with imposed transient eddy forcing as in the second part for basic flows given by these solutions. In the time integration for  $U \leq 14 \text{ m/s}$ , distinct diffluent flows similar to the blocking frequently appears and persists more than 10 days. We find that the formation of the blocking event in this model crucially depends on the wind speed  $U$ , i.e., the basic flow.

Examination of the tendency equation of the streamfunction decomposed into high- and low-frequency fields by using a 10-day low-pass filter, we find that the advection of the high-frequency vorticity by the low-frequency wind is the most important for the formation of the blocking flow. On the other hand, the development of the low-frequency field reveals that the eddy straining mechanism due to transient eddies is not essential for the formation of the blocking, but becomes important for the maintenance of the blocking after the onset of the blocking event. The important role of the low-frequency variability to trigger the onset of the blocking is also suggested. Thus, this study indicated that the effectiveness of the eddy straining mechanism crucially depends on the basic flow.

# Contents

<b>1</b>	<b>General Introduction</b>	<b>1</b>
<b>2</b>	<b>On the Effectiveness of the Eddy Straining Mechanism for the Maintenance of Blocking Flows</b>	<b>4</b>
2.1	Introduction . . . . .	4
2.2	Model . . . . .	7
2.2.1	Model description . . . . .	7
2.2.2	Modon solutions . . . . .	8
2.2.3	Parameter values and truncation level . . . . .	9
2.2.4	Method for linearized experiments . . . . .	10
2.3	Narrow channel model . . . . .	12
2.3.1	Multiple stationary solutions . . . . .	12
2.3.2	Second-order flow . . . . .	13
2.4	Wide channel model . . . . .	15
2.5	Sensitivity of the second-order flow to the imposed eddies . . . . .	17
2.5.1	Meridional shift of the wavemaker . . . . .	17
2.5.2	Horizontal size of the wavemaker . . . . .	18
2.6	Quantitative evaluation of the eddy straining effect . . . . .	19
2.7	Concluding Remarks . . . . .	22
<b>3</b>	<b>Effects of Transient Eddies and Low Frequency Variability on Blocking Formation and Maintenance</b>	<b>25</b>
3.1	Introduction . . . . .	25

3.2	Model . . . . .	27
3.3	Basic flow . . . . .	30
3.4	Effects of transient eddies . . . . .	32
3.4.1	Dependence on the basic flow . . . . .	32
3.4.2	Effectiveness of the eddy straining mechanism . . . . .	34
3.4.3	Formation of the blocking flow . . . . .	36
3.5	Concluding Remarks . . . . .	40
<b>4</b>	<b>General Conclusion</b>	<b>43</b>
	<b>References</b>	<b>48</b>

# Chapter 1

## General Introduction

Atmospheric blocking is one of the most prominent phenomena in large-scale atmospheric motions in the extratropical troposphere. The typical flow pattern of blocking is characterized by a dipole pressure system with an anticyclone centered to the north of a low pressure area, which splits the normal westerly jetstream into two distinct, widely separated flows (Rex 1950a, 1950b). This blocking high also has a quasi-stationary feature and tends to persist beyond the periods associated with synoptic-scale variability. It 'blocks' the eastward propagation of weather disturbances and deflects them from the usual storm tracks. This structure appears repeatedly at fixed geographical locations, off the western margins of the continents (e.g. Tibaldi and Molteni 1990), which coincide with the exit regions of the major storm tracks in the northern hemisphere. Moreover, since the occurrence of the blocking episode is intimately connected with the unusual weather, a better understanding of blocking has been a central objective of the meteorologists from the age of synoptic meteorology. Recently, the longer term variability of the occurrence frequency of the blocking events has been also discussed in relation to the climate change (Palmer 1999).

Although there are many theoretical and observational studies on atmospheric blocking, the consistent perspective on the dynamics of the blocking has not been established. In particular, the dynamical mechanism related with the formation, the maintenance, and the decay process of blocking events has not been fully resolved. However, the transient synoptic-scale disturbances have been considered to be one of the most important elements to maintain the blocking flow against surface friction since the work of Green (1977). He suggested that the European block-

ing anticyclone of July 1976 might be maintained by the meridional momentum flux associated with the synoptic-scale disturbances deformed by the diffluent field due to blocking. This “eddy straining mechanism” was further advanced by Shutts (1983). By using an equivalent barotropic quasi-geostrophic  $\beta$ -channel model, he showed in the framework of the quasi-linear theory that the imposed infinitesimal transient eddies which mimic the synoptic-scale disturbances are deformed by the assumed diffluent basic flow, and the induced flow by the potential vorticity flux divergence due to deformed eddies tends to enforce the original diffluent flow.

In the same line of approach, Haines and Marshall (1987) also examined the eddy straining mechanism by adopting the modon solution as a basic flow. The modon is a steady solution of the inviscid barotropic vorticity equation, and is used as a blocking prototype model in several theoretical studies on the blocking flow due to its similarity in the flow pattern (e.g. McWilliams 1980; Haines and Marshall 1987; Anderson 1995). Haines and Marshall (1987) also insisted the efficiency of the eddy straining mechanism for the maintenance of the diffluent flow due to the modon solution. However, there are several problems in their model experiments as revealed in this thesis, we think that the efficiency of the eddy straining mechanism has not been confirmed. In particular, the dependence of the efficiency of the eddy straining mechanism on the basic flow should be clarified. Furthermore, we should quantitatively evaluate the eddy straining mechanism in nonlinear framework to examine whether the eddy straining mechanism could sustain diffluent flows against surface friction.

As for the formation mechanism of the blocking flows, Shutts(1983) also insisted the importance of the eddy straining mechanism by illustrating the build up of diffluent flows from zonal flows by imposing transient eddies for some parameter ranges. Recently, Nakamura et al. (1997) indicated by careful analysis on the formation process of the blocking events in the north Pacific that low-frequency variability are another important factor for the the formation of blocking. The important role of low-frequency variability in the formation of the blocking was also reported Cash and Lee (2000) by analyzing output data of a general circulation model. However, the precise dynamical role of low-frequency variability could not be revealed in these observational studies since many other processes are involved in the blocking formation of the real atmosphere. Thus, we need more elaborate model experiments to examine the role of low-frequency variability. In these experiments, the relevance of the eddy straining mechanism in

the presence of low-frequency variability to the formation and the maintenance of blocking flows could be also revealed.

In chapter 2 in this thesis, we will examine the efficiency of the eddy straining mechanism in the quasi-linear framework as in the previous studies by adopting the modon solution as the basic flow. In this chapter, a quasi-geostrophic  $\beta$  channel model which is the same as in Haines and Marshall (1987) except for the meridional model width and horizontal resolution. Here, we use a wider channel model with a finer horizontal resolution to avoid distortion of the modon solution. In particular, we discuss the dependence of the efficiency of the eddy straining mechanism on the properties of the imposed transient eddies by showing a high sensitivity of second-order induced flows due to the transient eddy potential vorticity flux divergence. Furthermore, by conducting nonlinear experiments, we quantitatively evaluate the eddy straining mechanism for the maintenance of diffluent flows against surface friction.

The role of low-frequency variability for the formation and the maintenance of blocking flows will be investigated in chapter 3 by using barotropic  $\beta$ -channel model including an isolated topography with the aid of the bifurcation theory. The interaction between low-frequency variability and the imposed transient eddies will be shown to be essential for the formation of blocking events in this model. However, the eddy straining mechanism is irrelevant to this blocking formation while it plays a decisive role for the maintenance of the blocking flows after pronounced blocking patterns are established.

The summary of this thesis will be given in chapter 4 with some implication the observational analysis on the blocking flows. These observational studies (e.g. Illari 1984, Mullen 1986) documented the relevance of the eddy straining mechanism for the maintenance of the blocking flows by only examining the vorticity flux divergence field due to synoptic-scale eddies. However, since the second-order induced flows due to this field have a high sensitivity to the assumed basic flows as shown in this study, we cannot diagnose the relevance of eddy straining mechanism only by the vorticity flux divergence field.

## **Chapter 2**

# **On the Effectiveness of the Eddy Straining Mechanism for the Maintenance of Blocking Flows**

### **2.1 Introduction**

The blocking events in the extratropical troposphere are characterized by a well known vortex pair with the anticyclone to the north and the cyclone to the south of the ambient jetstreams. However, the most important feature of the blocking in the context of the dynamic meteorology is its own unusual persistence beyond the typical time scale of synoptic eddies and of the Ekman surface friction (Hoskins et al. 1983).

One promising hypothesis regarding the maintenance of blocking against dissipation is the “eddy straining mechanism” proposed by Shutts (1983). The mutual interaction between synoptic transient eddies and stationary blocking flows is the heart of this mechanism; when the migrating synoptic eddies advected by the zonal flow approach the diffluent straining field upstream of the blocking dipole, the eddies undergo an east/west compression and meridional extension, and are subsequently split meridionally. Associated with this strong deformation, a region of large eddy enstrophy is formed just upstream of the blocking dipole. By taking the balance in the time-averaged eddy enstrophy budgets into account, the enhanced dissipation of the eddy enstrophy has to be canceled by downgradient (i.e., southward) eddy vorticity flux

[see Eq.(1.2) in Shutts (1983)]. This vorticity flux will in turn form vorticity divergence (convergence) to the north (south) of the axis of the ambient jetstreams. Since this dipole pattern of eddy forcing has the same polarity as the blocking vortex pair, we could anticipate that migrating synoptic eddies maintain blocking flows in a time-averaged sense against the surface friction.

By using an equivalent barotropic  $\beta$ -channel model, Shutts (1983) also exemplified the eddy straining mechanism by denoting similarity between the time-mean second-order circulation induced by transient eddies and the assumed simple diffluent basic flow prescribed by a stationary Rossby wave in the framework of a quasi-linear theory. Infinitesimal transient eddies which mimic synoptic-scale waves were generated by a simple wavemaker forcing located far upstream of the diffluent region.

Haines and Marshall (1987, hereafter referred to as HM) conducted numerical experiments to examine the eddy straining mechanism in almost the same framework as in Shutts (1983), but they adopted an isolated modon solution in a uniform westerly flow as the basic state. The modon solution with an isolated north-south dipole vortex is a stationary solution in an inviscid equivalent barotropic atmosphere and resembles the blocking flow pattern in the real atmosphere (McWilliams, 1980). Because the obtained time-mean second-order circulation induced by imposed infinitesimal transient eddies is very similar to the basic flow, HM concluded that the eddy straining mechanism does work effectively for the maintenance of the basic flow comprised of the modon solution.

Although these two studies indicated the important role of the eddy straining mechanism in the maintenance of the diffluent flow, the sensitivity of the effectiveness of this mechanism to the assumed basic flow and the property of eddies generated by the wavemaker was not examined. Moreover, there are some problems in the numerical procedure in HM: first, the channel width assumed in HM is too narrow to represent the modon solution which is analytically derived in an infinite  $\beta$ -plane. The streamfunction field of the modon solution in their channel model is noticeably distorted not only near the channel walls but also in the dipole vortex region. Second, the linear stability of the basic flow in their channel model was not confirmed. Thus, the obtained second-order flow induced by perturbations could be contaminated by unstable modes and does not necessarily represent the effect of the eddies propagating from upstream of

the diffluent region.

Recently, Maeda et al. (2000) examined the eddy straining mechanism in a barotropic model on a sphere for realistic basic flows obtained from the observational data. They noted that the effectiveness of the eddy straining mechanism depends on the assumed basic flows and the imposed eddies. However, since the assumed basic flows are not any stationary solution, it is difficult to interpret the role of second-order induced flow by taking the time evolution of the basic flow itself into account. Moreover, the dependence of the effectiveness of the eddy straining mechanism on the characteristics of the imposed eddies was not revealed in detail.

In this study, we re-examine the effectiveness of the eddy straining mechanism for the maintenance of blocking flows, using an equivalent barotropic  $\beta$ -channel model identical to that in HM, except with a channel twice as wide. This model has two stationary solutions when a vorticity forcing associated with the modon solution is assumed as indicated by Pierrehumbert and Malguzzi (1984) in a barotropic  $f$ -plane model: one solution closely resembles the modon solution while another solution accompanies dominant zonal flows. Thus, by adopting these stationary solutions under linearly stable conditions as the basic flow, it is possible to argue in detail the effectiveness of the eddy straining mechanism without suffering from the interpretation of the second-order flow. We will also indicate that the results in HM are considerably affected by the channel walls in comparison with the results in our wide channel model, and the eddy straining mechanism is not so effective for the maintenance of the blocking flows. Moreover, the second-order flow is very sensitive to fine structures of the eddy PV flux divergence field. This sensitivity is designated by changing several properties of the imposed eddies.

Since the analysis in this study is performed restricted within the framework of quasi-linear theory, the result obtained in this study is valid for infinitesimal transient eddies, and it is necessary to conduct fully nonlinear experiments for the next study. However, we think that the quasi-linear analysis in this study is helpful to improve our understandings on the time evolution of blocking flows in the nonlinear experiments.

## 2.2 Model

### 2.2.1 Model description

We use an equivalent barotropic quasi-geostrophic potential vorticity equation on a  $\beta$ -channel with a vorticity source  $\nabla^2\psi^*$ , Ekman friction, and a scale-selective hyper-diffusion term:

$$\frac{\partial q}{\partial t} + J(\psi, q) = \lambda(\nabla^2\psi^* - \nabla^2\psi) - \nu(\nabla^2)^3\psi. \quad (2.1)$$

Here,  $\nabla^2$  and  $J$  denote the horizontal Laplacian and Jacobian operator,  $\lambda$  and  $\nu$  are the Ekman friction and the hyper-diffusion coefficient,  $\psi$  the streamfunction, and  $q$  the potential vorticity (PV) defined by

$$q = f_0 + \beta y + \nabla^2\psi - \gamma^2\psi. \quad (2.2)$$

In (2.2),  $f_0$  and  $\beta$  are the Coriolis and beta parameters, respectively;  $\gamma^2 \equiv f_0^2/gH$ , where  $g$  is the acceleration of gravity and  $H$  is the equivalent depth. Because we will examine isolated structures in a steady uniform zonal flow  $U$ ,  $\psi$  and  $q$  are split into zonal and isolated eddy components;

$$\left. \begin{aligned} \psi(x, y, t) &= -Uy + \tilde{\psi}(x, y, t), \\ q(x, y, t) &= q_\infty(y) + \tilde{q}(x, y, t), \end{aligned} \right\} \quad (2.3)$$

where

$$q_\infty \equiv f_0 + \beta_\infty y = f_0 + \beta y + \gamma_\infty^2 Uy,$$

and

$$\tilde{q} = \nabla^2\tilde{\psi} - \gamma^2\tilde{\psi}.$$

As shown in HM, for the existence of isolated stationary structures like modon solutions, which satisfy  $\tilde{\psi} \rightarrow 0$  for  $r \equiv (x^2 + y^2)^{1/2} \rightarrow \infty$ , the zonal flow  $U$  has to be more barotropic than the isolated structure, i.e.,

$$\gamma_\infty^2 > \gamma^2. \quad (2.4)$$

A cyclic boundary condition is imposed at  $x = -L_x\pi$  and  $x = L_x\pi$ :

$$\tilde{\psi}(x, y, t) = \tilde{\psi}(x + 2\pi L_x, y, t). \quad (2.5)$$

Since two rigid walls of the channel are assumed at  $y = -L_y\pi/2$  and  $y = L_y\pi/2$ , the following conditions for the meridional wind and the zonal mean of the zonal acceleration

$$\frac{\partial \tilde{\psi}}{\partial x} = 0 \quad \text{and} \quad \int_{-L_x\pi}^{L_x\pi} \frac{\partial}{\partial t} \left( -\frac{\partial \tilde{\psi}}{\partial y} \right) dx = 0, \quad (2.6)$$

are applied at these walls.

Substituting (2.3) into (2.1), we obtain the following equation for isolated eddy components:

$$\frac{\partial \tilde{q}}{\partial t} + J(\tilde{\psi} - y, \tilde{q} + \beta_\infty y) = \lambda(\nabla^2 \psi^* - \nabla^2 \tilde{\psi}) - \nu \nabla^6 \tilde{\psi}, \quad (2.7)$$

where all variables and constants are nondimensionalized:  $t$  by  $L_y/U$ ,  $x$  and  $y$  by  $L_y$ ,  $\tilde{\psi}$  and  $\psi^*$  by  $UL_y$ ,  $\tilde{q}$  by  $U/L_y$ ,  $\beta_\infty$  by  $U/L_y^2$ ,  $\gamma$  by  $L_y^{-2}$ ,  $\lambda$  by  $U/L_y$  and  $\nu$  by  $U/L_y^3$ . We expand  $\tilde{\psi}$  in the following truncated orthonormal functions which satisfy the boundary conditions (2.5) and (2.6):

$$\left. \begin{aligned} F_{A_m} &= \sqrt{2} \sin my, \\ F_{K_m^n} &= 2 \cos my \sin n\alpha x, \\ F_{L_m^n} &= 2 \cos my \cos n\alpha x, \end{aligned} \right\} \quad (2.8)$$

where  $m = 1, 2, \dots, M$ ,  $n = 1, 2, \dots, N$ , and  $\alpha = L_y/L_x$ ; the aspect ratio of this channel is given by  $2/\alpha$ . Substituting the spectral expansion (2.8) into (2.7), a set of  $M \times (2N + 1)$  ordinary differential equations for the expansion coefficients  $x_i(t)$  is obtained.

### 2.2.2 Modon solutions

For an infinite  $\beta$ -plane, if we assume different linear functional relationships between  $q$  and  $\psi$  for the interior and the exterior regions of a circle with the center at the origin  $(x, y) = (0, 0)$  and the radius  $r_0$ , i.e.,

$$\nabla^2 \tilde{\psi} - \gamma^2 \tilde{\psi} + \beta_\infty y = a(\tilde{\psi} - y), \quad (2.9)$$

where

$$a = \begin{cases} a_1 & \text{for } r < r_0, \\ a_2 & \text{for } r > r_0, \end{cases} \quad (2.10)$$

there is a set of isolated stationary solutions called “modon” for the inviscid case of  $\lambda = \nu = 0$  in (2.7) (Stern 1975). Isolated eddy components vanish in the far field, i.e.,  $\tilde{\psi} \rightarrow 0$  for  $r \rightarrow \infty$ . This gives

$$a_2 = -\beta_\infty \quad (2.11)$$

from (2.9). From the assumption of isolated structures, i.e.,  $\int \int |\nabla\psi|^2 dx dy$  is finite, the first order K-Bessel function is adopted as the solution of  $r > r_0$ . Moreover, the condition that  $\psi$  is finite at  $r = 0$  implies that  $a_1 < -\gamma^2$ . Here, the solution can be written as

$$\psi = \begin{cases} \left\{ r_0 \frac{K_1(kr)}{K_1(kr_0)} - r \right\} \frac{y}{r}, & \text{for } r > r_0 \\ \frac{k^2}{\kappa^2} \left\{ r - r_0 \frac{J_1(kr)}{J_1(kr_0)} \right\} \frac{y}{r}, & \text{for } r < r_0 \end{cases} \quad (2.12)$$

where  $k^2 \equiv \gamma^2 - \beta_\infty$ ,  $\kappa^2 = -(\gamma^2 + a_1)$ ,  $K_1$  and  $J_1$  are the first order K- and J-Bessel function, respectively. Finally, the condition that the velocity is continuous at  $r = r_0$  yields the relation between 1 and  $r_0$ .

### 2.2.3 Parameter values and truncation level

In the numerical experiments, we use the following parameter values according to HM:

$$\left. \begin{aligned} U &= 13.8 \text{ ms}^{-1}, \\ \beta &= 1.6 \times 10^{-11} \text{ m}^{-1}\text{s}^{-1}, \\ \beta_\infty &= 1.2\beta \text{ m}^{-1}\text{s}^{-1}, \\ L_\rho &\equiv 1/\gamma = 845 \text{ km}, \\ \alpha_1 &= -3.9 \times 10^{-12} \text{ m}^{-2}, \\ 2\pi L_x &= 42,000 \text{ km}. \end{aligned} \right\} \quad (2.13)$$

With these parameter values, Eq. (2.7) permits the existence of an analytical modon solution (2.12) with the radius of  $r_0 = 2,430$  km. In order to examine the effect of the lateral boundaries on the model behavior, we analyze the model behaviors with two different meridional channel widths: *narrow channel* ( $\pi L_y = 10,500$  km) corresponding to HM and *wide channel* ( $\pi L_y = 21,000$  km).

The truncation wave number adopted for the narrow channel is  $M = 21$ ,  $N = 42$  while  $M = 42$ ,  $N = 42$  for the wide channel. Thus, the horizontal resolution is the same for these two

models and is fine enough to represent the dynamics of the modon solution (see McWilliams et al. 1981). The hyper-diffusion coefficient  $\nu$  is given to have an  $e$ -folding time of 1 day for the component of  $M = 21$  and  $N = 42$  for both models.

## 2.2.4 Method for linearized experiments

In order to assess the role of the migrating disturbances, which correspond to the synoptic eddies, in the maintenance of the basic flow, we examine the time-mean flow induced by infinitesimal disturbances generated by an imposed wavemaker forcing. For this analysis, we use the following perturbation expansion by a small parameter  $\varepsilon$ :

$$\left. \begin{aligned} \tilde{\psi}(x, y, t) &= \psi_0(x, y) + \varepsilon\psi_1(x, y, t) + \varepsilon^2\psi_2(x, y, t) + O(\varepsilon^3), \\ \tilde{q}(x, y, t) &= q_0(x, y) + \varepsilon q_1(x, y, t) + \varepsilon^2 q_2(x, y, t) + O(\varepsilon^3). \end{aligned} \right\} \quad (2.14)$$

Substituting (2.14) into (2.7), and equating terms in the same order of  $\varepsilon$  gives

$$\frac{\partial q_0}{\partial x} + J(\psi_0, q_0) + \beta_\infty \frac{\partial \psi_0}{\partial x} = \lambda(\nabla^2 \psi^* - \nabla^2 \psi_0) - \nu \nabla^6 \psi_0, \quad (2.15)$$

$$\left(\frac{\partial}{\partial t} + \frac{\partial}{\partial x}\right)q_1 + J(\psi_1, q_0) + J(\psi_0, q_1) + \beta_\infty \frac{\partial \psi_1}{\partial x} + \lambda \nabla^2 \psi_1 + \nu \nabla^6 \psi_1 = F_1, \quad (2.16)$$

and

$$\left(\frac{\partial}{\partial t} + \frac{\partial}{\partial x}\right)q_2 + J(\psi_2, q_0) + J(\psi_0, q_2) + \beta_\infty \frac{\partial \psi_2}{\partial x} + \lambda \nabla^2 \psi_2 + \nu \nabla^6 \psi_2 = -J(\psi_1, q_1). \quad (2.17)$$

Here, the vorticity forcing  $\nabla^2 \psi^*$  is assumed to have a magnitude of  $O(1)$  such that the basic flow  $\psi_0$  is a stationary solution of (2.15), and  $F_1$  is an imposed wavemaker to generate migrating eddies  $\psi_1$ . We further prescribe  $\nabla^2 \psi^*$  by the vorticity distribution associated with the modon solution (2.12). Thus, we can expect that a stationary solution similar to the modon solution (2.12) is obtained as a basic flow  $\psi_0$  in the channel model. We use the revised Marquadt method to obtain stationary solutions of (2.15) (see Mukougawa 1988).

The linear stability of the basic flow  $\psi_0$  for infinitesimal disturbances  $\psi_1$  is examined by using (2.16) without wavemaker forcing, i.e.,  $F_1 = 0$ . By using the spectral expansion (2.8), Eq. (2.16) without  $F_1$  is symbolically written as:

$$\frac{d\mathbf{x}}{dt} + \mathbf{A}\mathbf{x} = 0, \quad (2.18)$$

where the vector  $\mathbf{x}(t)$  consists of the expansion coefficients of eddy streamfunction  $\psi_1$ , and  $\mathbf{A}$  is an  $M(2N + 1) \times M(2N + 1)$  Jacobian matrix. The stability property of the basic state  $\psi_0$  is examined by obtaining eigenvalues of the matrix  $\mathbf{A}$ .

Now, the time-mean effect of infinitesimal disturbances generated by the wavemaker  $F_1$  on the basic flow  $\psi_0$  is assessed in the framework of a quasi-linear theory by the following procedures. First, we perform time integration of (2.16) for 50 days by using a 4th-order Runge-Kutta method with an imposed wavemaker  $F_1$ . According to Shutts (1983), the wavemaker is prescribed by

$$F_1 = \tilde{F}_1 \sin\left\{\frac{\pi(x - x_0)}{\Delta x}\right\} \cos\left\{\frac{3\pi(x - x_0 - t)}{\Delta x}\right\} \sin\left\{\frac{\pi(y - y_0)}{\Delta y}\right\}, \quad (2.19)$$

for  $x_0 < x < x_1$ ;  $\Delta x = x_1 - x_0$ ;  $y_0 < y < y_1$ ;  $\Delta y = y_1 - y_0$  where  $\tilde{F}_1$  is a constant; otherwise  $F_1 = 0$ . Note that  $F_1$  generates disturbances propagating eastward with the background uniform zonal wind speed (unit). The rectangular wavemaker region defined by  $x_0$ ,  $x_1$ ,  $y_0$  and  $y_1$  is located well upstream of the model origin  $(x, y) = (0, 0)$  where the diffluence associated with the basic flow exists.

Second, the last 45 days of the integration period, which are quite long compared with the characteristic period of synoptic eddies, are used to compute the time-mean eddy PV flux divergence  $\overline{J(\psi_1, q_1)}$ , where the overbar means the time-average. Finally, we obtain the induced time-mean second-order flow  $\overline{\psi_2}$  by solving the time-averaged equation of (2.17):

$$\frac{\partial \overline{q_2}}{\partial x} + J(\overline{\psi_2}, q_0) + J(\psi_0, \overline{q_2}) + \beta_\infty \frac{\partial \overline{\psi_2}}{\partial x} + \lambda \nabla^2 \overline{\psi_2} + \nu \nabla^6 \overline{\psi_2} = -\overline{J(\psi_1, q_1)}. \quad (2.20)$$

Note that the eddy PV flux divergence  $\nabla \cdot (\mathbf{v}_1 q_1)$ , which is also expressed as  $\overline{J(\psi_1, q_1)}$  by using the wind vector  $\mathbf{v}_1 = (-\partial\psi_1/\partial y, \partial\psi_1/\partial x)$ , acts as the forcing term for  $\psi_2$ . From the similarity of the spatial structure of  $\overline{\psi_2}$  to the basic flows, we could infer a tendency of the time evolution of the basic flow against the dissipative process due to an ensemble effect of imposed transient eddies.

The steady response of the second-order flow  $\psi_2$  due to  $-\overline{J(\psi_1, q_1)}$  in (2.20) is also examined by the singular value decomposition (SVD) analysis (see Navarra 1993; Itoh and Kimoto 1999; Maeda et al. 2000). The analysis is based on the following symbolically written equation (2.20):

$$\mathbf{A}y = \mathbf{f}, \quad (2.21)$$

where the vectors  $\mathbf{y}$  and  $\mathbf{f}$  represent the spectral expansion coefficients of  $\overline{\psi}_2$  and  $-\overline{J(\psi_1, q_1)}$ , respectively; the matrix  $\mathbf{A}$  in (2.21) is the same that in (2.18). Then, the SVD of the matrix  $\mathbf{A}$  gives the expansion of the induced second-order flow  $\mathbf{y}$  in terms of the right singular vectors  $\xi_i$  ( $i = 1, 2, \dots, M(2N + 1)$ ):

$$\mathbf{y} = \sum_{i=1}^{M(2N+1)} \frac{\langle \mathbf{f} \cdot \zeta_i \rangle}{\sigma_i} \xi_i, \quad (2.22)$$

where  $\langle \cdot \rangle$  indicates the inner-product,  $\sigma_i$  ( $0 \leq \sigma_1 \leq \sigma_2 \dots$ ) and  $\zeta_i$  are the  $i$ -th singular value and the  $i$ -th left singular vector. The singular values satisfy  $\mathbf{A}\mathbf{A}^T \zeta_i = \sigma_i^2 \zeta_i$  or  $\mathbf{A}^T \mathbf{A} \xi_i = \sigma_i^2 \xi_i$ , where the superscript  $T$  means the transpose. Sets of vectors  $\{\xi_i\}$  and  $\{\zeta_i\}$  construct orthonormal basis, respectively.

From (2.22), we find that the flow pattern associated with  $\xi_j$  will dominate the  $\overline{\psi}_2$  field if the coefficient  $\langle \mathbf{f} \cdot \zeta_j \rangle / \sigma_j$  of this mode  $j$  is larger than the amplitude of the other modes  $i$  for  $i \neq j$ . In particular, if the smallest singular value  $\sigma_1$  is much smaller than the others while the projection of the forcing  $\mathbf{f}$  onto each left singular vector  $\zeta_i$ ,  $\langle \mathbf{f} \cdot \zeta_i \rangle$ , has a comparable magnitude among all modes, the second-order flow  $\overline{\psi}_2$  becomes very similar to  $\xi_1$ ; this is expected when the basic flow  $\psi_0$  satisfies near-resonant condition, i.e.,  $\sigma_1 \approx 0$ . For near-resonant basic flows, detailed structures of the forcing  $\mathbf{f}$  are irrelevant to determine the spatial structure of  $\overline{\psi}_2$  field except for the sign of  $\langle \mathbf{f} \cdot \zeta_1 \rangle$  which controls the polarity of  $\overline{\psi}_2$ .

## 2.3 Narrow channel model

In this section, we describe the results in the narrow channel model with lateral width  $\pi L_y = 10,500$  km which is the same as that in HM.

### 2.3.1 Multiple stationary solutions

We numerically obtain stationary solutions of (2.15) by assuming two initial guesses: one is the modon solution of (2.12) and the other is  $\psi_0 = 0$ . Obtained branches of stationary solutions are shown in Fig. 2.1 where the Ekman friction coefficient  $\lambda$  is used as a bifurcation parameter and the ordinate denotes the kinetic energy of stationary solutions  $\psi_0$  normalized by that of the analytic modon solution of (2.12). In this parameter range, the multiplicity of stationary

solutions is clearly observed. Since the flow pattern closely resembles the analytical modon solution, the upper branch solutions (Fig. 2.2a) will be referred to as “blocking solution”. On the other hand, the solutions belonging to the lower branch (Fig. 2.2b) have relatively weak zonally asymmetric components, and uniform zonal flow components dominate in the flow pattern. Thus, we will call this solution “zonal flow solution”. With the increase of  $\lambda$ , the lower branch approaches the upper branch very closely, but a bifurcation point does not exist in this parameter range. The existence of similar multiple equilibria of isolated solutions was reported in Pierrehumbert and Malguzzi (1984) for an  $f$ -plane barotropic model, and also in Yamagata et al. (1990) for a  $\beta$ -plane equivalent barotropic model.

The linear stability property of stationary solutions is also depicted by two different symbols in Fig. 2.1. The blocking solution becomes unstable for  $\lambda < 0.13 \text{ day}^{-1}$ , while the zonal flow solution is stable in this parameter range. The growth rate of the most unstable mode for the blocking solution becomes larger with the decrease of  $\lambda$  as shown in Fig. 2.3a: when  $\lambda = 0$ , the growth rate attains the maximum value of  $0.15 \text{ day}^{-1}$ ; this unstable mode is stationary with zero frequency.

We also confirm the instability of the analytical modon solution ( $\lambda = \nu = 0$ ) in a higher horizontal resolution model with  $M = 42$  in (2.8). The numerically obtained fastest growing mode (Fig. 2.3b) for the analytical modon solution has a large amplitude in the center of the channel. The flow pattern of this unstable mode is similar to that obtained by the time integration from the initial condition composed of the westward-propagating modon solution as shown in Nycander (1992), which also gave a theoretical proof on the linear instability of the modon solution.

### 2.3.2 Second-order flow

Now, we will examine the second-order induced flow  $\overline{\psi}_2$  associated with transient perturbations forced by a prescribed wavemaker of (2.19). When the basic flow is unstable to infinitesimal perturbations by assuming a small value of  $\lambda$ , it is difficult to assess the effect of imposed perturbations on the basic flow because the obtained induced flow will be contaminated by growing unstable modes. On the other hand, if we assume a large Ekman friction coefficient  $\lambda$  to assure the stability of the basic flow, the transient eddies forced far upstream of the diffluent

region of the basic flow will fade away before reaching the diffuence and producing significant vorticity flux. Thus, we set  $\lambda = 0.12 \text{ day}^{-1}$  (denoted by open circles in Fig. 2.1) at which the blocking solution is marginally stable.

First, we consider the effect of perturbations on the blocking solution. Figure 2.4a shows an instantaneous field of the perturbation streamfunction  $\psi_1$  at day 30 superimposed on the basic flow  $\psi_0$ . The hatched rectangular area denotes the wavemaker region given by (2.19), where we set  $\alpha x_0 = -3\pi/4$ ,  $\alpha x_1 = -\pi/4$ ,  $y_0 = -\pi/6$ ,  $y_1 = \pi/6$ . The zonal wavelength and the period of the eddies forced by this wavemaker are 7,000 km and 5.8 days. The meridional wavelength of this perturbation is the same as the zonal wavelength i.e., the imposed eddy is isotropic. Approaching the diffuence region, perturbations expand in the lateral direction and shrink in the zonal direction. We also see a phase tilt associated with the differential advection by the basic flow  $\psi_0$  in the upstream of the diffuence. The time-averaged PV flux divergence  $\overline{J(\psi_1, q_1)}$  in (2.20) associated with the perturbations is shown in Fig. 2.4b where the wavemaker region is masked. In the upstream of the diffuence, the horizontal distribution of eddy PV flux divergence is anti-symmetric with respect to the center of the channel  $y = 0$ . There is enhanced divergence to the north of  $y = 0$  and convergence to the south in just upstream of the diffuence.

Second-order induced flow  $\overline{\psi_2}$  forced by the eddy PV flux divergence in the downstream region of  $x_1$  in Fig. 2.4b is shown in Fig. 2.4c. The flow pattern is characterized by a north/south, anticyclonic/cyclonic vortex dipole, and is almost identical to that obtained in HM. Since the second-order flow has a similar horizontal structure to the basic flow and the polarity is also the same, we can anticipate that the transient disturbances have a tendency to enforce the diffuence of the basic blocking flow and the eddy straining mechanism does work in the narrow channel.

In order to investigate the sensitivity of the second-order flow  $\overline{\psi_2}$  to the characteristic of the imposed forcing, we proceed the singular value decomposition analysis for the matrix  $A$  in (2.18). Figure 2.5a indicates that the smallest singular value  $\sigma_1$  is almost two orders of magnitude smaller than the second smallest one. Moreover, the right singular vector  $\xi_1$  associated with  $\sigma_1$  has a similar horizontal pattern to the second-order flow  $\overline{\psi_2}$  in Fig. 2.4c. On the other hand, the corresponding inner-product  $\langle \xi_1 \cdot f \rangle$  has a comparable magnitude with  $\langle \xi_i \cdot f \rangle$  for  $i \neq 1$  (not shown). Thus, in this narrow channel, we find that the basic flow is in a near-resonant condition, and the induced second-order flow is irrelevant to the characteristic of the eddy forc-

ing except for the polarity of the dipole structure. We also confirmed that the results for the blocking basic flow do not depend on the Ekman friction  $\lambda$  when the basic flow is stable.

We have also performed the analysis on the second-order flow for the zonal flow solution but refrain from describing the results here because the obtained results are identical to those in the wide channel model documented in the next section.

## 2.4 Wide channel model

The streamfunction of the blocking solution in the narrow channel is noticeably deformed from the analytical modon solution, especially near the lateral boundaries. In order to reduce the influence of the boundaries to the results, we extend the channel width into twice the narrow channel width ( $\pi L_y = 21,000$  km). We also increase the lateral truncation wave number  $M$  in (2.8) from 21 to 42 so as to retain the same horizontal resolution as in the narrow channel.

Figure 2.6 shows the bifurcation diagram of the blocking solution and the zonal flow solution as in Fig. 2.1. The distortion of the streamfunction of the blocking solution (Fig. 2.7a) is rather reduced not only near the boundaries but also in the center of the channel: the amplitude of the dipole structure is slightly larger in the wide channel. Note that the contour interval in Fig. 2.7 is one half of that in Fig. 2.4 due to the nondimensionalization. The structure of the zonal flow solution (Fig. 2.7b) is noticeably unchanged. The linear stability property of both stationary solutions remains almost the same as that in the narrow channel: the blocking solution becomes unstable when  $\lambda$  is smaller than  $0.13 \text{ day}^{-1}$ ; the zonal flow solution is stable in the parameter range examined in this study. The analytical modon solution represented in the wide channel is also linearly unstable to infinitesimal perturbations. Thus, we could infer that the lateral boundaries in this channel model does not directly affect the stability property of the analytical modon solution. The growth rate and horizontal structure of the most unstable mode for the analytical modon solution are almost the same as those in the narrow channel.

Figure 2.8a shows an instantaneous streamfunction field of the perturbation  $\psi_1$  at day 30 when the blocking solution is assumed as the basic flow. Since we focus upon the behavior in the center of the channel, only the central domain of  $-\pi/4 < y < \pi/4$  in the model will be shown in the following figures. The eddies are forced by the wavemaker  $F_1$  of which region is

denoted by the hatched rectangle in Fig. 2.8; the wavemaker region has the same dimensional horizontal size as in the narrow channel model. The deformation of eddy structure and the horizontal distribution of the accompanied PV flux divergence upstream of the diffuence (Fig. 2.8b) are almost the same as those in the narrow channel model.

However, we find a remarkable difference in the second-order flow  $\psi_2$  induced by the eddy forcing. In Fig. 2.8c, a quadruple structure is evident instead of the dipole structure in Fig. 2.4c. The downstream north-south vortex pair has a comparable magnitude to that of the upstream vortex pair. The polarity of these vortex pairs is opposite to each other, and the second-order flow has a tendency to shift the basic blocking vortex pair downstream instead of enforcing them.

The difference in the response of the second-order flow to almost the same PV flux divergence is also confirmed in the singular value decomposition analysis in Fig. 2.9a for the wide channel. The smallest singular value  $\sigma_1$  is several times as large as that in the narrow channel, and its magnitude is comparable to the second smallest singular value. Although there is a weak quadrupole pattern in the streamfunction field of the first right singular vector  $\xi_1$  (Fig. 2.9b), the zonal flow component which is absent in Fig. 2.8c dominates in its flow pattern. Moreover, the magnitude of the coefficient  $\langle \zeta_1 \cdot f \rangle / \sigma_1$  in (2.22) associated with  $\xi_1$  is not dominant as shown in Fig. 2.10 but  $\langle \zeta_3 \cdot f \rangle / \sigma_3$  and  $\langle \zeta_{11} \cdot f \rangle / \sigma_{11}$  are significant instead. Each pattern of  $\xi_3$  and  $\xi_{11}$  has a quadruple structure (not shown). Thus, the second-order flow  $\overline{\psi_2}$  for the blocking solution in the wide channel has relatively strong sensitivity to the characteristic of the imposed eddy forcing. This implies that the resonant enhancement mechanism of the blocking solution by the transient eddies found in the narrow channel as well as in HM is due to the narrow meridional extent of the channel model. We will further examine the sensitivity of the second-order flow to several eddy forcing characteristics in the next section.

Figure 2.11a shows an instantaneous perturbation streamfunction field at day 30 when the zonal flow solution (Fig. 2.7b) is assumed as the basic flow  $\psi_0$ . The perturbations induced by the same wavemaker  $F_1$  (hatched region) as in Fig. 2.8 have rather complicated structure. Eddies in the center of the channel become fragmented associated with the stagnation region of the basic flow, and fade away due to the Ekman friction and the biharmonic viscosity. On the other hand, the meridionally split eddies due to weak diffuence of the basic flow survive

further downstream compared with those for the blocking solution. Thus, the distribution of the time-mean eddy PV flux divergence (Fig. 2.11b) is concentrated in the center of the channel and has a smaller meridional scale compared with that for the blocking solution (Fig. 2.8b). The second-order flow induced by the time-mean eddy PV flux divergence is shown in Fig. 2.11c. Because its horizontal pattern is similar to the zonal flow solution (Fig. 2.7b) and its polarity is also the same, it is suggested that the imposed perturbation has an effect to maintain the basic zonal flow solution. The singular value decomposition analysis of the zonal flow solution shows that the resonant enhancement mechanism of the basic flow is not efficient, and the second-order induced flow crucially depends on the characteristic of the imposed wavemaker (not shown).

## 2.5 Sensitivity of the second-order flow to the imposed eddies

The results in the previous section suggest that the second-order induced flow for the blocking basic flow is very sensitive to the characteristic of the imposed eddies. In order to illustrate this high sensitivity, we examine the dependence of the second-order flow on the meridional location and the horizontal size of the wavemaker. The blocking solution is assumed as the basic flow in this section.

### 2.5.1 Meridional shift of the wavemaker

Figure 2.12 shows a result when the wavemaker is shifted to the south by 15% of the modon radius  $r_0$ . The instantaneous streamfunction field of  $\psi_1$  at day 30 (Fig. 2.12a) is almost identical to that in Fig. 2.8a except that eddies in the southern jetstreams retain larger amplitude compared with those in the northern jetstreams. The eddy PV flux divergence pattern (Fig. 2.12b) is also almost identical to that in Fig. 2.8b: a north/south, divergence/convergence dipole pattern resides upstream of the diffluence. On the other hand, the  $\overline{\psi}_2$  flow pattern in Fig. 2.12c is drastically deformed in comparison with Fig. 2.8c: a dominant anticyclonic vortex is located near  $y = 0$  instead of the quadrupole pattern, therefore this second-order flow tends to shift the vortex pair of the blocking basic flow southward from its original position. This second-order flow will destroy the blocking dipole since the anti-symmetry with respect to  $y = 0$  in the blocking dipole is totally lost in Fig. 2.12c; the meridional shift of the wavemaker only by 5% of the modon

radius is enough to extinguish the anti-symmetry of the second-order flow. This is an example of high sensitivity of the second-order flow to the meridional shift of the wavemaker.

### 2.5.2 Horizontal size of the wavemaker

Next, we examine the sensitivity of the second-order flow to the horizontal scale of the imposed wavemaker  $\Delta x$  and  $\Delta y$  in (2.19) while the aspect ratio of the wavemaker is kept constant as in section 2.4.

The further increase of the horizontal scale of the wavemaker does not give rise to qualitative change in the second-order flow; the second-order flow retains a tendency to advect the blocking dipole downstream (not shown). On the other hand, the decrease of horizontal scale of the wavemaker brings about a drastic change in the second-order flow. Figures 2.13 and 2.14 show the results for the prescribed zonal wavelength of eddies are 6,300 km and 5,600 km, respectively. The horizontal deformation of eddies associated with the blocking dipole in these two figures is apparently the same. The time-mean eddy PV flux divergence in Fig. 2.13b is also almost the same as that in Fig. 2.14b except that there is a slight enhancement of the north/south, divergence/convergence along the split jets around the blocking dipole in the former. However, the second-order flow is distinctively different between them; in Fig. 2.13c, a weak dipole with the opposite polarity to the blocking dipole exists within the dipole of the basic flow while strong dipoles with the same polarity as the blocking resides outside the dipole of the basic flow. This pattern will tend to diffuse the vortex pair associated with the blocking; The flow in Fig. 2.14c has a quadrupole structure with the opposite polarity to that in Fig. 2.8c, and tends to shift the blocking dipole upstream.

These two experiments suggest that a small difference in the time-mean eddy PV flux divergence has a possibility to raise a large difference in the second-order induced flow. Moreover, the effectiveness of the eddy straining mechanism is very sensitive to parameters prescribing the horizontal structure of migrating eddies.

## 2.6 Quantitative evaluation of the eddy straining effect

In sections 3,4 and 5 in this chapter it has been shown that the effectiveness of the eddy straining mechanism depends on the basic flow and the horizontal structure of the prescribed eddy forcing, and that the modon solution is not maintained by the eddy straining mechanism in the quasi-linear framework studied in sections 3, 4 and 5. Here, we will re-examine the eddy straining mechanism in fully nonlinear framework including the interaction between the basic flows and transient eddies, with particular we pay attention to the eddy straining mechanism compared with the dissipation of diffluent flow due to the Ekman friction.

We use the following fully nonlinear, nondimensionalized PV equation with the imposed eddy forcing term  $F$ :

$$\frac{\partial \tilde{q}}{\partial t} + J(\tilde{\psi} - y, \tilde{q} + \beta_{\infty} y) = \lambda(\nabla^2 \psi^* - \nabla^2 \tilde{\psi}) + F - \nu(\nabla^2)^3 \tilde{\psi}, \quad (2.23)$$

where  $\tilde{\psi}$  and  $\tilde{q}$  are the streamfunction and the PV (see section 2 in detail). Based on the time integration of Eq. (2.23), the eddy straining effect is quantitatively evaluated by examining the time evolution of the PV field from the initial condition given by the blocking solution (Fig. 2.2a). If the dipole structure associated with the blocking solution will be maintained against the dissipation without the forcing term  $\lambda \nabla^2 \psi^*$  in Eq. (2.23), we could conclude that the eddy straining mechanism is effective to maintain the diffluent flow.

Parameter values, boundary conditions and time integration scheme are the same as those in Section 2 in this chapter: the Ekman friction coefficient  $\lambda$  is  $0.13 \text{ day}^{-1}$  corresponding to  $e$ -folding time of 7.7 days; the hyper-diffusion coefficient  $\nu$  is determined to have an  $e$ -folding time of 1 day for the wave component  $(m, n) = (21, 42)$ . The blocking solution adopted for the initial condition is linearly stable for these parameter values. The eddy forcing  $F$  is imposed in the rectangular region in Fig. 2.15a, and is given by the following wavemaker forcing:

$$F = \begin{cases} \tilde{F} \sin\left\{\frac{\pi(x - x_0)}{(x_1 - x_0)}\right\} \cos\left\{\frac{3\pi(x - x_0 - t)}{(x_1 - x_0)} - \theta\right\} \sin\left\{\frac{\pi(y - y_0)}{y_1 - y_0}\right\} & \text{for } x_0 \leq x \leq x_1, y_0 \leq y \leq y_1 \\ 0 & \text{elsewhere.} \end{cases} \quad (2.24)$$

The forcing function of Eq. (2.24) is almost the same as in Eq. (2.19) except for the phase factor  $\theta$ , which specifies phase of the imposed transient eddies.

The amplitude of the wavemaker  $\tilde{F}$  is set at  $5.2 \times 10^{-11} \text{ s}^{-2}$  (120.0 in nondimensionalized unit) which will enforce the maximum value of the relative vorticity  $\nabla^2 \tilde{\psi}$  for the blocking solution during 9.8 days, corresponding to  $5.2 \times 10^{-11} \text{ s}^{-2}$ . This value of  $\tilde{F}$  is 1.3 times larger than the maximum value of the dissipation rate  $\lambda \nabla^2 \tilde{\psi}$  for the blocking solution. We have also performed another experiment with  $\tilde{F} = 60.0$ . Results of these two experiments are qualitatively the same, and we only describe the results for  $\tilde{F} = 120.0$  in the following.

In the quasi-linear framework, the effectiveness of the eddy straining mechanism is evaluated by examining the second-order flow induced by the time-mean PV flux divergence associated with transient eddies for a fixed basic flow. In the nonlinear experiments, however, this method based on the time-mean is not applicable to evaluate the eddy straining mechanism since the “basic flow” will evolve in time during the period of the time average. Thus, we use the following “ensemble mean” technique to obtain the phase-independent effect of transient eddies on the basic flow. The average over the time integrations with different phase factor  $\theta$  in  $F$  of Eq. (2.24): we perform 20 integrations by changing the phase factor  $\theta$  by  $\pi/10$  in the range of  $0 \leq \theta < 2\pi$ . The vorticity forcing  $\nabla^2 \psi^*$  is also retained during the first 3.3 days in the integration to maintain the diffluent flow until the maximum (or minimum) value of PV associated with the imposed transient eddy encounters at the diffluent region at  $\alpha x = -8/\pi$ , which indicated by the vertical thick line in Fig. 2.15a.

The time evolution of the PV field  $\tilde{q}$  of the ensemble mean of each integration with the transient eddy forcing of the zonal wavelength of 7000 km is shown in Fig. 2.15a. In this case,  $\alpha x_0 = -3\pi/4$ ,  $\alpha x_1 = -\pi/4$ ,  $y_0 = -\pi/6$ ,  $y_1 = \pi/6$  in Eq. (2.24). The vorticity forcing  $\nabla^2 \psi^*$  is removed at day 0. On the other hand, time evolution of the PV for the integration without the transient eddy forcing is shown in Fig. 2.15b. The maximum value of  $\tilde{q}$  in the ensemble mean decreases monotonically (Fig. 2.15a) at almost the same rate as that in the time integration without transient forcing (Fig. 2.15b) due to the dissipation terms. The horizontal pattern in PV is also very similar to each other except for a little deformation in the diffluent region in Fig. 2.15a. Thus, we find that the eddy straining mechanism is not effective to maintain the diffluent field against the dissipation.

To further evaluate the quantitative contribution of the eddy straining mechanism in the non-linear framework, time evolution of the maximum value in  $\tilde{q}$  for transient eddy forcing with zonal wavelength of 7,000km (asterisk), 6,300km (open circle) and 5,600km (open square) is shown in Fig. 2.16, respectively. The result for integration without eddy forcing is also shown by closed circles. From this figure, we find that the dipole structure in the experiments with transient eddy forcing decreases faster than that without eddy forcing. This fact does not depend on the horizontal size of the imposed transient eddies. Thus, we confirmed that the eddy straining mechanism in the nonlinear framework is not effective to maintain the dipole structure of the blocking solution compared with the dissipation rate due to the Ekman friction. This is consistent with the results obtained in the quasi-linear framework in section 2.5.

## 2.7 Concluding Remarks

In order to examine the effectiveness of the eddy straining mechanism on the maintenance of the blocking flow proposed by Shutts (1983), we investigate the mutual interaction between migrating eddies and stationary basic flows by using an equivalent barotropic  $\beta$ -channel model, which is all the same as in HM except that the channel width is enlarged twice to reduce the distortion of the flow field near the channel walls. The eddies which mimic the synoptic-scale waves are generated by an upstream wavemaker forcing. Their amplitude is assumed to be small enough so that the interaction is described by a quasi-linear framework as in HM. The model possesses two stationary solutions accompanying isolated structures in prescribed uniform westerlies when the vorticity forcing associated with the analytical modon solution is assumed: a “blocking solution” which closely resembles the modon solution and a “zonal flow solution” which is characterized by dominant zonal flows. The effectiveness of the eddy straining mechanism is assessed by the resemblance between the basic flow and the second-order flow induced by the time-averaged eddy potential vorticity (PV) divergence as in HM. The following results are obtained.

- When the basic flow is prescribed by linearly stable blocking solutions, the second-order flow induced by eddies has a quadruple structure, which tends to shift the blocking dipole downstream, instead of the dipole structure enforcing the blocking as shown in HM. On the other hand, the time-averaged eddy PV flux divergence has almost the same pattern as in HM: north/south, divergence/convergence dipole upstream of the diffluence of the basic flow.
- The superficial enhancement of the blocking dipole by the eddy straining mechanism indicated by HM is attributed to the false resonance characteristic of the basic flow due to the narrow channel model. This is also confirmed by the SVD analysis.
- The second-order flow for the linearly stable zonal flow solutions has a tendency to enforce the weak diffluence associated with the basic flow. The enhancement is not due to the resonant property of the basic flow but depends on the properties of imposed eddies.
- The second-order induced flow for the blocking solution is drastically deformed by a

negligible distortion of the eddy PV flux divergence field due to a small change in the property of imposed eddies, such as their horizontal scale and the meridional position of the trains of eddies relative to the diffluent region.

- The eddy straining mechanism is not effective to maintain the dipole structure of the blocking solution against the dissipation.

Thus, our study revealed that the eddy straining mechanism for the maintenance of the blocking flow against the dissipation is not so effective as indicated in the previous studies, and its effectiveness is also very sensitive to the properties of migrating eddies as well as the assumed basic flow.

Furthermore, the high sensitivity of the second-order flow to a fine structure in the eddy PV flux divergence field will suggest that the downgradient eddy PV flux divergence structure upstream of the blocking flow does not necessarily imply the enforcement of the blocking flow by the synoptic eddies; observational studies (*e.g.*, Shutts 1986; Mullen 1987) usually insist the enforcement only by indicating such a PV flux divergence field, or the corresponding geopotential tendency field simply obtained with an inverse Laplacian operator. In order to designate a large difference between the second-order flow and the tendency field from the PV flux divergence field, Fig. 2.17a and Fig. 2.17b show the streamfunction tendency fields  $\partial\tilde{\psi}/\partial t$  obtained by  $-\nabla^{-2}\overline{J(\psi_1, q_1)}$  for the eddy PV flux divergence field in Fig. 2.13b and Fig. 2.14b, respectively. These two streamfunction fields are too similar to be distinguished while there is noticeable difference in the second-order flow as already shown. This difference suggests the importance of zonal asymmetry of the basic flow in computing the second-order flow. Moreover, the high sensitivity of the second-order flow to a fine structure of the eddy PV flux divergence implies that a data set with high spatial resolution is necessary to assess the role of the synoptic eddies on the maintenance of the blocking flow although a resultant second-order flow has a relatively large horizontal scale.

These results obtained in the framework of a quasi-linear theory are confirmed by the non-linear framework. Since it is suggested in this study that the effectiveness of the eddy straining mechanism depends on the basic flow, the examination of the eddy straining mechanism for another basic flow is necessary to understand further the role of the synoptic disturbances on

the blocking flow. Moreover, the possibility to form the blocking flows only by the synoptic eddies from basic states with prevailing zonal flows suggested by Shutts (1983) has to be also examined in order to reveal the role of synoptic eddies in the dynamics of the blocking.

## **Chapter 3**

# **Effects of Transient Eddies and Low Frequency Variability on Blocking Formation and Maintenance**

### **3.1 Introduction**

Although there is downgradient time-averaged eddy PV flux due to transient eddies, the diffluent flow associated with the modon solution is not maintained against the Ekman dissipation as indicated in the previous chapter. This could suggest the sensitivity of the eddy straining mechanism on the prescribed basic flow. The important property of the basic flow which affects this sensitivity could be its temporal behavior as well as its spatial structure. The basic flow prescribed in the previous chapter is essentially stationary in time except for the gradual damping due to the Ekman dissipation, where the interaction between transient eddies and basic flow might be weak. On the other hand, low-frequency variabilities of the basic flows would perhaps enhance the efficiency of the eddy straining effect to build up the blocking flows. To make clear the effectiveness of the eddy straining mechanism, thus, it is necessary to reveal the most important property of the basic flows to affect the effectiveness of the eddy straining mechanism.

In fact, recent studies analyzing the observational data (Nakamura et al. 1997) and general circulation model (GCM) output data (Cash and Lee 2000) suggest the important role of low

frequency variability as well as the synoptic disturbances in the formation process of blocking. By examining the respective contribution of the low-frequency variability and high-frequency synoptic scale eddy to the time tendency of the geopotential height field of composite blocking flows, Nakamura et al. (1997) indicated that the following property of blocking flows in the Pacific and Atlantic sectors: contribution of synoptic eddies is dominant for the formation of the blocking flows in the Pacific sector while the existence of the low-frequency variability is crucial for the formation of the blocking in the Atlantic sector, where the eastward energy propagation associated with low-frequency variability in the upstream region of the diffluence due to blocking is frequently observed before the onset of blocking event.

Cash and Lee (2000) also examined each contribution of synoptic-scale transient eddies and low-frequency variabilities to the formation and maintenance of blocking events reproduced in an atmospheric GCM (AGCM) long-term integration. The contribution is quantitatively evaluated in terms of the streamfunction tendency based upon the barotropic vorticity equation applied to a single pressure level (300 hPa) of the AGCM. They found several blocking events in which the low-frequency variabilities have a major contribution to the formation of the diffluent flows: the downstream energy propagation associated with low frequency variability in the upstream of the diffluent region before the onset of the blocking events emerges frequently. They also noticed that the effect of synoptic scale transient eddies as represented by the eddy straining mechanism might be secondary during the onset of the blocking formation while it is crucial for the maintenance of blocking flow.

Although these two studies suggested that the importance of low frequency variation on the blocking flows, there is an inevitable restriction in their evaluation since their analyses are basically based upon the barotropic equation. Thus, the inevitable existence of large residual term which results from the vortex stretching term associated with the divergent winds as well as the dissipation terms makes the exact evaluation impossible. In addition, the thermodynamic processes such as heat flux and diabatic heating involved in the blocking events are totally neglected in their analyses, which could also obscure the results on the importance of the low-frequency variability during the blocking formation. Thus, in this chapter, we try to evaluate exactly each contribution of low-frequency variability and synoptic scale eddies on the formation and maintenance of blocking flows occurring in a barotropic mechanistic model. In this framework, the

blocking flows could be caused only due to barotropic mechanical process, and we could figure out the whole process of blocking flows without any residuals.

In this chapter, we also use a  $\beta$ -channel barotropic model with an isolated topography, which would force low-frequency variations (Jin and Ghil 1990), and an imposed eddy forcing, which would generate transient eddies resembling the synoptic scale eddies. This model is basically the same as that used by Kalnay-Rivas and Merkin (1981) who showed that transient eddies could enhance the ridge of quasi-stationary eddies and forms diffluent flows akin to blocking. However, the imposed eddy forcing in their study is located upstream of the isolated topography opposed to the real atmosphere, where the transient synoptic scale eddies are generated in high baroclinicity regions located in the downstream of major large scale topographies: the Pacific (Atlantic) storm tracks resides the downstream of the Himalaya (the Rockies). With this unrealistic position of eddy forcing, blocking flows occurs simultaneously in the upstream and downstream of the isolated topography in their study. In this chapter, the eddy forcing will be placed downstream of the isolated topography to avoid unrealistic features in their study. In addition, we will carefully examine each contribution of low-frequency variations and eddy straining mechanism associated with transient eddies in the formation of blocking flows, which is not discussed in their study.

At first, the blocking criterion is established based on 10-day low-pass filtered streamfunction field. To assess the contribution of low-frequency variations and high-frequency eddies to the formation and maintenance of blocking flows, the high-frequency eddy field is defined as the raw field subtracted from the low-pass filtered field, i.e., the low-frequency variations. The separation of high-frequency eddies and low-frequency variations enables us to evaluate the efficiency of the eddy straining mechanism for the maintenance of the blocking flows based upon the low-pass filtered barotropic vorticity equation.

## 3.2 Model

The model used in this study is based on an barotropic quasi-geostrophic vorticity equation with topography in a cyclic  $\beta$ -channel whose width is  $\pi L_y$  and length is  $2\pi L_x$ :

$$\frac{\partial}{\partial t} \nabla^2 \psi + J(\psi, \nabla^2 \psi + \beta y + f_0 \frac{h}{H}) = -\lambda \nabla^2 \psi + \mathcal{F} - \nu (\nabla^2)^3 \psi, \quad (3.1)$$

where  $\psi$  denotes the streamfunction,  $h$  the height of the topography,  $H$  the mean depth of the atmosphere, and  $\lambda$  and  $\nu$  are the Ekman friction and the hyper-diffusion coefficient,  $\nabla^2$  and  $J$  the horizontal Laplacian and Jacobian operator, and  $\mathcal{F}$  is the forcing function of transient eddies, which will be described in detail in section 3.4.

Boundary conditions are the same as that in chapter 1: cyclic condition in the zonal direction,

$$\psi(x, y, t) = \psi(x + 2\pi L_x, y, t)$$

at  $x = -L_x\pi$  and  $x = L_x\pi$  is imposed; the two prescribed rigid walls at  $y = -L_y\pi/2$  and  $y = L_y\pi/2$  set the meridional boundary condition,

$$\frac{\partial\psi}{\partial x} = 0, \quad \int_{-L_x\pi}^{L_x\pi} \frac{\partial}{\partial t} \left( -\frac{\partial\psi}{\partial y} \right) dx = 0,$$

at  $y = -y/2$  and  $y/2$ . We also assume a constant uniform zonal wind ( $U$ ), and the streamfunction  $\psi$  is

$$\psi(x, y, t) = -Uy + \phi(x, y, t). \quad (3.2)$$

The following orthonormal functions

$$\left. \begin{aligned} F_{A_m} &= \sqrt{2} \sin my, \\ F_{K_m^n} &= 2 \cos my \sin n\alpha x, \\ F_{L_m^n} &= 2 \cos my \cos n\alpha x, \end{aligned} \right\} \quad (3.3)$$

where  $m = 1, 2, \dots, M$ ,  $n = 1, 2, \dots, N$ , and  $\alpha = L_y/L_x$  are used for the spectral expansion of the streamfunction  $\phi$  in the channel domain as in chapter 1. The aspect ratio of this channel is given by  $2/\alpha$ . By using these orthonormal functions, a set of  $M \times (2N + 1)$  ordinary differential equations for the expansion coefficients  $x_i(t)$  is obtained.

An isolated topography is assumed to have a Gaussian shape in the zonal direction as in Kalnay-Rivas and Merkin (1981):

$$h = h_0 \cos(\pi y/L_y) \exp\{-((x - x_0)/\Delta x)^2\},$$

where,  $h_0$  is the height of the topography,  $\Delta x$  the zonal width of the mountain, and  $x_0$  the location of the peak of the topography.

Equation (3.1) is then nondimensionalized;  $t$  is nondimensionalized by  $1/f_0$  where  $f_0$  is  $2\Omega \sin \phi_0$  at the central latitude of the channel:  $x$  and  $y$  by  $L_y$ . The following parameter values are used in this chapter: the central latitude  $\phi_0$  of the channel is placed at  $45^\circ$  N, and  $f_0 = 1.03 \times 10^{-4} \text{s}^{-1}$ ,  $\beta = 1.62 \times 10^{-11} \text{m}^{-1} \text{s}^{-1}$ , the zonal length of the channel  $\pi L_x$  is given by that of the latitude circle at  $45^\circ$  N (28,342 km), the two walls of the channel is placed at  $15^\circ$  N and  $75^\circ$  N,  $L_y = 6,679$  km, and the scale height  $H$  is  $8.3 \times 10^3 \text{m}$ . The truncation wave number  $M$  and  $N$  in (3.3) used in this chapter is  $M = 21$  and  $N = 42$ , which provides sufficient spatial resolution to resolve synoptic-scale eddies. The assumed value of Ekman friction coefficient  $\lambda$  and the hyper diffusion coefficient  $\nu$  correspond to the damping time scale of 10 days ( $\lambda = [\text{s}^{-1}]$ ) and 1/6 hours for the smallest horizontal scale component of  $M = 21$ ,  $N = 42$  ( $\nu = [\text{s}^{-1}]$ ).

Time integration in this chapter is carried out by using the 4th order Runge-Kutta scheme with the time step of 1 hour. The model data are stored every 12 hours.

### 3.3 Basic flow

In order to specify the basic states in Eq. (3.1) without  $\tilde{\mathcal{F}}$ , we examine the bifurcation of stationary solutions in a wide range of parameter values of the zonal wind speed  $U$  and the topographic height  $h$  ( $10 \text{ m/s} \leq U \leq 20 \text{ m/s}$ ,  $600 \text{ m} \leq h \leq 1000 \text{ m}$ ). Stationary solutions are numerically obtained by the revised Marquadt method, which obtain local minimum point from a specified initial guesses (Mukougawa 1988). Here, several hundreds of initial guesses are given for several prescribed values of  $U$  and  $h$ .

In the framework of the linear theory, the wave component of  $(m, n) = (1, 4)$  in Eq. (3.2) is expected to dominate the flow pattern in this parameter range since its resonant wind speed  $U_R = \beta / \{(m/L_y)^2 + (n/\alpha L_x)^2\}$  is given by 17.8 m/s. The bifurcation diagram of solutions for  $h=900 \text{ m}$  is shown in Fig. 3.1a, where the ordinate shows the amplitude of the wave component  $(m, n) = (1, 4)$ , i.e.,  $(\psi_{K_1^4}^2 + \psi_{L_1^4}^2)^{1/2}$  for  $h = 900 \text{ m}$ . We obtain two solution branches as in Fig. 3.1a. The upper branch denoted by squares in Fig. 3.1a comprises of stationary solutions which may have a pitchfork bifurcation point at  $U=15 \text{ m/s}$ , and becomes linearly unstable for  $U \leq 15 \text{ m/s}$  (we do not obtain branch of stationary solution bifurcating from this bifurcation point). The stationary solutions belonging to the lower branches denoted by circles in Fig. 3.1a also becomes unstable at  $U=13 \text{ m/s}$ , and a stable periodic solution emerges for  $U \geq 13 \text{ m/s}$ . Thus, this bifurcation is classified as the super-critical Hopf bifurcation. Each vertical bar in Fig. 3.1a shows the range of the amplitude variation in the periodic solution, which becomes larger with the increase of  $U$ . Thus, for  $U \geq 16 \text{ m/s}$ , one stable stationary solution and one periodic solutions co-exist. The period of the limit cycles is about 16 days, and is almost independent of  $U$  for this parameter range.

Figures 3.1b and 3.1c show the streamfunction of the unstable stationary solution and time-averaged streamfunction of the periodic solution during one period for  $U = 14 \text{ m/s}$ , respectively. The wave component of  $(m, n) = (1, 4)$  dominates in both fields as expected by the linear theory. The ridge just downstream of the isolated topography ( $\alpha x \sim 2/5\pi$ ) in the stationary solution (Fig. 3.1b) is enhanced compared with that in the time-averaged field of the periodic solution (Fig. 3.1c). This is also seen in Fig. 3.1a.

These two solution branches are also obtained in a wide range of parameter value of the

topographic height  $h$ . While Hopf bifurcation in the lower branch appears for smaller  $U$  than 13 m/s when  $h$  is larger than 900 m, it appears at larger  $U$  for smaller  $h$ . The stationary solution in the upper branch becomes stable at larger  $U$  for larger  $h$ . Thus, the parameter range of  $U$  where two stable solutions co-exist becomes narrow for larger  $h$ . However the linear stability of solutions depends upon the value of  $h$ ; the zonal wind speed  $U$  at the Hopf bifurcation for the lower branch becomes small with the increase of  $h$ , while  $U$  at the pitchfork bifurcation point in the upper branch becomes large with the increase of  $h$ .

## 3.4 Effects of transient eddies

### 3.4.1 Dependence on the basic flow

The obtained stationary solutions and the periodic solutions in this parameter range explored in our study do not exhibit distinct diffluent flow such as the blocking. Thus, we impose a transient eddy forcing on the basic flow prescribed by the stationary solutions or the periodic solutions, and examine whether a distinct diffluent flow is formed. In this section, the relationship between the formation of blocking flows and the basic flows is examined.

The eddy forcing  $\mathcal{F}$  in Eq. (3.1) is given by

$$\mathcal{F} = \begin{cases} \tilde{\mathcal{F}} \sin\left\{\frac{\pi(x-x_0)}{\Delta x}\right\} \cos\left\{\frac{3\pi(x-x_0-Ut)}{\Delta x}\right\} \sin\left\{\frac{\pi(y-y_0)}{\Delta y}\right\} & \text{for } x_0 < x < x_1; \Delta x = x_1 - x_0; \\ & y_0 < y < y_1; \Delta y = y_1 - y_0 \\ 0 & \text{elsewhere.} \end{cases} \quad (3.4)$$

Here, the eddy forcing region denoted by  $x_0$ ,  $y_0$ ,  $\Delta x$  and  $\Delta y$  is shown by the the rectangular in Fig. 3.2 ( $\alpha x_0 = -7\pi/12$ ,  $y_0 = -\pi/8$ ,  $\alpha\Delta x = \pi/4$ ,  $\Delta y = \pi/4$ ). The forced transient eddies have a zonal wavelength of 4724 km, and their phase speed is given by  $U$ . The eddy forcing is located in the trough region of the basic flow just downstream of the isolated topography. The amplitude of the eddy forcing  $\tilde{\mathcal{F}}$  is varied between the nondimensionalized parameter range of  $0.2 \leq \tilde{\mathcal{F}} \leq 0.5$ , where the value of 0.2 corresponds to form the vorticity which is given by the maximum value of the periodic solution in 3 hours for  $h=900$  m and  $U=14$  m/s.

The time integrations are performed for  $h=900$  m and  $11 \text{ m/s} \leq U \leq 17 \text{ m/s}$  from the initial condition given by the stationary solution or the periodic solution. Distinct diffluent flow patterns similar to the blocking frequently emerged for  $U \leq 15 \text{ m/s}$  when the amplitude of eddy forcing  $\tilde{\mathcal{F}}$  is larger than 0.45. Thus, we set  $\tilde{\mathcal{F}}=0.5$  in the following experiments. With this forcing amplitude, the asymptotic behavior of this system does not depend on the initial condition.

For example, Fig. 3.2 shows the instantaneous streamfunction field at the day 928 for  $h=900$  m and  $U=14$  m/s. The enhanced anticyclonic circulation is located at  $\alpha x=0$  (Fig. 3.2a), and associated difffluence is formed just upstream of this anticyclone as in Fig. 3.2b where the

streamfunction of  $\psi = \phi - Uy$  is depicted.

Since the variation accompanied by the diffluent flow has a distinct low frequency component, we apply a 10-day low-pass filter to the output data so as to extract the low-frequency variability. Variations associated with each transient eddy are mostly removed by this filter since the imposed eddies has a period of 3.2-5.0 days for  $11 \text{ m/s} \leq U \leq 17 \text{ m/s}$ .

We also apply an empirical orthogonal function (EOF) analysis to the 10-day low-pass filtered data in order to obtain the dominant low frequency variation and to define the “blocking event” during which the diffluent flow pattern as in Fig. 3.2b becomes prominent. The EOF analysis on the covariance matrix of the streamfunction is applied for the rectangular region of  $-\pi/2 < \alpha x < \pi/2$  in the channel model (see Fig. 3.3).

The first mode called EOF1 for  $U = 14 \text{ m/s}$ ,  $F = 0.5$  and  $h = 900 \text{ m}$  accounts for 81.4% of the total variance, and is characterized by an enhanced anticyclonic circulation located near  $\alpha x=0$  as shown in Fig. 3.3. The flow pattern is very similar to the “blocking” flows (Fig. 3.2a). Figure 3.4 shows the time variation of the principal component (PC) associated with EOF1 scaled by its standard deviation (thick horizontal line). From this figure, we find that PC1 intermittently has a large value except for long quiescent periods during which PC1 has small negative values. Moreover, most of the excited events with large PC1 last more than 10 days.

Hence, we define the blocking event in this channel model when PC1 exceeds one standard deviation for more than 10 days. To ensure separation of events for compositing and filtering purposes, two blocking events occurring less than 10 days apart are treated as a single event. For other experiments with different values of  $U$ , we also use EOF1 for  $U=14 \text{ m/s}$  to define the blocking event; “PC1” time series for these experiments is obtained by projecting streamfunction field onto EOF1 for  $U=14 \text{ m/s}$ . This procedure will facilitate to examine the dependence of the statistical property of the blocking event on the uniform zonal flow  $U$ <sup>1</sup>.

Table 1 show the number and total days of blocking events occurring during 2500 days for  $11 \text{ m/s} \leq U \leq 17 \text{ m/s}$ . The number of blocking events attains a maximum value at  $U = 14 \text{ m/s}$ , and blocking events hardly occur for  $U \geq 16 \text{ m/s}$ . This result shows that the formation of blocking events depends crucially on the basic flow.

---

<sup>1</sup>The flow pattern which is very similar to EOF1 for  $U = 14 \text{ m/s}$  can be seen in EOF1 in the wide range of  $U$ . In fact, this definition is verified by comparing with the time evolution of the streamfunction field

### 3.4.2 Effectiveness of the eddy straining mechanism

In the previous section, we found that persistent diffluent flows similar to the blocking are formed for some basic flows when the transient eddies are imposed in this model. In order to examine the effectiveness of the eddy straining mechanism for the formation and maintenance of diffluent flows, we will analyze the model behavior for  $h=900$  m,  $U=14$  m/s,  $\tilde{\mathcal{F}}=0.5$  in detail. The blocking events occur most frequently at  $U = 14$  m/s in the range of  $11 \text{ m/s} \leq U \leq 17 \text{ m/s}$  (Table 1).

In the nonlinear framework, the examination on the eddy straining mechanism by computing the second-order flows due to PV flux divergence associated with high-frequency transient eddies is not adequate since the assumption of the basic flow stationarity does not hold. On the contrary, the basic flow evolves in time, and diffluent flow states (blocking flows) emerge spontaneously from non-blocking states in this model. Fortunately, this evolution is mostly captured by the low-pass filtered field as shown in the previous section. Thus, we will assess the eddy straining mechanism, by integrating the following vorticity equation, which governs the evolution of the low-pass filtered field:

$$\frac{\partial \nabla^2 \overline{\psi}^L}{\partial t} + J(\overline{\psi}^L, \nabla^2 \overline{\psi}^L + \beta y + f_0 \frac{h}{H}) = -\nabla \cdot \overline{\mathbf{v}' \nabla^2 \psi'^L} - \lambda \nabla^2 \overline{\psi}^L - \nu (\nabla^2)^3 \overline{\psi}^L. \quad (3.5)$$

Here,  $\overline{(\ )}^L$  denotes the low-pass filtered field defined by the 10-day low-pass filter (Blackmon et al. 1986), and  $(\ )'$  the high-pass filtered one defined as the residual, i.e.  $\psi = \overline{\psi}^L + \psi'$ . Equation (3.5) could be obtained by applying the low-pass filter to Eq. (3.1) after decomposing the streamfunction into the low-frequency part and high-frequency part. We also assume  $\overline{\psi}'^L = 0$ , and ignore the high- and the low-frequency nonlinear interactions, such as  $\nabla \cdot \overline{\mathbf{v}' \nabla \cdot \overline{\psi}^L}$ . We found these terms to be unimportant compared with  $\nabla \cdot \overline{\mathbf{v}' \nabla^2 \psi'^L}$  retained in Eq. (3.5).

The transient eddy forcing term  $\nabla \cdot \overline{\mathbf{v}' \nabla^2 \psi'^L}$  is obtained by using the data generated by a long-term integration of the model in the previous section. Thus, we could diagnose a one-way effect of high-frequency transient eddy on the low-frequency field by integrating Eq. (3.5) forward in time. We initialize Eq. (3.5) with the low-pass filtered streamfunction  $\overline{\psi}^L$  at the onset of each blocking event (day 0), 2.5 days prior to the onset (day -2.5), and 5 days prior to the onset (day -5). By comparing these results with time evolution of the low-pass filtered field in the model, we could assess the effectiveness of the eddy straining mechanism for the maintenance of the

blocking flow.

Figures 3.5, 3.6, and 3.7 show the composite streamfunction of the time integrated results for individual blocking events (see Table 1). The key day for the composite is set at day 0. Although we find a distinct confluence just downstream of the wavemaker region a diffluent region at  $\alpha x = -\pi/3$  for the low-pass filtered streamfunction at day 0 (Fig. 3.7), the composite of the time integration of Eq. (3.5) from day -5 and day -2.5 does not indicate such distinct diffluence downstream of the wavemaker region at day 0 in Fig. 3.5c and Fig. 3.6b, respectively. Thus, we find that the eddy straining mechanism is not effective to excite blocking states from non-blocking zonal states.

In order to quantitatively evaluate the contribution of high-frequency transient eddies to the formation and maintenance of the diffluent flow, we show the time evolution of the projection of each composite  $\overline{\psi}^L$  onto EOF1 (Fig. 3.3) along with PC1 time series (solid line) in Fig. 3.8. The projection for the time integrations from day -5 (broken line) and day -2.5 (dotted line) remains almost constant before day 0 is consistent with Figs. 3.5 and 3.6. The value is also scaled by the standard deviation of PC1. The variance of the projection among the blocking events at day 0 denoted by the vertical lines for these two series of the experiments. Thus, we confirm that the contribution of PV flux convergence associated with the high-frequency eddies is not significant to form the blocking event in this model.

On the other hand, eddy straining mechanism due to high-frequency eddies does work to maintain the diffluent flows after the onset of the blocking event. For example, the composite projection of the time integrations from day 0 (dash-dotted line) remains larger than unity (the horizontal line) as in Fig. 3.8. Moreover, the projection for the time integrations from day -5 (broken lines) and day -2.5 (dotted line) increases near day 0, and keeps a large value around the threshold for the definition of the blocking after the onset of the blocking event. Note that we use the same value of the transient eddy forcing  $\nabla \cdot \overline{\mathbf{v}' \nabla^2 \psi}^L$  for these three kinds of integration from diffluent initial conditions. Thus, we find that PV flux convergence due to transient eddies has an important contribution to *maintain* the blocking state after the establishment of the diffluent flow.

### 3.4.3 Formation of the blocking flow

As shown in the previous subsection, the eddy straining mechanism due to transient eddies does not play an important role during the developing stage of the distinct diffluent flows similar to the blocking, while this mechanism is relevant for the maintenance of the diffluent flow against dissipation. In this subsection, we will examine the formation process of the diffluent flows from the zonal, non-blocking state in detail. In particular, we pay our attention to the interaction between low- and high-frequency transient motions.

First of all, we show the time evolution of the vorticity field during a non-blocking state for day 845 - day 849, and the onset period of a blocking event for day 922.5 - day 926.5 for  $U=14$  m/s in Fig. 3.9a and Fig. 3.9b, respectively, to obtain an intuitive understanding for the blocking formation in this model. The low-pass filtered streamfunction fields for day 922.5 - day 926.5 are also shown in Fig. 3.10. During the non-blocking state (Fig. 3.9a), vortices associated with high-frequency transients are advected eastward along the center of the channel ( $y=0$ ) by almost zonal “basic flow”. On the other hand, high-frequency eddies are gradually meandering in the meridional direction before the onset (day 922.5 in Fig. 3.9b), and anticyclonic vortices eventually move far northward, and stay near the northern wall around  $\alpha x = \pi/8$  just before the onset (day 924.5-day 926.5 in Fig. 3.9b). Then, a dominant anticyclonic circulation is abruptly built up, and the blocking state is established (day 926.5 in Fig. 3.10).

The contributions of low- and high-frequency eddies to the formation of the blocking event could be examined quantitatively by using the following streamfunction tendency equation decomposed into the low-pass filtered field  $\bar{\psi}^L$  and the residual  $\psi' = \psi - \bar{\psi}^L$  (high-frequency transients) as in Cash and Lee (2000):

$$\frac{\partial \psi}{\partial t} = \sum_{i=1}^4 \xi_i - \lambda \psi - \nu(\nabla^2) \psi \quad (3.6)$$

where

$$\begin{aligned} \xi_1 &= \nabla^{-2} J(\bar{\psi}^L, \nabla^2 \bar{\psi}^L + \beta y + \frac{f_0 h}{H}) \\ \xi_2 &= \nabla^{-2} J(\bar{\psi}^L, \nabla^2 \psi') \\ \xi_3 &= \nabla^{-2} J(\psi', \nabla^2 \bar{\psi}^L + \beta y + \frac{f_0 h}{H}) \\ \xi_4 &= \nabla^{-2} J(\psi', \nabla^2 \psi'), \end{aligned} \quad (3.7)$$

which is obtained by applying the inverse Laplacian to Eq. (3.5), and low-frequency field is obtained by using the same low-pass filter as in the previous subsection.

The physical interpretations of the  $\xi_i$  terms are as follows. The advection of the low-frequency and the planetary vorticity by the low-frequency wind is  $\xi_1$ . The advection of the high-frequency vorticity by the low frequency wind is  $\xi_2$ , while  $\xi_3$  is the advection of the low-frequency and planetary vorticity by the high-frequency wind. The vorticity flux divergence due to high-frequency eddies is represented by  $\xi_4$ .

The contribution of each term  $\xi_i$  for the blocking event (day 926.5-day 945) of Fig. 3.9b is shown in Fig. 3.11, which indicates the cumulative increment of the streamfunction due to each term  $\xi_i$  from day 919.5 to day 929.5 (the onset of the blocking event is day 926.5), i.e.,

$$\int_{\text{day } 919.5}^{\text{day } 929.5} \xi_i dt \quad (3.8)$$

along with the difference field of the streamfunction between day 919.5 and day 929.5 ( $\psi_{\text{day } 929.5} - \psi_{\text{day } 919.5}$ ). Day 919.5 (929.5) corresponds to 7 days before (3 days after) the onset of the blocking (day 0). In the difference field of the streamfunction (Fig. 3.11a), a dominant anticyclonic circulation is seen in the northern half of the channel around the region of  $-\pi/8 < \alpha < 0$ , consistent with the buildup of the blocking high in this region. By comparing other four figures in Fig. 3.11 with Fig. 3.11a, we find that only Fig. 3.11c indicating the contribution of the term  $\xi_2$  (advection of high-frequency vorticity by low-frequency wind) shows the anticyclonic circulation around the blocking region as in Fig. 3.11a, while other terms do not have any contribution to the onset of the blocking formation. Thus, these figures suggest the important contribution of the term  $\xi_2$  in the blocking formation. We also find that the  $\xi_1$  term (Fig. 3.11b) corresponding to the low-frequency contribution creates a confluent flow upstream of the blocking region. This flow pattern in the upstream is also seen in the difference field of Fig. 3.11a.

In order to further evaluate the contribution of each term  $\xi_i$  in Eq. (3.6) to the blocking formation, we calculate the projection of the cumulative contribution of each term  $\int_{\text{day } -7}^{\text{day } 3} \xi_i dt + \psi_{\text{day } -7}$  onto EOF1 of Fig. 3.3 for 11 blocking events (see Table 1). Figure 3.12 shows the composite value of the projection for these events along with that of PC1 time series (solid line). From Fig. 3.11, we find that the dominant term is  $\xi_2$  (Fig. 3.11c) and  $\xi_3$  (Fig. 3.11d), i.e., the interaction between low- and high-frequency field, and they have almost the same magnitude with the opposite sign before the onset of the blocking event. In the composite value, the sum

of these terms (dotted line) abruptly increase after day -1. This abrupt increase is also seen for PC1 time series. Thus, the blocking in this model is formed rapidly in time with the time-scale of high-frequency eddies due to the interaction terms between low- and high-frequency eddies. In particular, the contribution of the advection of the high-frequency vorticity by the low-frequency wind  $\xi_2$  is important for the formation since the term  $\xi_2$  has the same sign as PC1. We also denote that the contribution of the high-frequency eddies ( $\xi_4$ ; dash-dotted line) becomes gradually important after the establishment of the blocking, which has already been shown in the previous subsection.

Figure 3.13 also shows that the contribution of low-frequency contribution  $\xi_1$  gradually increases before the onset of the blocking. Moreover, Fig. 3.12 also indicates significant contribution of the low-frequency variability to the formation of the confluent flow upstream of the blocking region during the blocking formation. Thus, these facts suggest that the onset of the blocking formation is triggered by the low-frequency variation in this model. In order to examine this possibility, we show the time evolution of the composited streamfunction fields associated with the low-frequency variation  $\bar{\psi}^L$  for 11 blocking events from day -5 to day 0 in Fig. 3.13. In this onset period, the vortex dipole (cyclone/anticyclone in north/south) at  $\alpha x = -2\pi/5$  upstream of the blocking region is gradually enhanced. This is caused mainly by the term  $\xi_1$  in Eq. (3.9) as shown in Fig. 3.11b. In the just downstream region of this confluence, another vortex pair (anticyclone/cyclone in north/south) corresponding to the blocking is gradually amplified with a slightly downstream shift of the northern anticyclone. Thus, these figures suggest that the buildup of the confluence upstream of the blocking region in the low-frequency variability  $\bar{\psi}^L$  seems to be a precursor of the blocking formation.

In order to examine this hypothesis on the precursor of the blocking, we calculate the inner product of the streamfunction field during the non-blocking states and that of the composited low-frequency variation at each day in Fig. 3.13 for the rectangular region of  $-3\pi/4 < \alpha x < 0$  and  $-\pi/2 < y < \pi/2$ . The non-blocking state is defined as periods except for the time interval from day -10 to the end of each blocking event. For each day in Fig. 3.13, we also compute the inner product of the streamfunction at the corresponding day in each blocking event and that of the composited value (closed circles in Fig. 3.14). If the inner products at a day for each blocking event have significantly different values from those values during

the non-blocking states, we could think that the composited low-frequency field at that day is inherent to the blocking formation. Moreover, the low-frequency field of the first day after which this separation between blocking and non-blocking states is distinct is the precursor for the blocking formation. In Fig. 3.14, the variation of the inner product during non-blocking states is shown by the vertical lines which cover the two standard deviation from the mean value. From this figure, we find that the separation between blocking and non-blocking states becomes evident after day -4. Thus, this result also implies that the enhancement of the dipole structure accompanying the confluent region upstream of the blocking in low-frequency variation might be a precursor for the blocking formation.

### 3.5 Concluding Remarks

The formation and the maintenance mechanisms of blocking flows were investigated using a quasi-geostrophic barotropic  $\beta$ -channel model with an isolated topography. A periodic wave forcing was included just downstream of the topography in order to represent the transient synoptic eddies in this barotropic model. In particular, we paid attention to clarify the role of eddy straining effect due to the deformation of transient eddies and that of the low-frequency variation in the formation and the maintenance of the blocking flow.

We obtained stationary and periodic solutions in a wide parameter range of the zonally uniform flow  $U$  ( $10 \text{ m/s} \leq U \leq 20 \text{ m/s}$ ) and the topographic height  $h$  ( $600 \text{ m} \leq h \leq 1000 \text{ m}$ ) to specify the basic flow in this model. These solutions, however, do not accompany distinct diffluent flow. However, when the wave forcing is imposed on this basic flow, we find that distinct difffluence fields similar to the blocking frequently occur for some parameter values. Since the intrinsic lifetime of this distinct diffluent event is much longer than the period of the imposed transient eddies (3.9 days), we apply a 10-day low-pass filter (Blackmon et al. 1986) to the model output to extract the low-frequency variability including the blocking event in this model. The EOF analysis to the 10-day low-pass filtered streamfunction reveals that the most dominant variability for  $U = 14 \text{ m/s}$  and  $h = 900$  is closely related to the occurrence of the distinct diffluent flow. Thus, we define the blocking event in this model by using the principal component (PC1) associated with EOF1 for  $U = 14 \text{ m/s}$  and  $h = 900 \text{ m}$ . By using this definition we find that the total number and the total duration of blocking events for the parameter range  $11 \text{ m/s} \leq U \leq 17 \text{ m/s}$  show a clear dependence on the zonally uniform flow: there is no blocking event for  $U > 16 \text{ m/s}$ . This might be connected with the resonance of the zonal wavenumber 4 component in this parameter range.

The effectiveness of the eddy straining mechanism for the formation of the blocking event in this model is quantitatively evaluated by integrating the low-pass filtered vorticity equation, and we find that after the onset of the blocking event the difffluence flow associated with the blocking is maintained by the low-pass filtered vorticity flux divergence associated with the imposed high-frequency eddies. On the other hand, before the onset of the blocking, the contribution of low-pass filtered vorticity flux divergence is too small to explain the enhancement of the

blocking dipole. Thus, the eddy straining mechanism is not effective to establish the diffluence associated with the blocking state.

The importance of the low-frequency variability in the formation of the blocking is confirmed by decomposing the streamfunction tendency equation into low-frequency and high-frequency contributions, and the interaction between low- and high-frequency eddies. The blocking event in this model is built up on a synoptic time scale, and this abrupt establishment is caused by the advection of the high-frequency vorticity due to low-frequency winds. Moreover, the blocking formation seems to be caused by an irreversible mixing of PV due to the wave breaking as mentioned by Nakamura et al. (1997).

The low-frequency variations might be important to trigger the blocking formation. In particular, we find that the enhancement of the confluent flow associated with the low-frequency variation upstream of the blocking region could be a precursor of the blocking onset since the confluence is not sustained for the non-blocking state. However, the successive downstream development from the confluence connected with the blocking formation is not simply explained by the energy propagation of low-frequency eddies, since the development before the onset is mainly due to the interaction between high- and low-frequency eddies.

In a similar barotropic model experiment, Shutts (1983) indicated the importance of the eddy straining mechanism due to transient eddies in the formation of the diffluent flows as well as their maintenance. However, our result on the blocking formation is apparently in contradiction to Shutts (1983), in which blocking flows develop spontaneously only when the zonal flow satisfies the resonance condition for Rossby waves with dipole meridional structure. Thus, we think that the eddy straining mechanism becomes effective for the blocking formation only under these restricted conditions, and is not so important for other more general conditions.

The formation mechanism of the blocking event in our study is the same as that of the blocking in the Atlantic sector in Nakamura et al. (1997) and the upstream blocking case in Cash and Lee (2000). These studies denote the importance of the interaction between low- and high-frequency eddies in the formation by applying a barotropic equation to the development of the observational data or AGCM output data at one pressure level. However, there were large residual terms in their vorticity budgets, which obscure the obtained conclusion. Ignored processes such as the thermodynamics in these studies might play role in the blocking formation. More-

over, the “basic flow” has to be maintained by artificial forcings in their barotropic model, which is also critical to interpret the result. On the other hand, our analysis avoids these deficiencies and is able to clearly show each contribution of the high- and low-frequency eddies in the formation and maintenance of the blocking flow.

For further studies, it is necessary to perform similar experiments in a baroclinic model, in which the artificial transient eddy forcing is not necessary, and the baroclinic waves spontaneously develop. The dependence of the effectiveness of the eddy straining mechanism on the horizontal structure of the imposed eddies and the basic flows must be reexamined in the baroclinic model.

# Chapter 4

## General Conclusion

We made a series of numerical experiments by using a barotropic quasi-geostrophic  $\beta$ -channel model to reexamine the efficiency of the eddy straining mechanism proposed by Shutts (1983) and Haines and Marshall (1987) (hereafter referred to as HM) on the formation and the maintenance of blocking flows. In this mechanism, synoptic-scale transient eddies propagating from the upstream region of the diffluence would tend to reinforce the diffluence of the blocking flow due to the potential vorticity (PV) flux divergence associated with the deformed eddies by the diffluence. However, the sensitivity of the effectiveness of this mechanism on the basic diffluent flows and the property of synoptic-scale transient eddies have not been elucidated. The important role of low frequency variability on the formation of blocking events denoted by recent observational studies (e.g., Nakamura et al. 1997) was also examined in detail in this thesis by using the same model with an isolated topography which could force low-frequency variations in barotropic models (Jin and Ghil 1990).

In the first part of this thesis, the effectiveness of eddy straining mechanism was carefully examined by using the same model as in HM except that the channel width was enlarged twice to avoid the influence of channel walls to fluid motions. When we assume a vorticity forcing associated with the analytical modon solution with Ekman friction in this model, two stationary solutions accompanying isolated structures in the uniform westerlies are obtained: one is referred to as "blocking solution" closely resembling the modon solution; the other is referred to as "zonal flow solution" characterized by dominant zonal flows. In order to examine the dependence of eddy straining mechanism on the basic flows, we adopted each stationary solu-

tion as a basic flow, and imposed transient eddies, which mimic the synoptic-scale waves, by a wavemaker forcing located further upstream of the diffluence associated with basic flows. The amplitude of transient eddies is also assumed to be small enough so that the interaction with the basic flow could be described by a quasi-linear framework as in HM. The effectiveness of the eddy straining mechanism is assessed by the resemblance between the basic flow and the second-order flow induced by the time-averaged eddy PV flux divergence as in HM.

When the basic flow is prescribed by linearly stable blocking solutions, second-order flows induced by eddies have quadruple structures, which tend to shift the blocking dipole downstream, instead of the dipole structure enforcing the blocking as shown in HM. However, the time-averaged eddy PV flux divergence has almost the same pattern as in HM: north/south, divergence/convergence dipole upstream of the diffluence of the basic flow. On the other hand, second-order flows for the linearly stable zonal flow solutions have a tendency to enforce the weak diffluence associated with the basic flow. The enhancement is not due to the resonant property of the basic flow but depends on the property of imposed eddies. The second-order induced flow for the blocking solution is drastically deformed by a negligible distortion of the eddy PV flux divergence field due to a small change in the property of imposed eddies, such as their horizontal scale and the meridional position of the trains of eddies relative to the diffluent region.

These results obtained in the above quasi-linear framework were also confirmed in a nonlinear framework by examining the nonlinear evolution of the blocking solution without vorticity forcing associated with the analytical modon: the amplitude of the blocking high diminish faster when the transient eddy forcing are included in the model. Thus, the eddy straining mechanism is not so effective to maintain the diffluence of blocking flows against surface friction, and its effectiveness is also very sensitive to the properties of migrating eddies as well as the assumed basic flow.

In the second part of this thesis, the mechanism related to the formation and the maintenance of blocking flows when there is low-frequency variability as in the real atmosphere was investigated. The model used in this part was almost the same as in the first part except for the inclusion of an isolated topography. A wavemaker forcing was also imposed at the trough region just downstream of the topography. The surface topography forces planetary-scale quasi-stationary

waves in this model.

We obtained stationary and periodic solutions in a wide parameter range of the uniform zonal flow speed  $U$  ( $10 \text{ m/s} \leq U \leq 20 \text{ m/s}$ ) and the topographic height  $h$  ( $600 \text{ m} \leq h \leq 1000 \text{ m}$ ) to specify the basic flow in this model. Although these solutions do not have distinct diffluent flows, we could find frequently prominent diffluence fields similar to the blocking for some parameter values when the wave forcing is imposed on these basic flows. Since the intrinsic lifetime of this distinct diffluent event is much longer than the period of the imposed transient eddies (3.9 days), we apply a 10-day low-pass filter (Blackmon et al. 1986) to the model output to extract the low-frequency variability including blocking events in this model. The EOF analysis to the 10-day low-pass filtered streamfunction reveals that the most dominant variability for  $U = 14 \text{ m/s}$  and  $h = 900 \text{ m}$  is closely related to the occurrence of the distinct diffluent flow. Thus, we define the blocking event in this model when the projection of the streamfunction field to EOF1 for  $U = 14 \text{ m/s}$  and  $h = 900 \text{ m}$  becomes greater than a prescribed threshold value. By using this definition we find that the total number and the total duration of blocking events for the parameter range  $11 \text{ m/s} \leq U \leq 17 \text{ m/s}$  with  $h = 900 \text{ m}$  show a clear dependence on the uniform zonal wind speed  $U$ : there is no blocking event for  $U > 16 \text{ m/s}$ .

The effectiveness of eddy straining mechanism for the formation of the blocking event in this model was quantitatively evaluated by integrating the low-pass filtered vorticity equation. We found that the low-pass filtered transient eddy vorticity flux divergence corresponding to the eddy straining mechanism is too small to set up the blocking dipole during the onset of the blocking event. Thus, the eddy straining mechanism is not effective to establish the diffluence associated with the blocking state. On the other hand, eddy straining mechanism plays a major role to maintain the blocking event in the mature stage of the blocking event.

With the analysis on the streamfunction tendency during the onset of the blocking event by decomposing it into low-frequency contribution, high-frequency contribution, and the interaction between low- and high-frequency eddies, we found that low-frequency variability plays a key role in the formation of the blocking. Moreover, the blocking event in this model is built up in a synoptic time scale, and this abrupt establishment is caused by the advection of the vorticity field associated with high-frequency variability due to low-frequency winds. The low-frequency variation might trigger the blocking formation. The enhancement of the confluent flow associ-

ated with the low-frequency variation upstream of the blocking region could be a precursor of the blocking onset since the confluence is not sustained for the non-blocking state. However, the successive downstream development from the confluence connected with the blocking formation is not simply explained by the energy propagation of low-frequency eddies since the development before the onset is mainly due to the interaction between high- and low-frequency eddies.

From this study, we could suggest that the discussion on the eddy straining mechanism by adopting a stationary solution such as modon solution as the basic state may be inadequate. As we noted, the slowly varying component during the blocking event may be essential to understand the whole life cycle of the blocking event. Thus, we should pay our attention to the transience of the blocking event.

The efficiency on the eddy straining mechanism for the maintenance of the blocking flow in the real atmosphere has been insisted in observational studies (*e.g.*, Illari 1984; Mullen 1987) only by indicating the downgradient PV flux divergence structure upstream of the blocking flow (Illari 1984), or the corresponding geopotential tendency field obtained with an inverse Laplacian operator (Mullen 1987) based upon the result of Shutts (1983). However, the high sensitivity of the second-order flow to a fine structure in the eddy PV flux divergence field in this study suggests that these evidences in the PV fields does not necessarily mean the enforcement of the blocking flow by the synoptic eddies. We should compute the second-order induced flow due to the PV flux divergence based on a zonally varying basic flow and discuss the similarity between the induced flow and the basic flow to assess the efficiency of the eddy straining mechanism.

In this study, transient eddies are forced by a imposed wavemaker forcing since transient eddies do not spontaneously develop in this barotropic model. Thus, we should examine the efficiency of the eddy straining mechanism in a baroclinic model where transient eddies emerge through the baroclinic instability. Moreover, since the activity and the horizontal scale of eddies are determined in connection with the structure of the basic flow upstream of the blocking, the enhancement of the jetstream, which might be a precursor of the blocking indicated in the second part of this thesis, could activate the transient eddy in baroclinic models. This may in turn enhance the possibility to set up the blocking onset through the interaction between low- and high-frequency variability as indicated in this thesis.

## Acknowledgement

First of all, I wish to express my deepest gratitude to my major advisor Dr. Hitoshi Mougawa for his many invaluable suggestions, discussions, and great patience. The members of this dissertation committee, Prof. Atsushi Kubokawa, Prof. Koji Yamazaki, Dr. Masahiro Watanabe and Prof. Masahide Kimoto, read an earlier version of this manuscript and gave me many valuable comments which made this dissertation better one. I would like to thank my present advisor Prof. Atsushi Kubokawa for his many useful comments about geophysical fluid dynamics.

I am indebted to all the teaching staff and students of Division of Ocean and Atmospheric Science, Environmental Earth Science, Hokkaido University for their helpful suggestions in various seminars. Especially, I wish to thank colleagues of Nonlinear Atmospheric Dynamics seminar: Dr. Masaru Inatsu, Ms. Mutsumi Abe, Mr. Kei Shimoda, Mr. Rui Nakazawa, Mr. Hirokazu Sakai and Ms. Keiko Yamashita. Many discussions in this seminar are very useful for me.

I would like to express my gratitude to my parents for their generosity to continue my graduate career, and to Dr. Masami Nonaka for his understanding of my study and for his constant encouragement. Finally, I thank our unborn child for his/her silent encouragement.

The GFD-DENNOU library were used for the graphics and the numerical calculations.

## References

- Anderson, J. L. 1995: A simulation of atmospheric blocking with a forced barotropic model. *J. Atmos. Sci.*, **52**, 2593-2608.
- Blackmon, M. L, S. L. Mullen and G. T. Bates, 1986: The climatology of blocking events in a perpetual January simulation of a spectral general circulation model. *J. Atmos. Sci.*, **43**, 1379-1405.
- Cash, B. A and S. Lee, 2000: Dynamical processes of blocking evolution. *J. Atmos. Sci.*, **57**, 3202-3218.
- Haines, K. and J. Marshall, 1987: Eddy-forced coherent structures as a prototype of atmospheric blocking. *Quart.J.Roy.Meteor.Soc.*, **113**, 681-704.
- Hoskins, B.J., I.N. James and G.H. White 1983: The shape, propagation and mean-flow interaction of large-scale weather systems. *J. Atmos. Sci.*, **40**, 1595-1612.
- Illari, L. 1984: A diagnostic study of the potential vorticity in a warm blocking anticyclone. *J. Atmos. Sci.*, **41**, 3518-3526.
- Itoh, H. and M. Kimoto, 1999: Weather regimes, low-frequency oscillations, and principal patterns of variability : A perspective of extratropical low-frequency variability. *J. Atmos. Sci.*, **56**, 2684-2705.
- Jin, F-F and M. Ghil, 1990: Intraseasonal oscillations in the extratropics: Hopf bifurcation and topographic instabilities. *J. Atmos. Sci.*, **47**, 3007-3022.
- Kalnay-Rivas, E. and L. Merkine, 1981: A simple mechanism for blocking. *J. Atmos. Sci.*, **38**, 2077-2091.

- Maeda, S., C. Kobayashi, K. Takano and T. Tsuyuki, 2000: Relationship between singular modes of blocking flow and high-frequency eddies. *J. Meteor. Soc. Japan*, **78**, 631-645.
- McWilliams, J.C., 1980: An application of equivalent modons to atmospheric blocking. *Dyn. Atmos. Ocean*, **5**, 43-66.
- McWilliams, J.C., G.R. Flierl, V.D. Larichev and G.M. Reznik, 1981: Numerical studies of barotropic modons. *Dyn. Atmos. Ocean*, **5**, 219-238.
- Mukougawa, H., 1988: A dynamical model of “quasi-stationary” states in large-scale atmospheric motions. *J. Atmos. Sci.*, **45**, 2868-2888.
- Mullen, S. L., 1987: Transient eddy forcing of blocking flows. *J. Atmos. Sci.*, **44**, 3-22.
- Nakamura, H, M. Nakamura and J.L. Anderson, 1997: The role of high- and low-frequency dynamics in blocking formation. *Mon. Wea. Rev.*, **125**, 2074-2093.
- Navarra, A., 1993: A new set of orthonormal modes for linearized meteorological problems. *J. Atmos. Sci.*, **50**, 2569-2583.
- Nycander, J., 1992: Refutation of stability proofs for dipole vortices. *Phys. Fluids. A*, **4**, 467-476.
- Palmer, J., 1999: A numerical dynamical perspective on climate prediction. *J. Climate*, **12**, 575-591.
- Pierrehumbert, R.T. and P. Malguzzi, 1984: Forced coherent structures and local multiple equilibria in a barotropic atmosphere. *J. Atmos. Sci.*, **41**, 246-257.
- Rex, D. F., 1950a: Blocking action in the middle troposphere and its effect upon regional climate. I. An aerological study of blocking action. *Tellus*, **2**, 196-211.
- , 1950b: Blocking action in the middle troposphere and its effect upon regional climate. II. The climatology of blocking action. *Tellus*, **2**, 275-301.
- Shutts, G.J., 1983: The propagation of eddies in diffluent jetstreams: eddy vorticity forcing of ‘blocking’ flow fields. *Q.J.R.Meteor.Soc.*, **109**, 737-761.

—, 1986: A case study of eddy forcing during an atlantic blocking eposode. *Adv. Geophys.*, **29**, 135-162.

Stern, M. E. 1975: Minimal properties of planetary eddies. *J. Mar. Res.*, **33**, 1-13.

Tibaldi, S. and F. Molteni, 1990: On the operational predictability of blocking. *Tellus*, **42A**, 343-365.

Yamagata, T., K. Sakamoto and M. Arai, 1990: Locally-induced nonlinear modes and multiple equiribria in planetary fluids. *PAGEOPH*, **133**, 733-748.



Figure 2.2

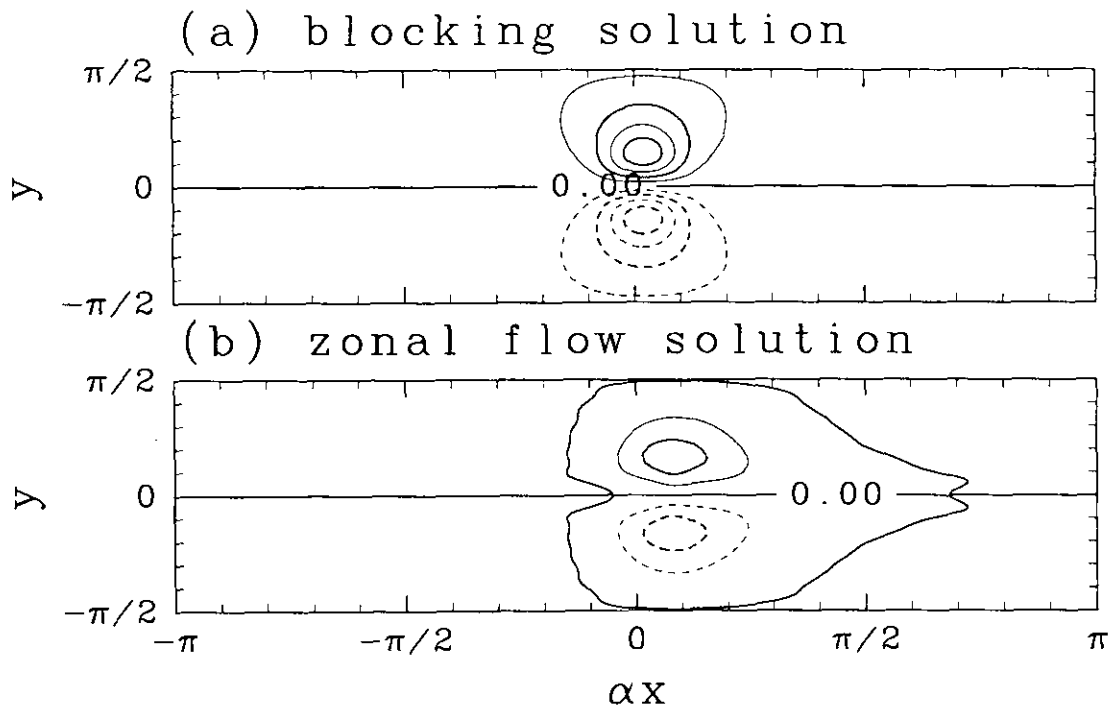


Figure 2.2: Streamfunction of the steady solutions  $\psi_0$  at  $\lambda = 0.13 \text{ day}^{-1}$  denoted by open circles in Fig.1.1. Contour interval is 0.2. Negative values are contoured by dashed lines. (a) Blocking solution. (b) Zonal flow solution.

Figure 2.3

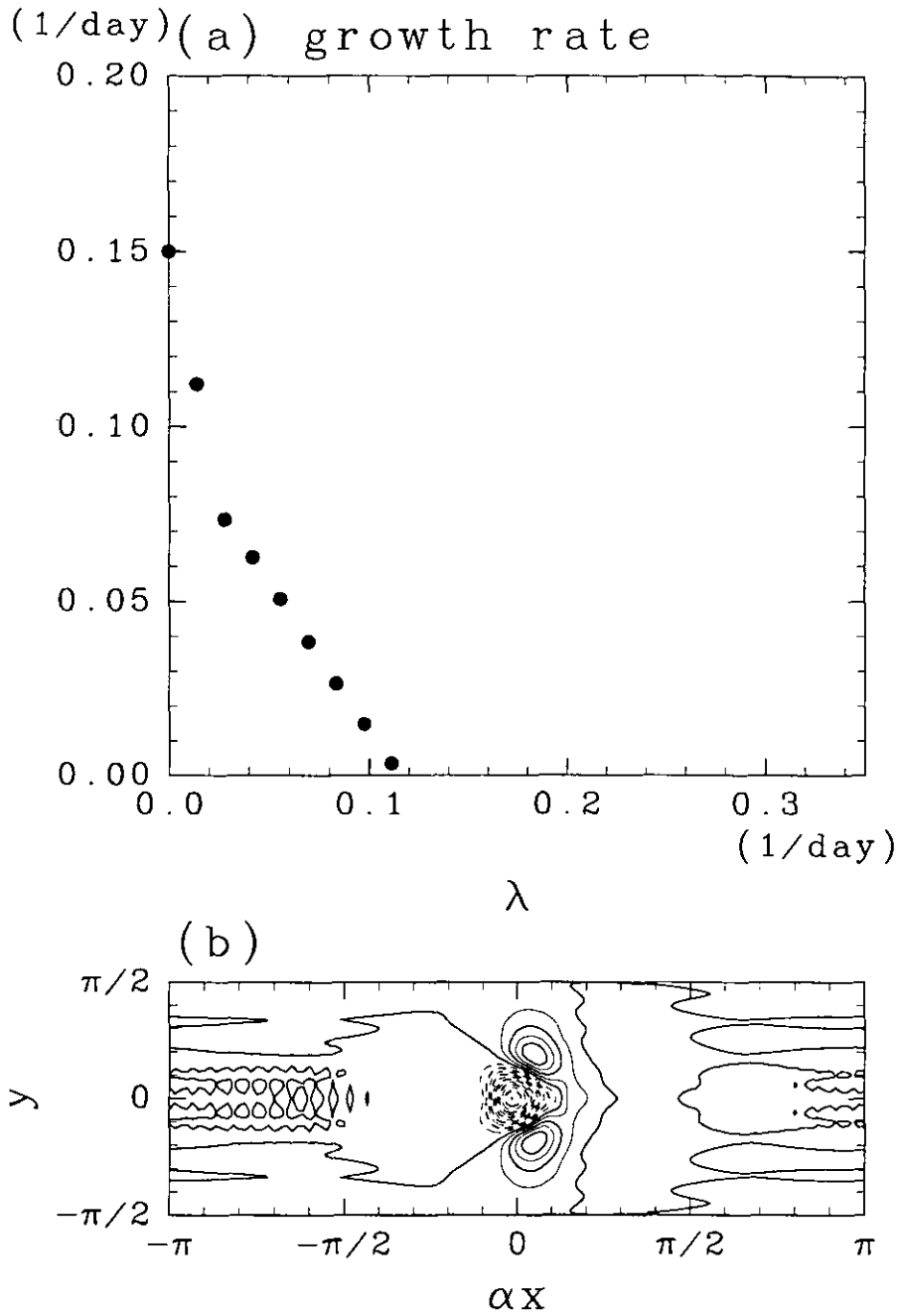


Figure 2.3: (a) Dependence of the growth rate of the most unstable mode for the blocking solution on the Ekman friction coefficient  $\lambda$ . (b) The eigenvector of the most unstable mode for the analytical modon solution (2.12). This is a stationary mode with the growth rate of  $0.15 \text{ day}^{-1}$ . Negative values are contoured by dashed lines.

Figure 2.4

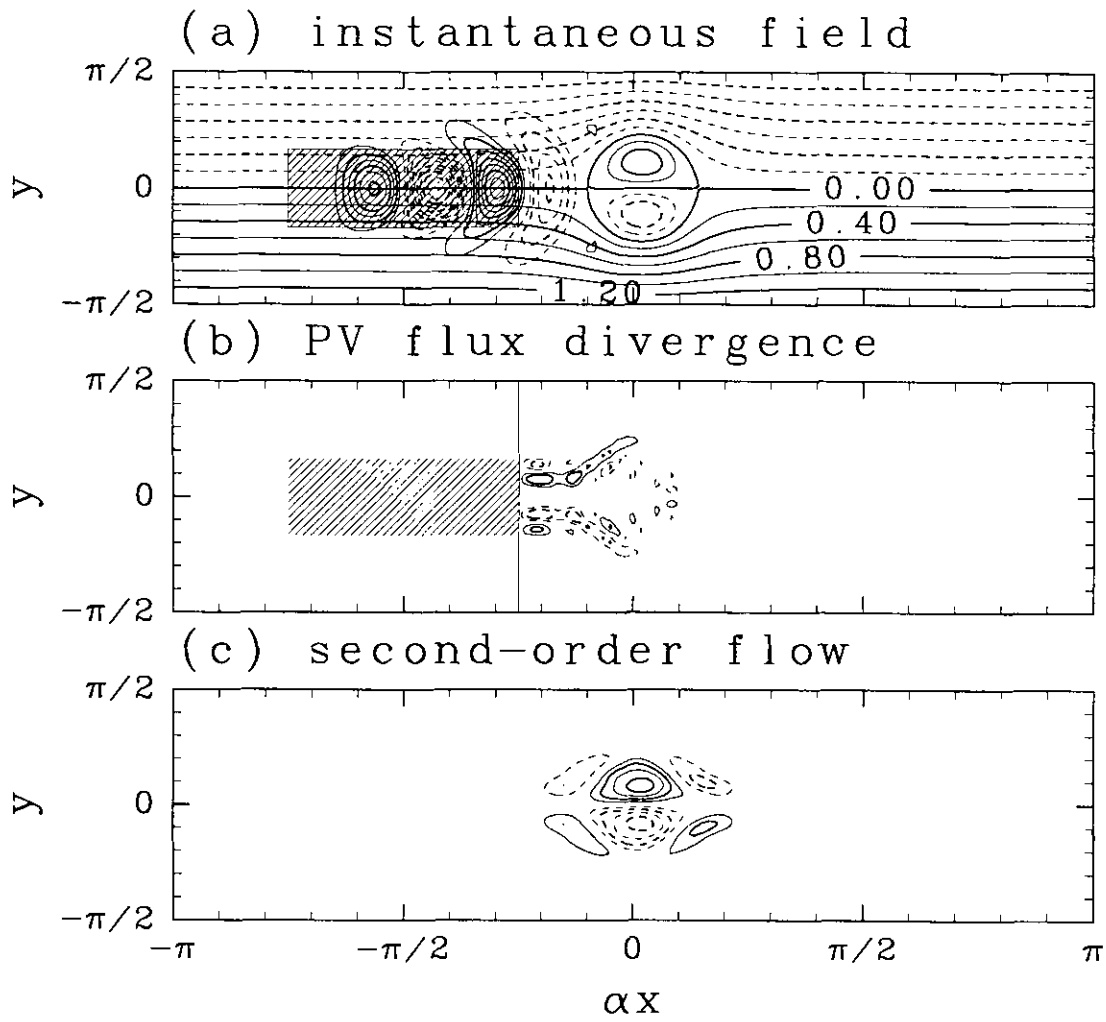


Figure 2.4: Transient eddy forcing for the blocking basic flow in the narrow channel. Negative values are contoured by dashed lines. Zero contours are omitted. (a) Instantaneous streamfunction field of the disturbances  $\psi_1$  at day 30 with the basic flow  $\psi_0 - Uy$ . Contour interval is  $2.0 \times 10^{-4}$ . The shaded rectangle denotes the eddy forcing region. (b) Time-averaged eddy PV flux divergence  $\nabla \cdot (\overline{v_1 q_1})$  during 45 days. Contour interval is  $1.0 \times 10^{-5}$ . (c) Second-order flow  $\overline{\psi_2}$  induced by the time-averaged eddy PV flux divergence downstream of the solid vertical line in (b). Contour interval is  $1.0 \times 10^{-5}$ .

Figure 2.5

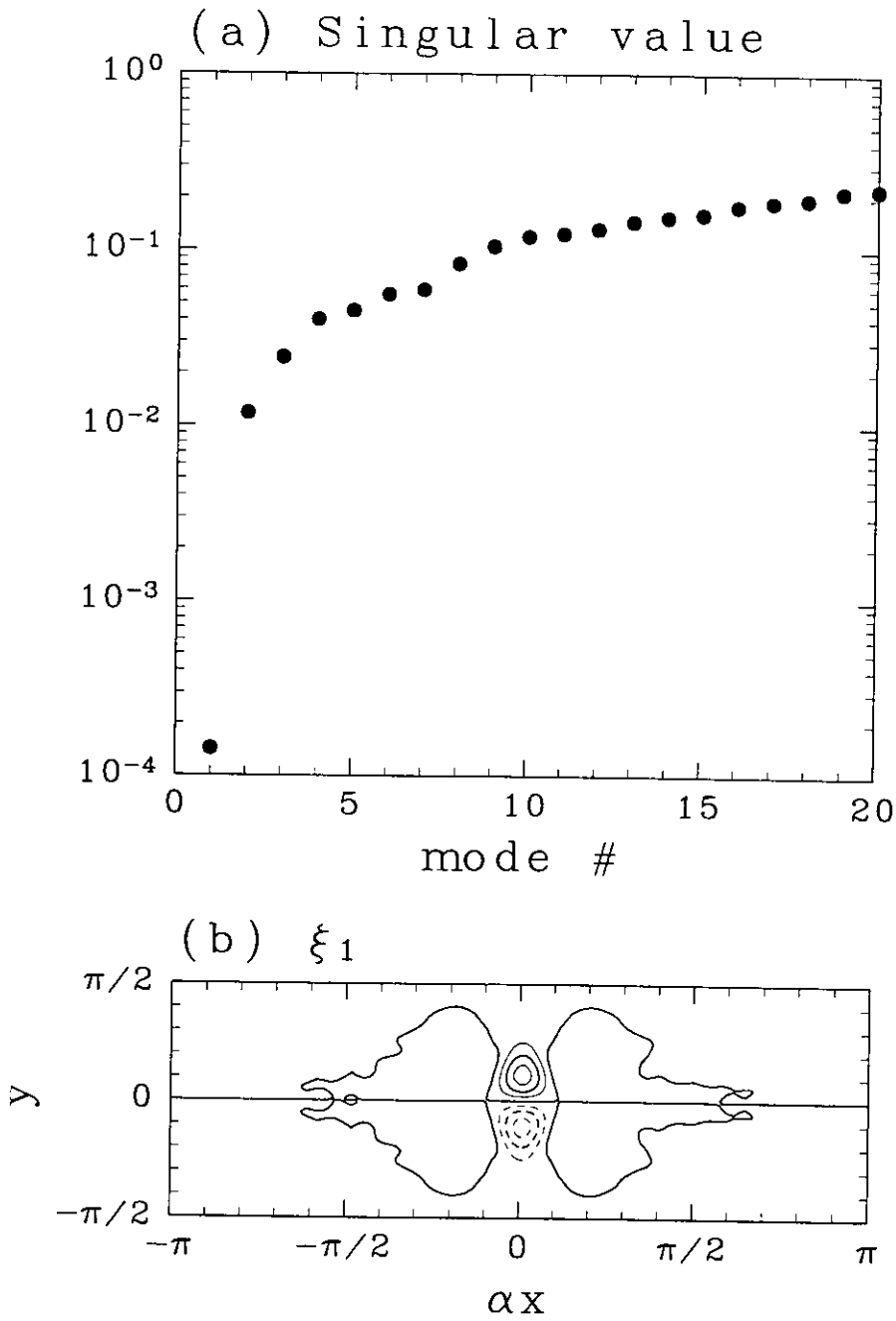


Figure 2.5: SVD analysis for the blocking solution in the narrow channel model. (a) Distribution of the 20 smallest singular value  $\sigma_i$ . (b) Streamfunction field for the first right singular vector  $\xi_1$ . Contour interval is 1.0 and negative values are contoured by dashed lines.

Figure 2.6

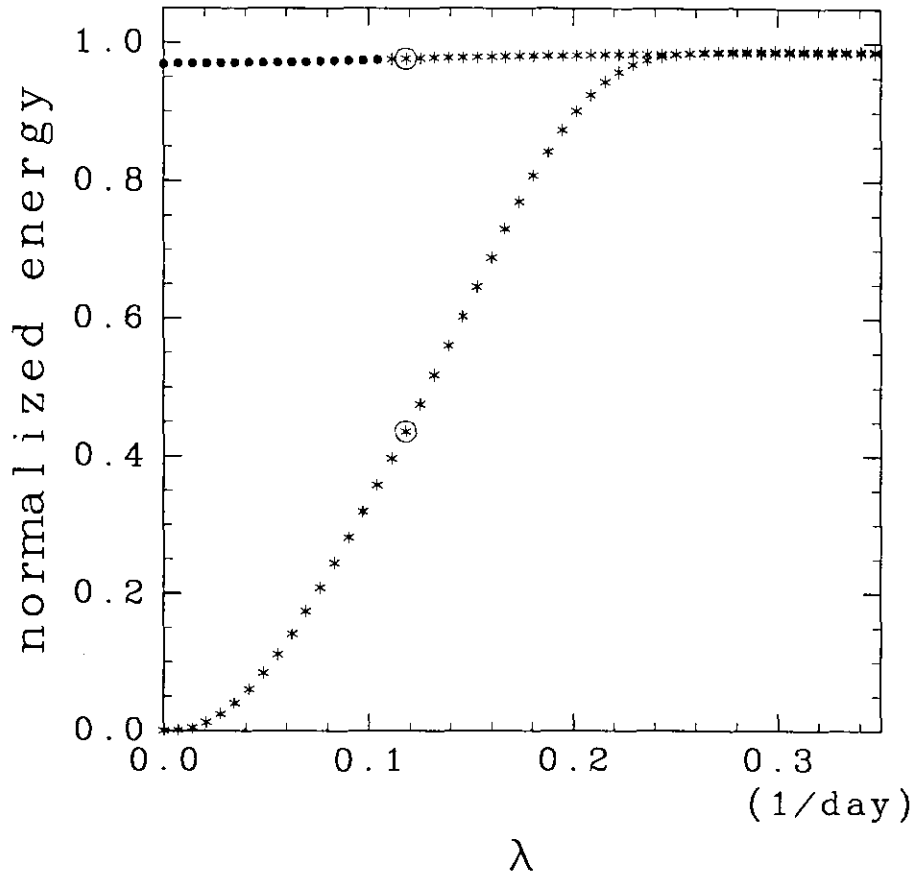


Figure 2.6: As in Fig.1.1 but for the wide channel model.

Figure 2.7

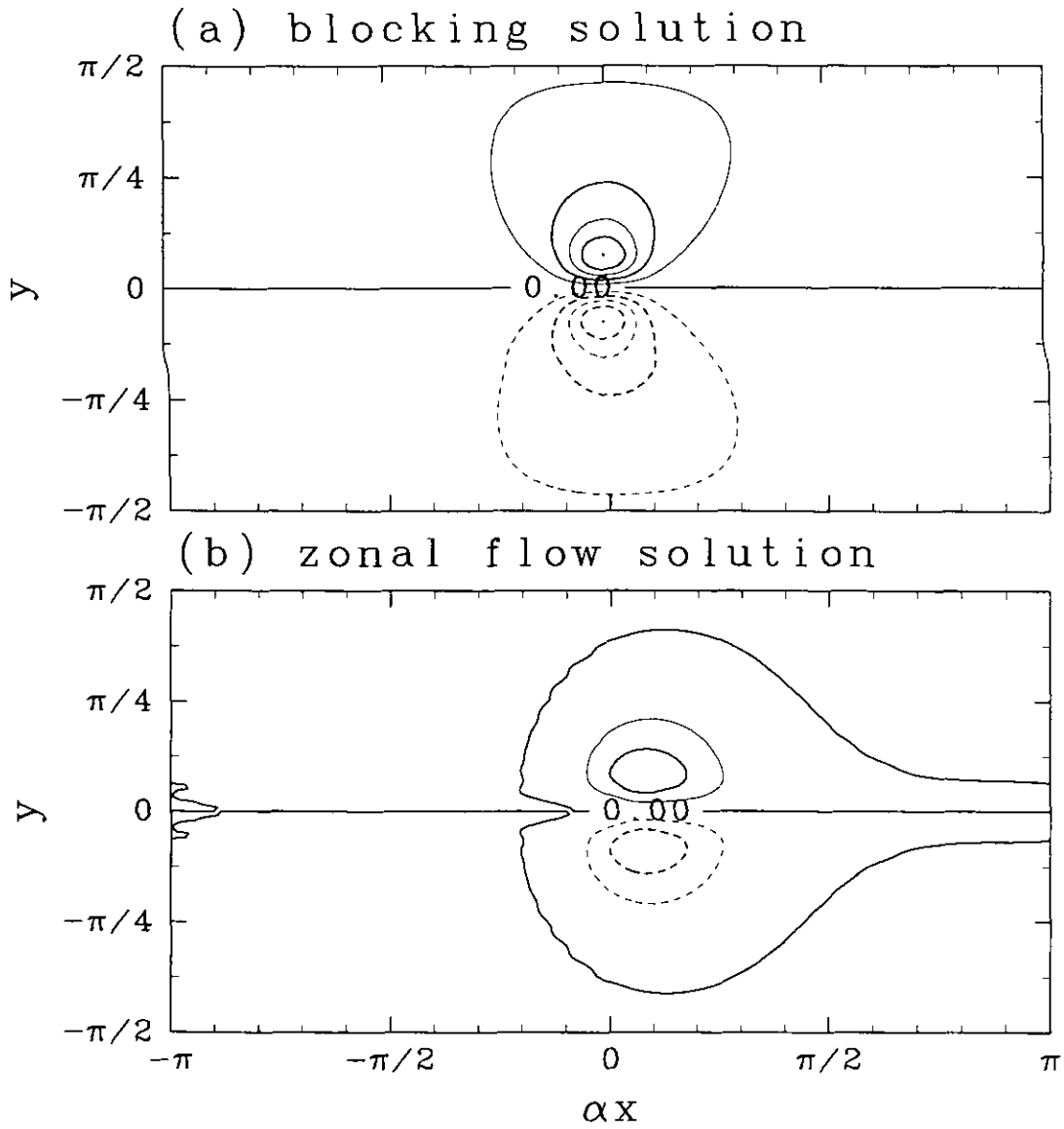


Figure 2.7: Streamfunction  $\psi_0$  of steady solutions at  $\lambda = 0.12 \text{ day}^{-1}$  denoted by open circles in Fig. 1.6. Contour interval is 0.1 and negative values are contoured by dashed lines. (a) Blocking solution. (b) Zonal flow solution.

Figure 2.8

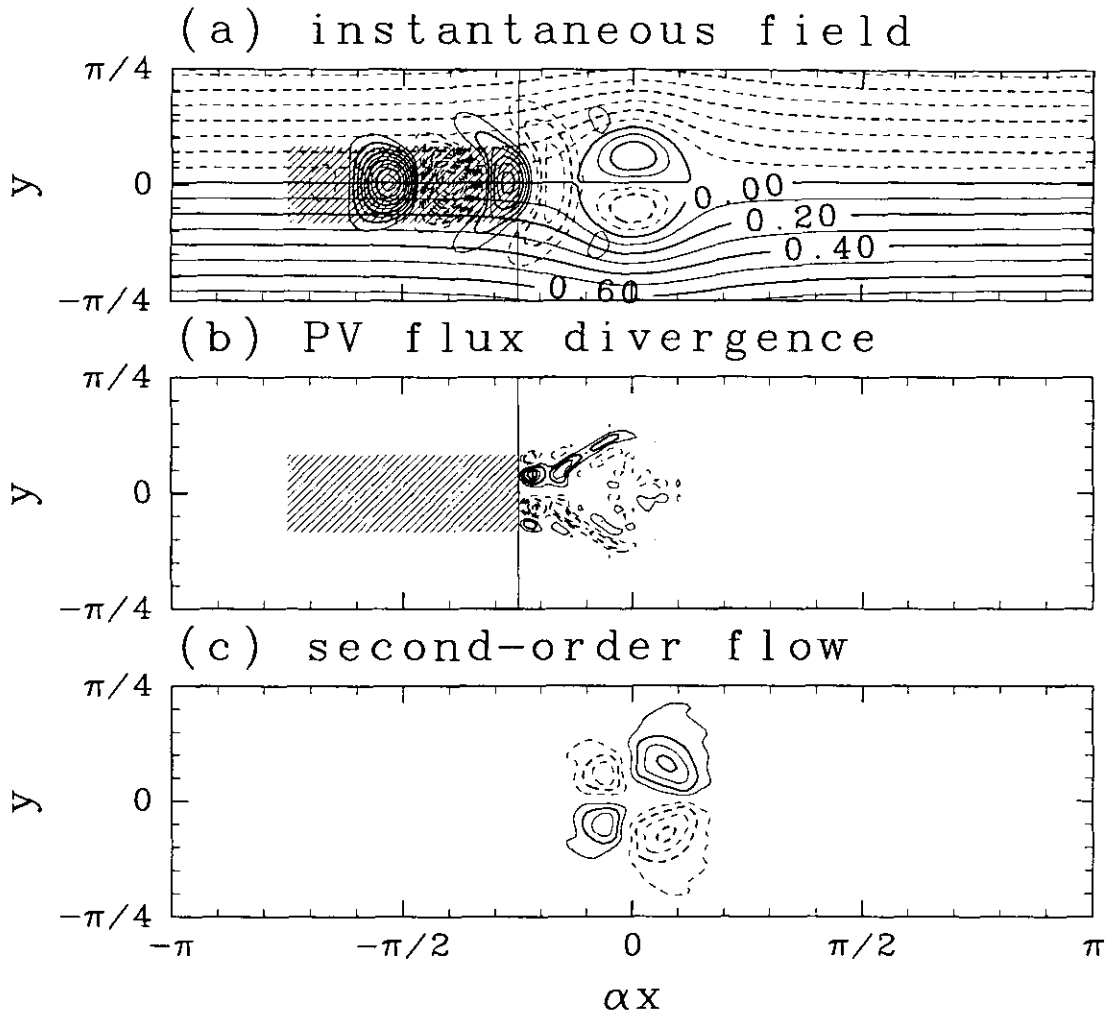


Figure 2.8: As in Fig. 1.4 but for the blocking solution in the wide channel model. Only the half region of the model,  $-\pi/4 < y < \pi/4$  is shown. Contour intervals for (a), (b), (c) are  $2.0 \times 10^{-5}$ ,  $2.0 \times 10^{-6}$ ,  $2.0 \times 10^{-6}$ .

Figure 2.9

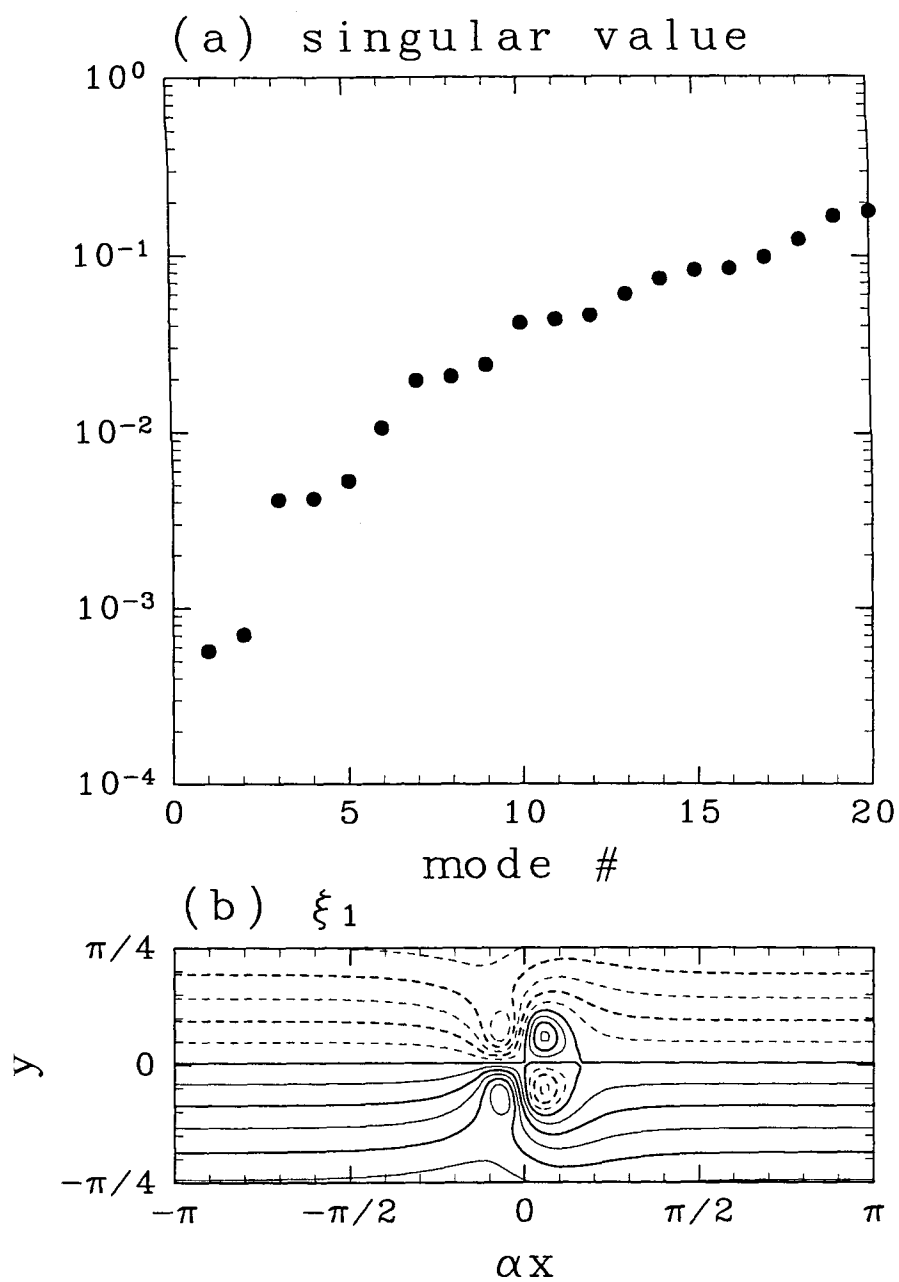


Figure 2.9: As in Fig. 1.5 but for the blocking solution in the wide channel model. Contour interval for (b) is 0.2.

Figure 2.10

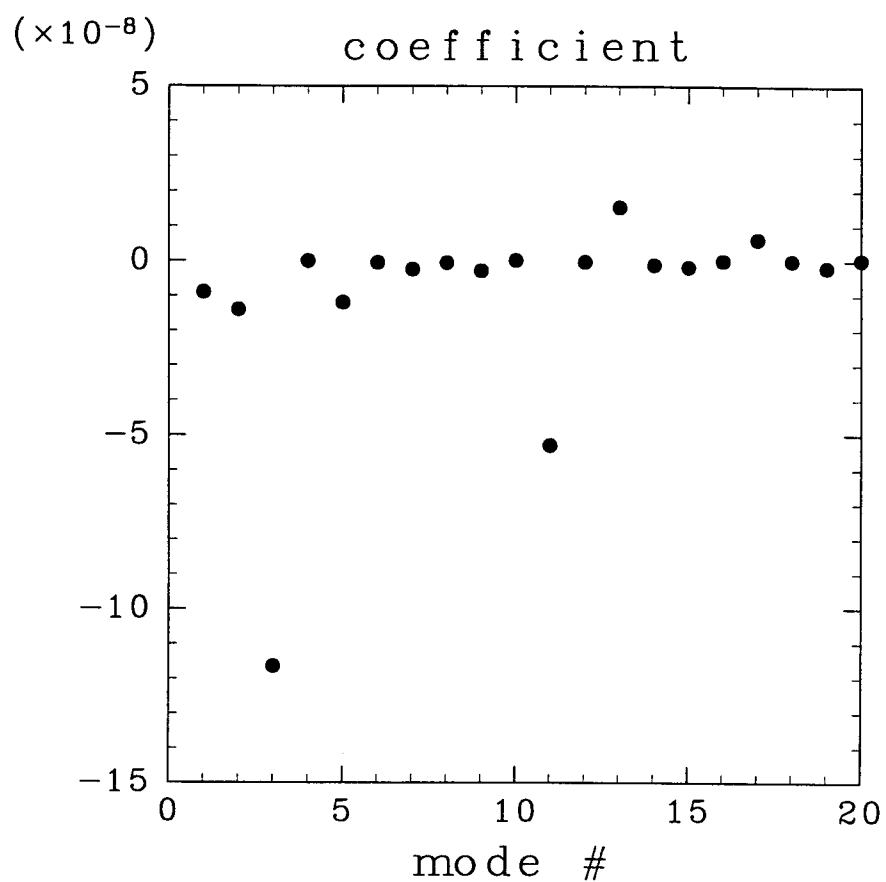


Figure 2.10: Projection  $\xi_i$  of the eddy PV convergence  $f$  onto each right singular vector  $\langle \xi_i \cdot f \rangle / \sigma_i$  with the smallest 20 singular values  $\sigma_i$  for the blocking solution in the wide channel.

Figure 2.11

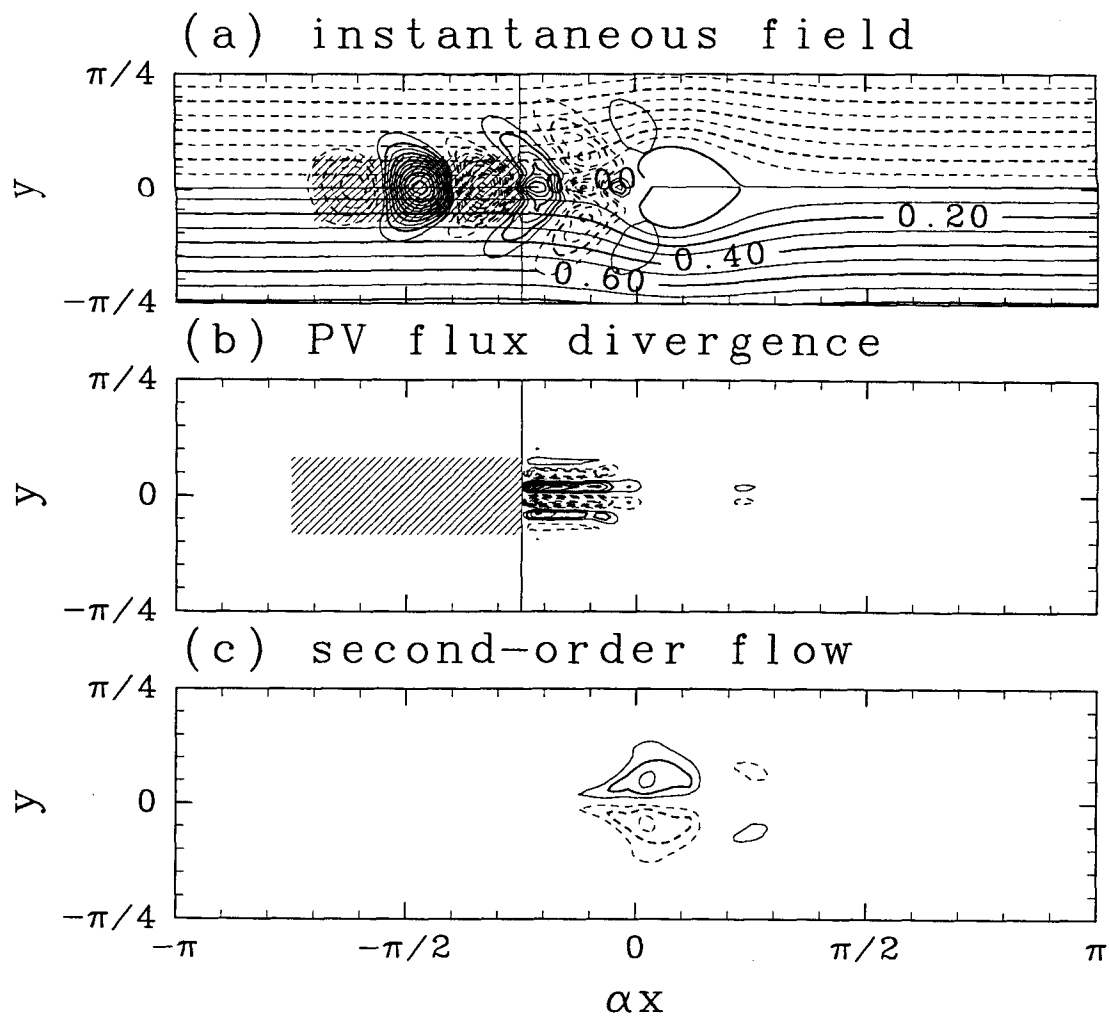


Figure 2.11: As in Fig. 1.8 but for the zonal flow solution in the wide channel model.

Figure 2.12

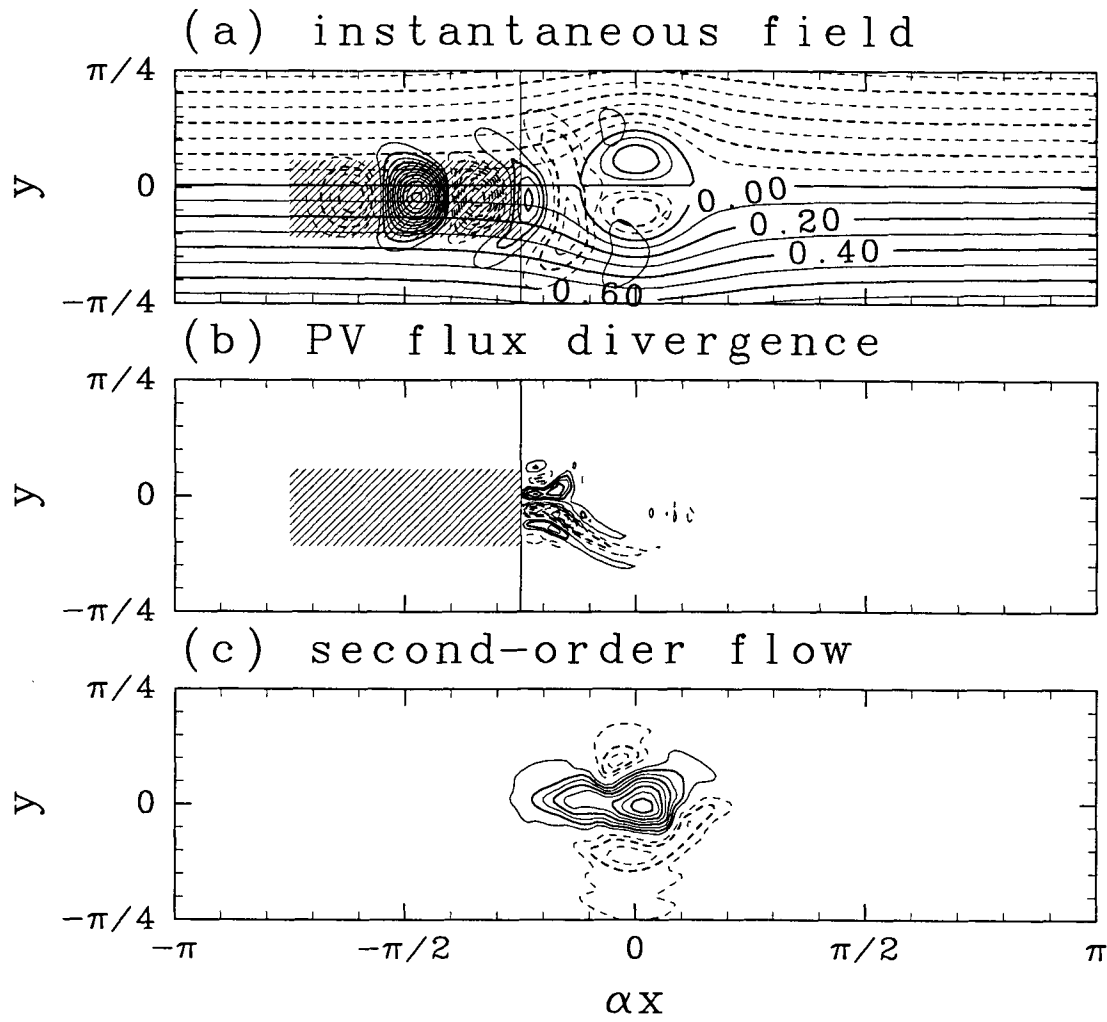


Figure 2.12: Same as in Fig. 1.8 except that the wavemaker is shifted to the south by 15% of the modon radius  $r_0$ .

Figure 2.13

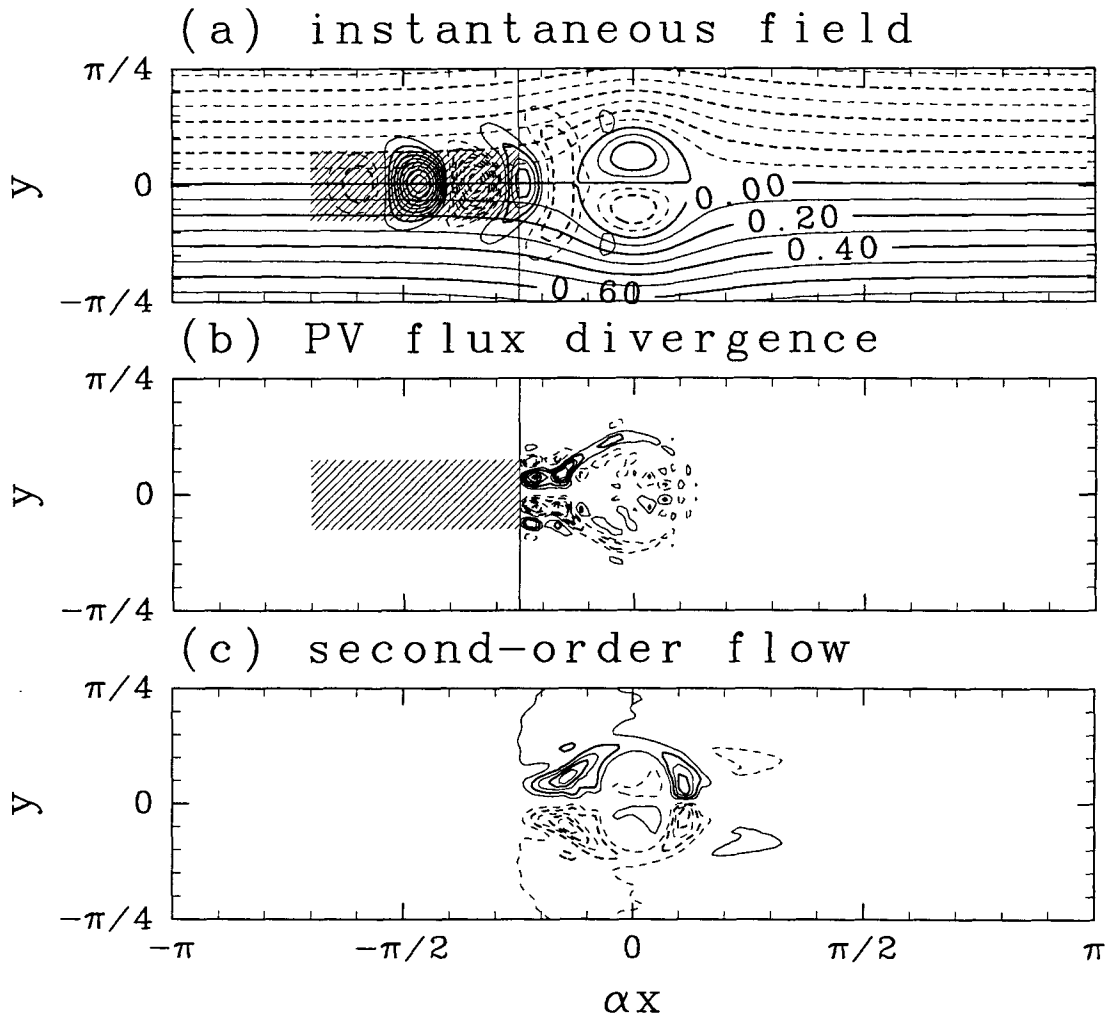


Figure 2.13: Same as in Fig. 1.8 except that the zonal wavelength of the imposed eddies is 6,300km, and the eddy streamfunction at day 29 is drawn in (a).

Figure 2.14

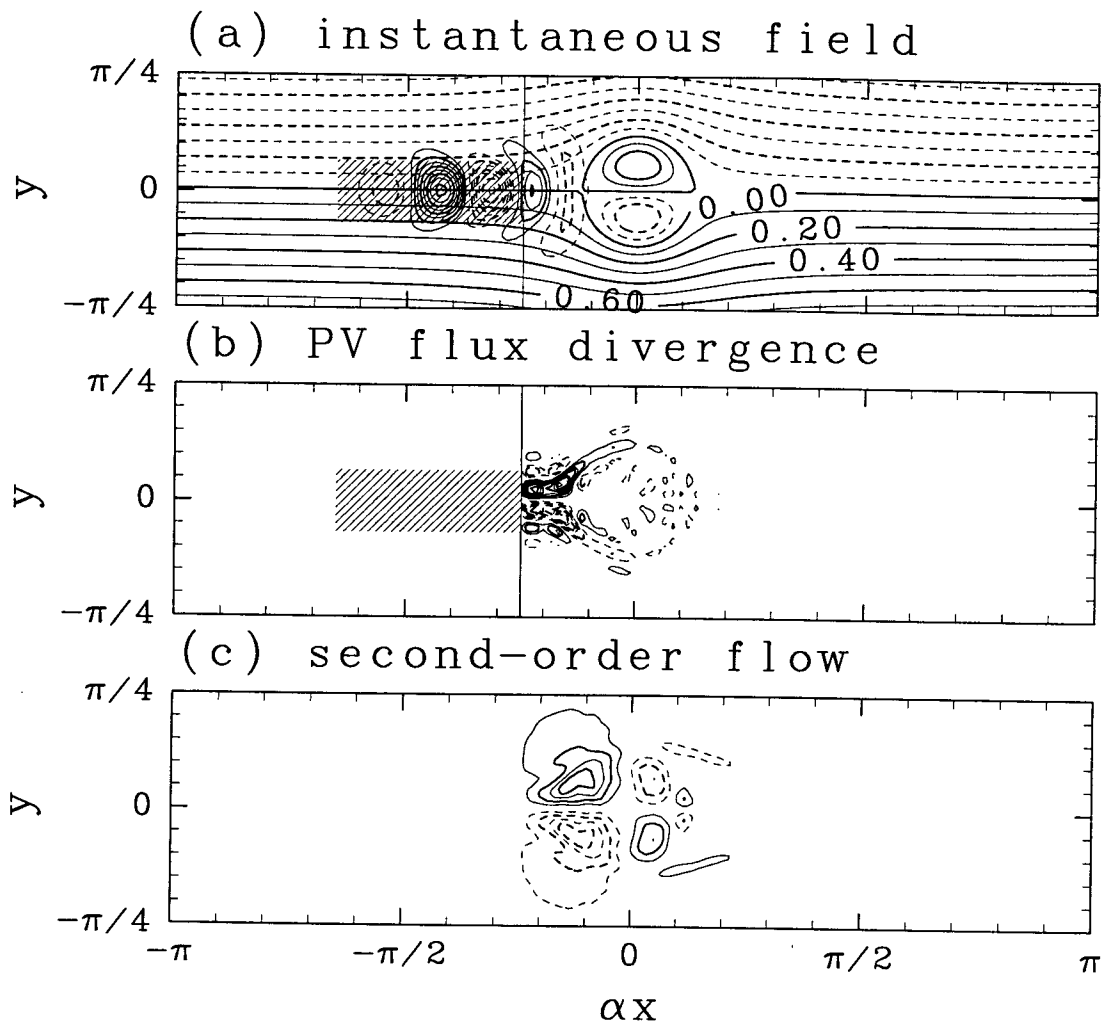


Figure 2.14: Same as in Fig. 1.8 except that the wavelength of the eddies is 5,600km, and the eddy streamfunction at day 28 is drawn in (a).

Figure 2.15

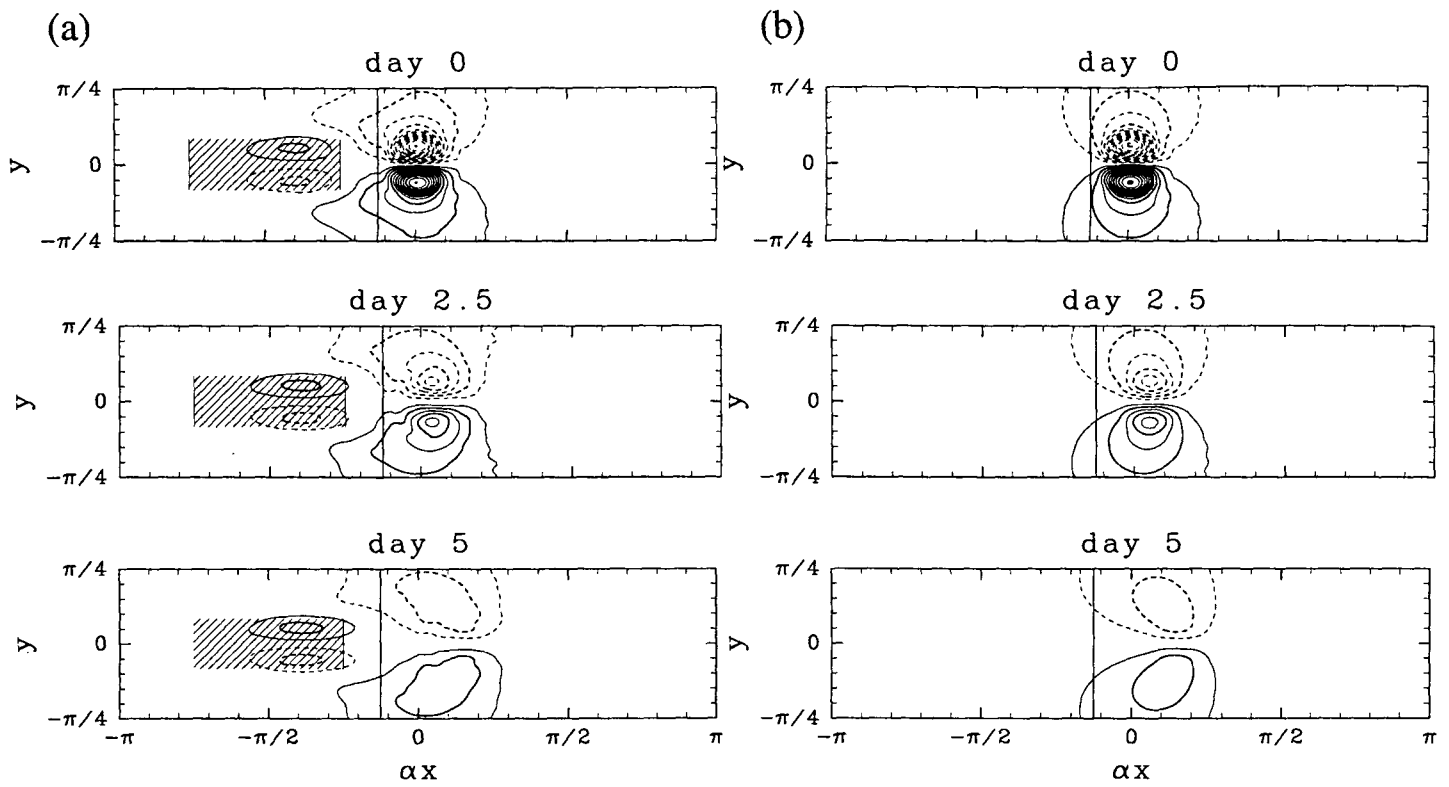


Figure 2.15: Ensemble mean of PV field (a) with and (b) without the eddy forcing of the zonal wavelength of 7000 km (shaded rectangular region). The upper panel, the middle panel and the lower panel denote day 0, day 2.5 and day 5, respectively. Contour intervals are 5.0 and negative values are contoured by dashed lines. Zero contours are omitted.

Figure 2.16

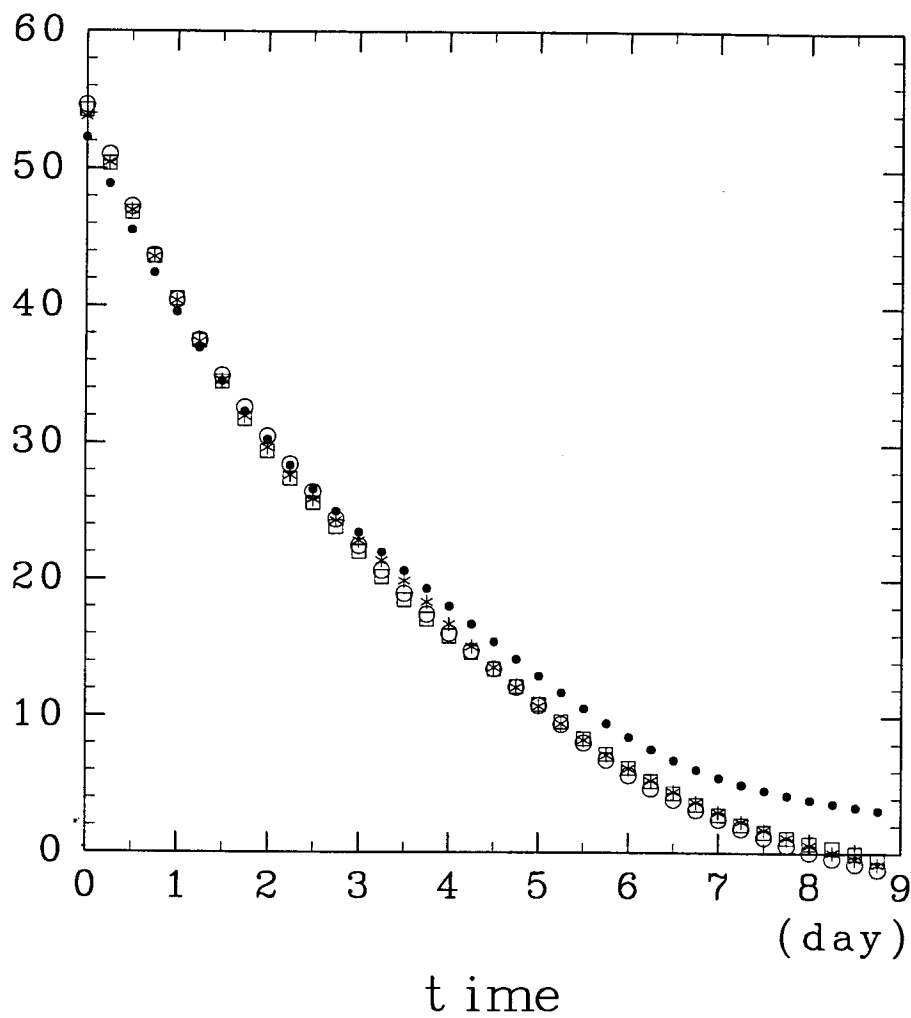


Figure 2.16: Time evolution of the maximum value of the PV with the transient eddy forcing of zonal wavelength of 7000 km (asterisks), 6,300km (open circles), 5,600km (open squares) and without eddy forcing (closed circles).

Figure 2.17

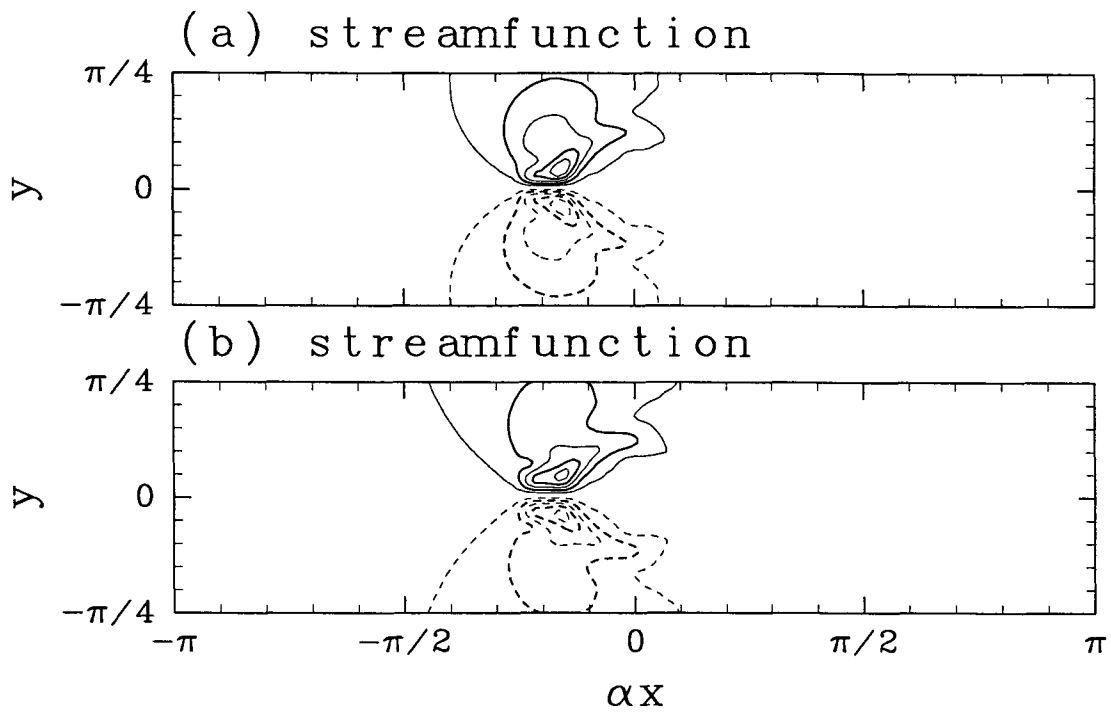


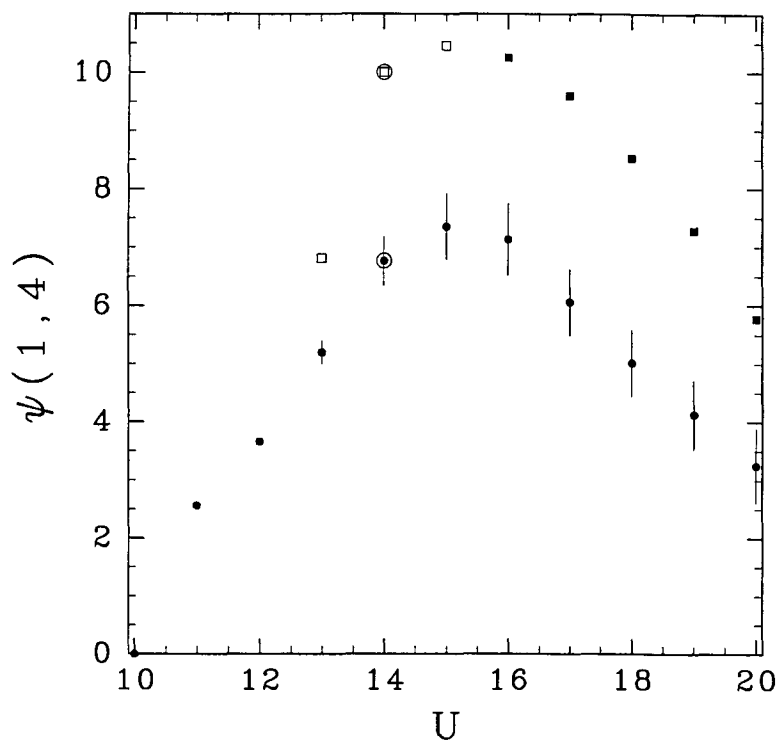
Figure 2.17: Streamfunction tendency  $-\nabla^{-2}\overline{J(\psi_1, q_1)}$  obtained from the eddy PV flux divergence of Fig. 1.13b for (a) and of Fig. 1.14b for (b), respectively. Contour intervals are  $1.0 \times 10^{-8}$  and negative values are contoured by dashed lines. Zero contours are omitted.

Figure 3.1

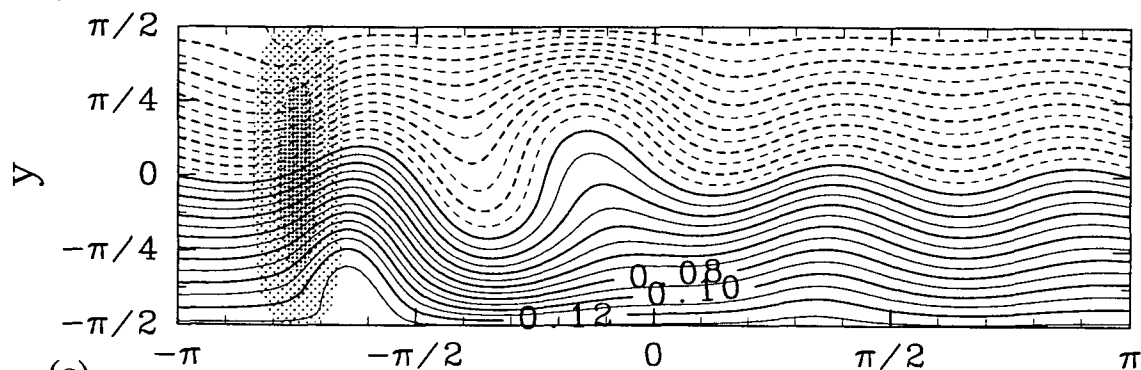
(a)

( $\times 0.001$ )

$h = 900 \text{ m}$



(b)



(c)

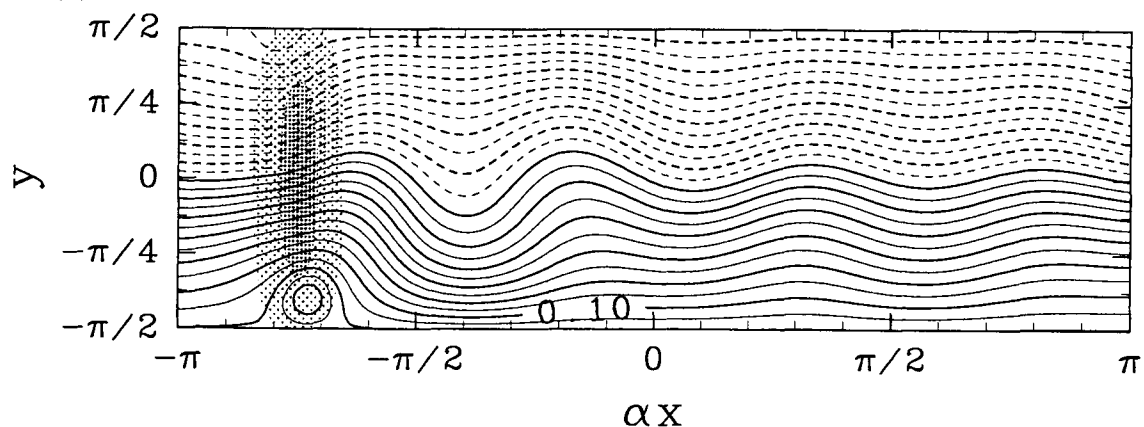
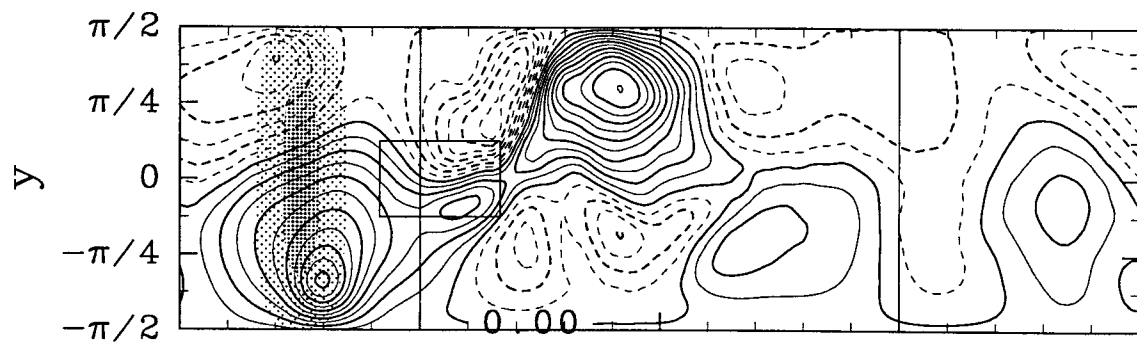


Figure 3.1: (a) Bifurcation diagram of the steady solutions for  $h=900$  m. The abscissa is zonally uniform wind  $U$  and the ordinate is the amplitude of the wave component  $(m, n) = (1, 4)$  of steady solutions. Closed squares and closed circles are linearly stable stationary solutions, open squares are linearly unstable stationary solutions. The closed circles with vertical bars denote the stable periodic solutions whose amplitude are the range of the vertical bars. The streamfunction fields for  $U=14$  m/s (indicated as large open circles in (a)) of the unstable stationary solution for (b) and time-averaged field of the periodic solution for (c).

Figure 3.2  
(a)



(b)

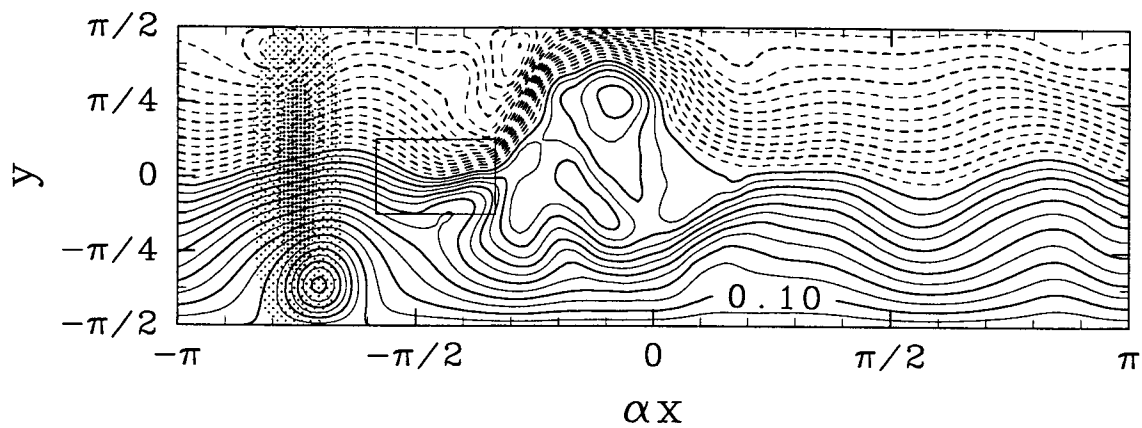


Figure. 3.2: Instantaneous streamfunction field of (a)  $\phi$  and (b)  $\psi = \phi - Uy$  at day 928 for  $h=900$  m and  $U=14$  m/s. Contour intervals are 0.01 and negative values are contoured by dashed lines.

Figure 3.3

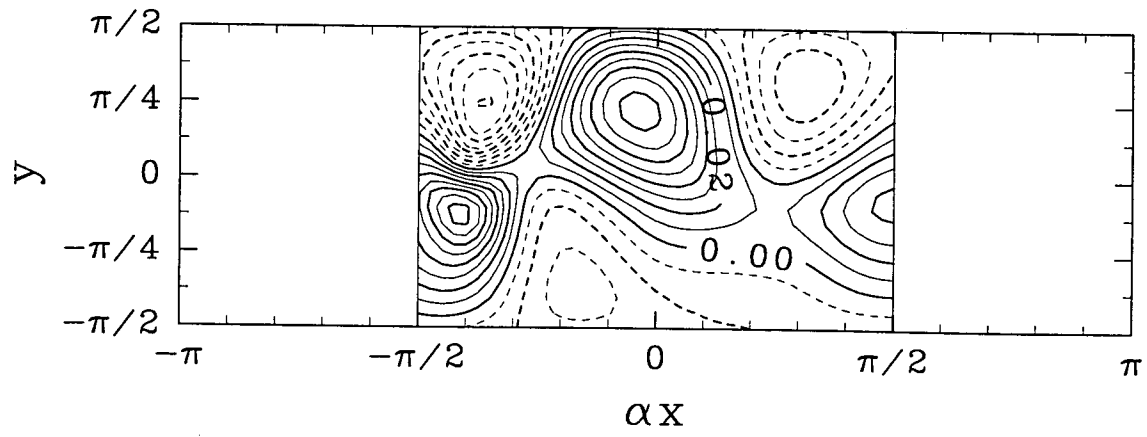


Figure 3.3: Pattern of EOF1 for  $U=14$  m/s,  $F=0.5$  and  $h=900$  m. Contour intervals are 0.01.

Figure 3.4

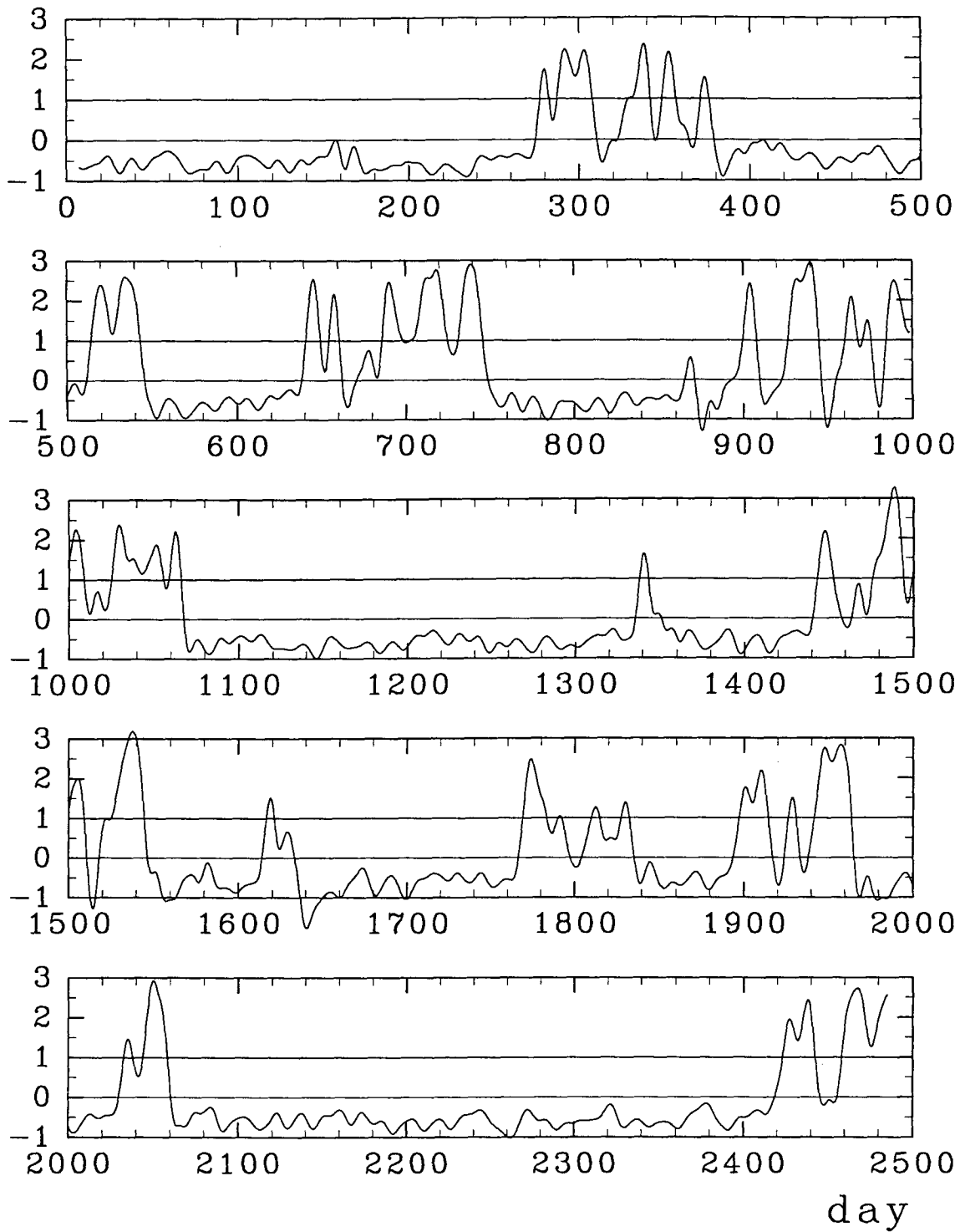


Figure 3.4 Time series of PC1 scaled by its standard deviation (denoted by a horizontal line).

Figure 3.5

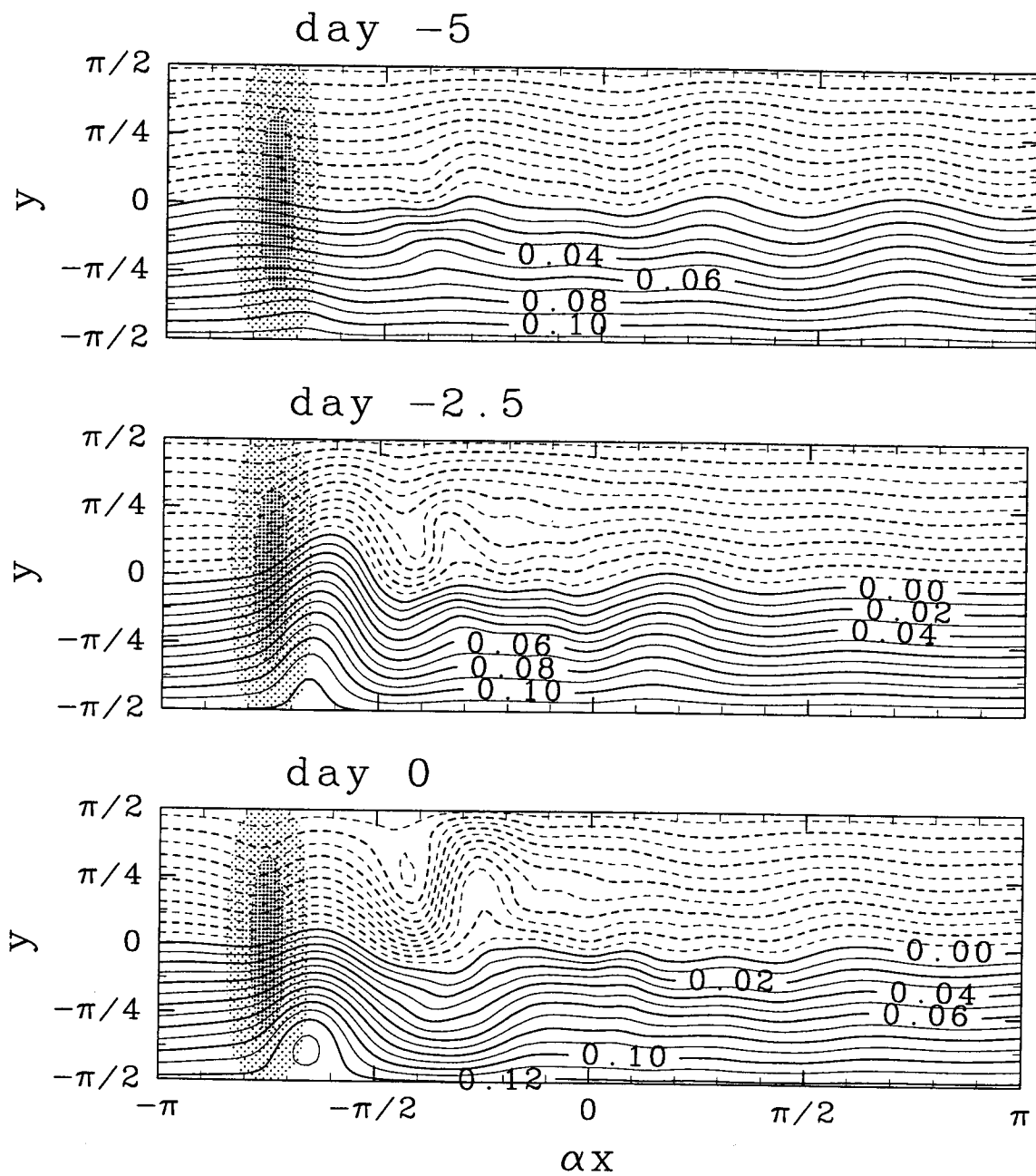


Figure 3.5 Composite streamfunction field  $\bar{\psi}^L$  obtained by the time integration of Eq. (3.5) initialized with the low-pass filtered streamfunction of day -5 (the upper panel). The middle panel and the lower panel show  $\bar{\psi}^L$  of day -2.5 and of day 0. Contour intervals are 0.01.

Figure 3.6

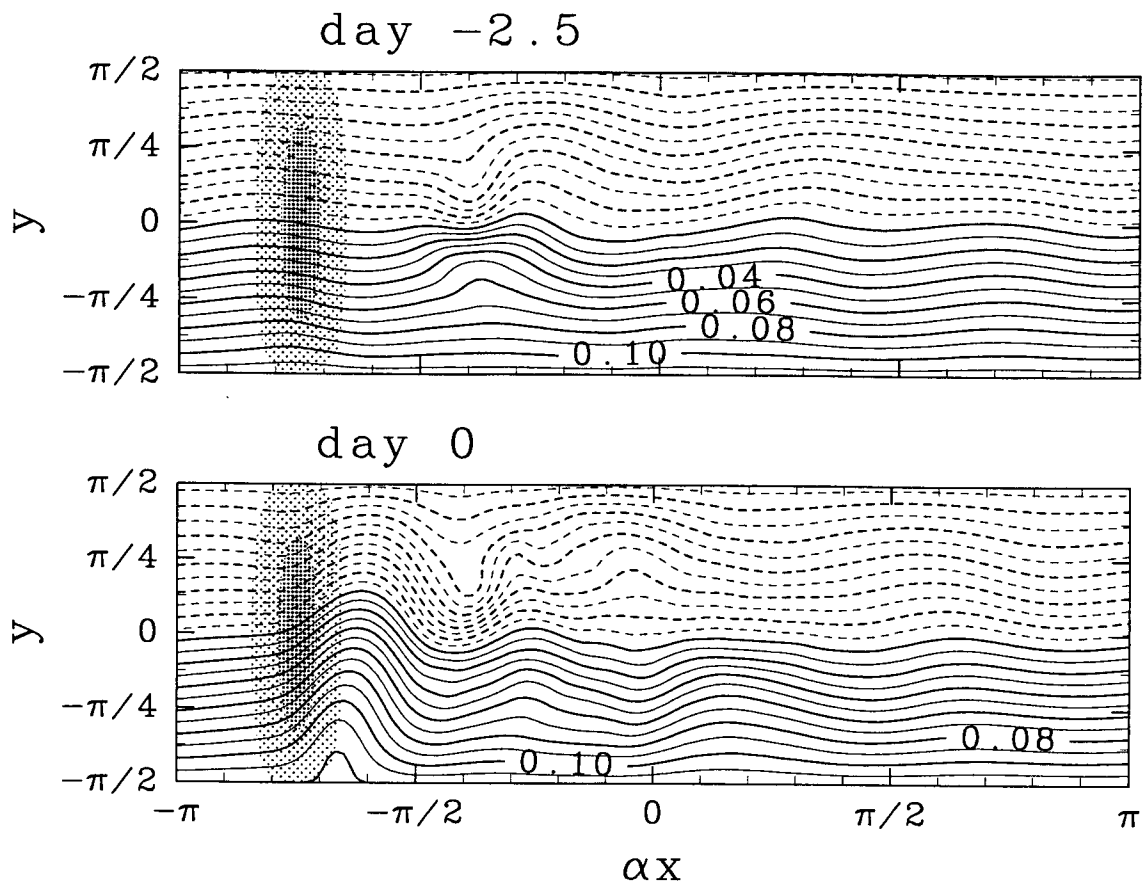


Figure 3.6: Same as Fig. 2.5 but initialized with the streamfunction of day -2.5 (the upper panel) and the lower panel shows  $\bar{\psi}^L$  of day 0.

Figure 3.7

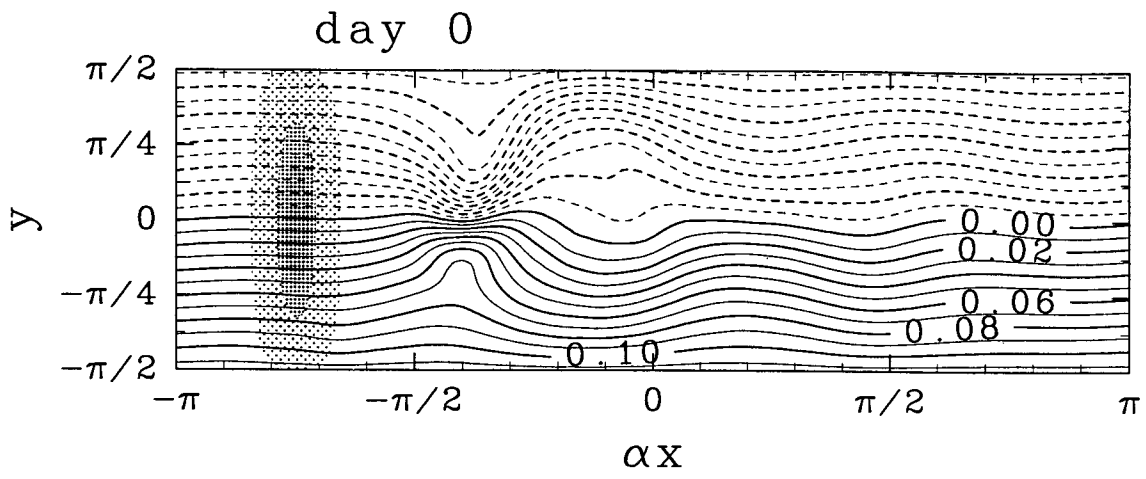


Figure 3.7: Low-pass filtered streamfunction field of day 0 (onset of the blocking event).

Figure 3.8

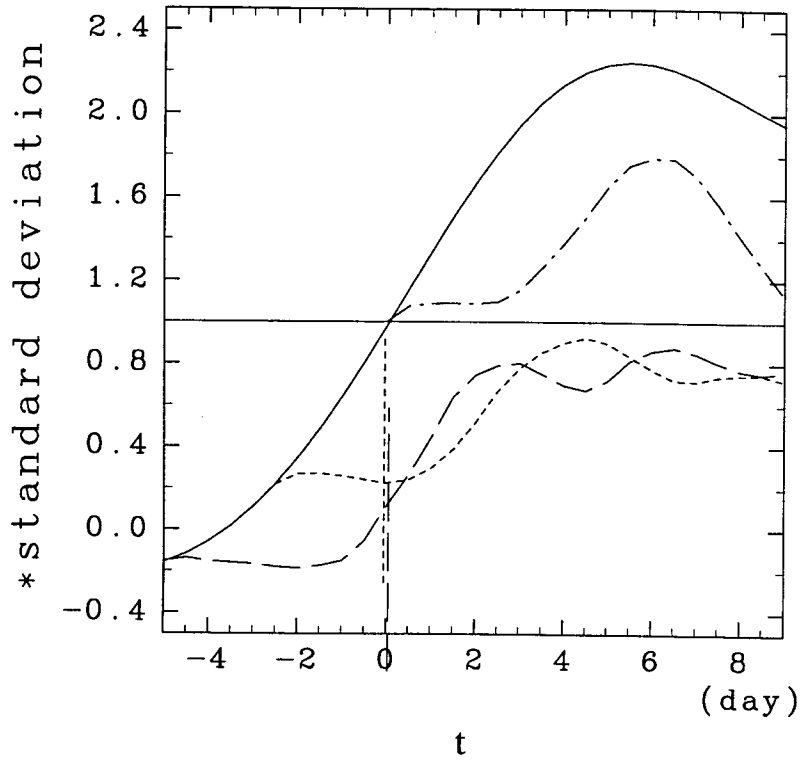


Figure 3.8: Time evolution of the projection of composite  $\bar{\psi}^L$  onto EOF1. Solid line denotes the time evolution of PC1. The projection for the time integration from day -5, -2.5, 0 are depicted by broken line, dotted line and dotted broken line, respectively. The variance of the projection at day 0 in each blocking event are shown by vertical lines.

Figure 3.9

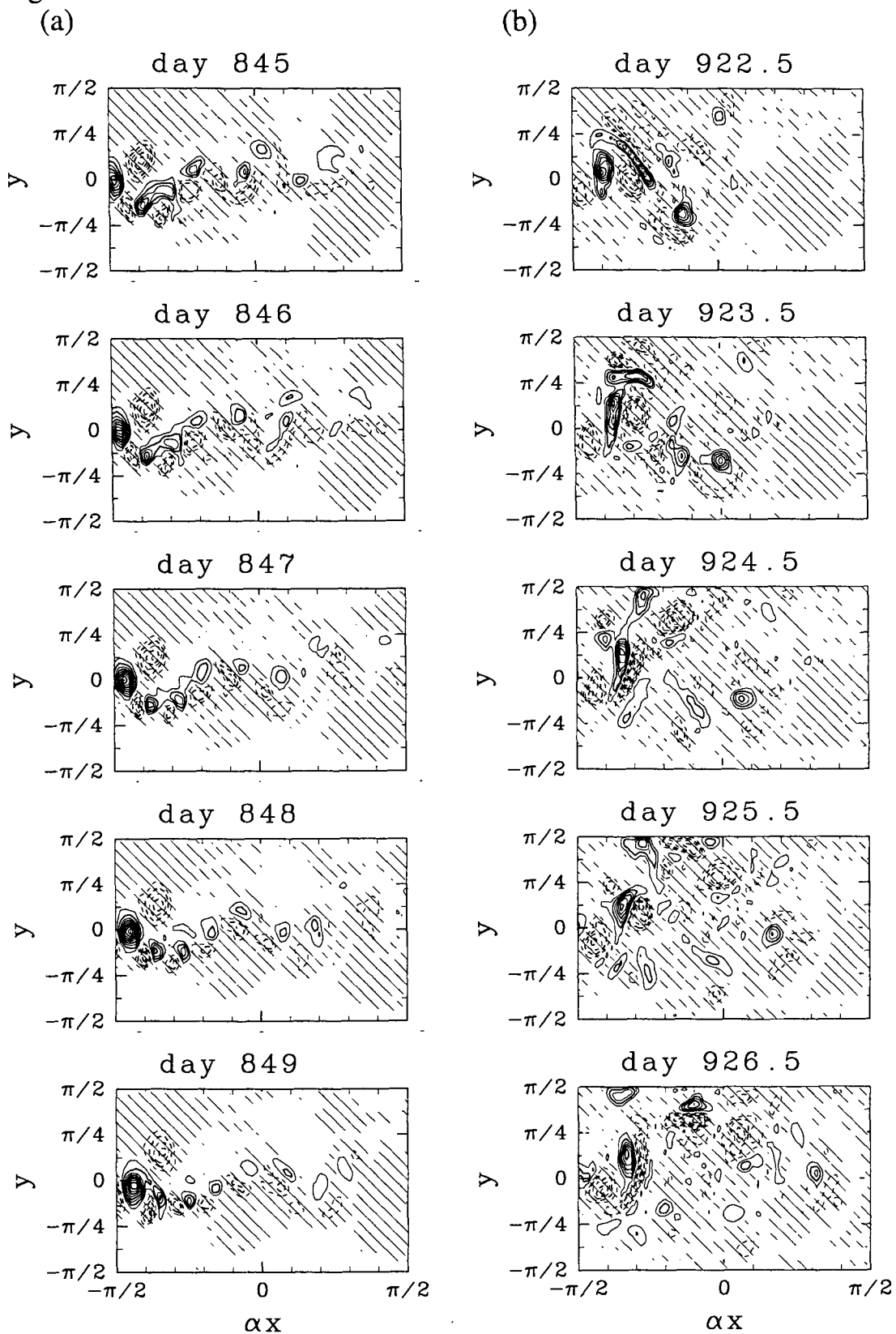


Figure 3.9: Time evolution of the relative vorticity field  $\nabla^2\psi$  during (a) non-blocking state of day 845-849, (b) before the blocking onset of day 922.5-926.5. Only the half of region of the model,  $-\pi/2 < \alpha x < \pi/2$  is shown. Contour intervals are 0.25 and negative values are contoured by dashed lines and shaded. Zero contours are omitted.

Figure 3.10.

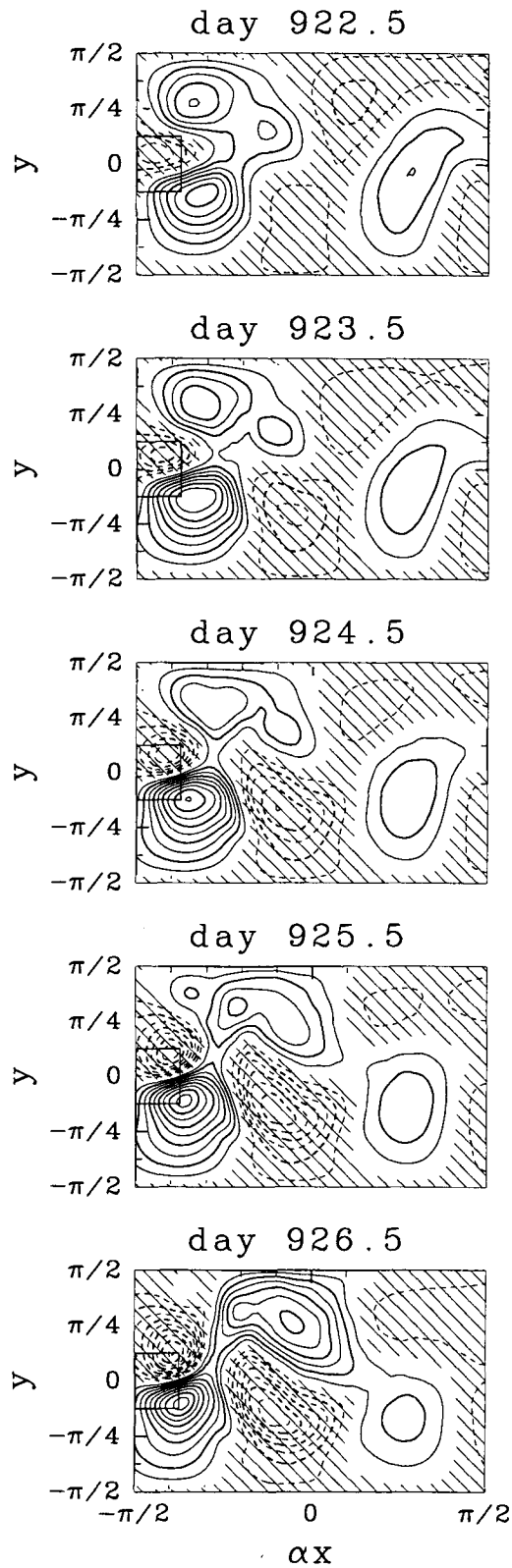


Figure 3.10: Time evolution of the low-pass filtered streamfunction field  $\bar{\phi}^L$  before the blocking onset of day 922.5-926.5 (corresponding to Figure 3.9b). Only the half of region of the model,  $-\pi/2 < \alpha x < \pi/2$  is shown. Contour intervals are 0.005 and negative values are contoured by dashed lines and shaded. Zero contours are omitted.

Figure 3.11

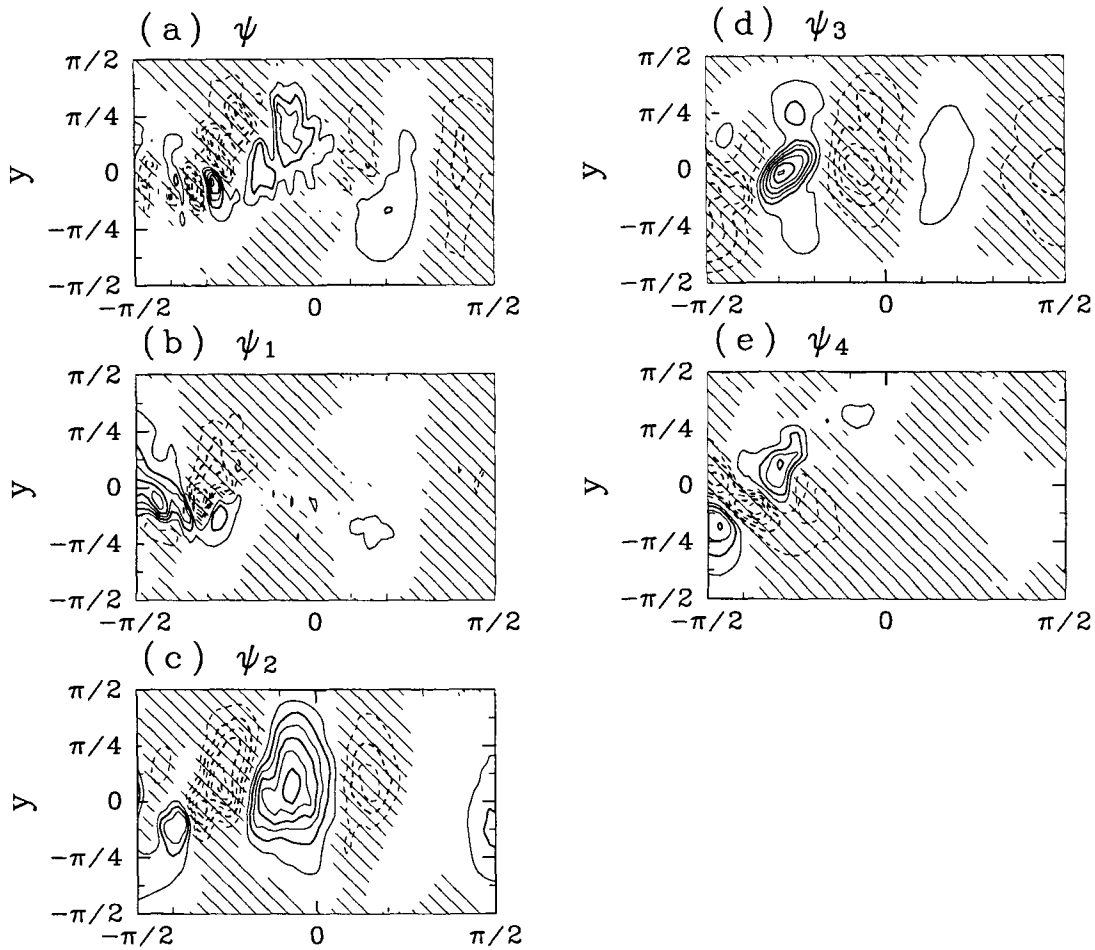


Figure 3.11: Difference of the streamfunction field evaluated by Eq. (3.8). The difference streamfunction field  $\psi_{\text{day}929.5} - \psi_{\text{day}919.5}$  is (a), and that due to  $\xi_1$ ,  $\xi_2$ ,  $\xi_3$  and  $\xi_4$  are shown in (b), (c), (d) and (e), respectively. Only the half of region of the model,  $-\pi/2 < \alpha x < \pi/2$  is shown. Contour intervals are 0.02 and negative values are contoured by dashed lines and shaded. Zero contours are omitted.

Figure 3.12

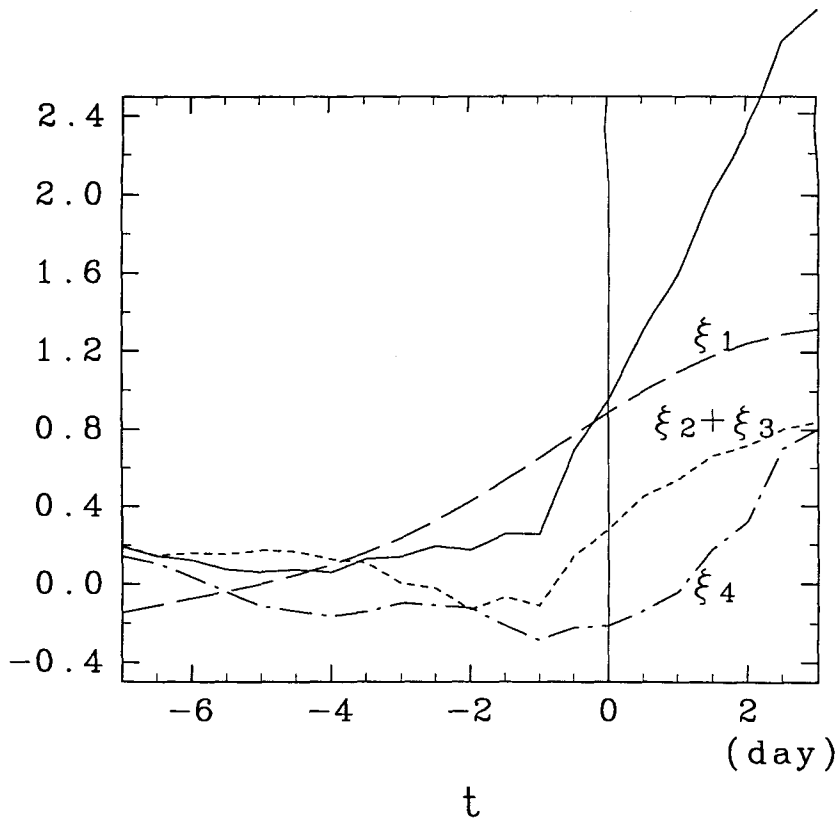


Figure 3.12: The time evolution of projection of 11 blocking composite of the cumulative contribution of each term of Eq. (3.7) onto EOF1. The projection of contribution of  $\xi_1$ ,  $\xi_2 + \xi_3$  and  $\xi_4$  are depicted by broken line, dotted line and dotted-broken line and that of PC1 is depicted by solid line.

Figure 3.13

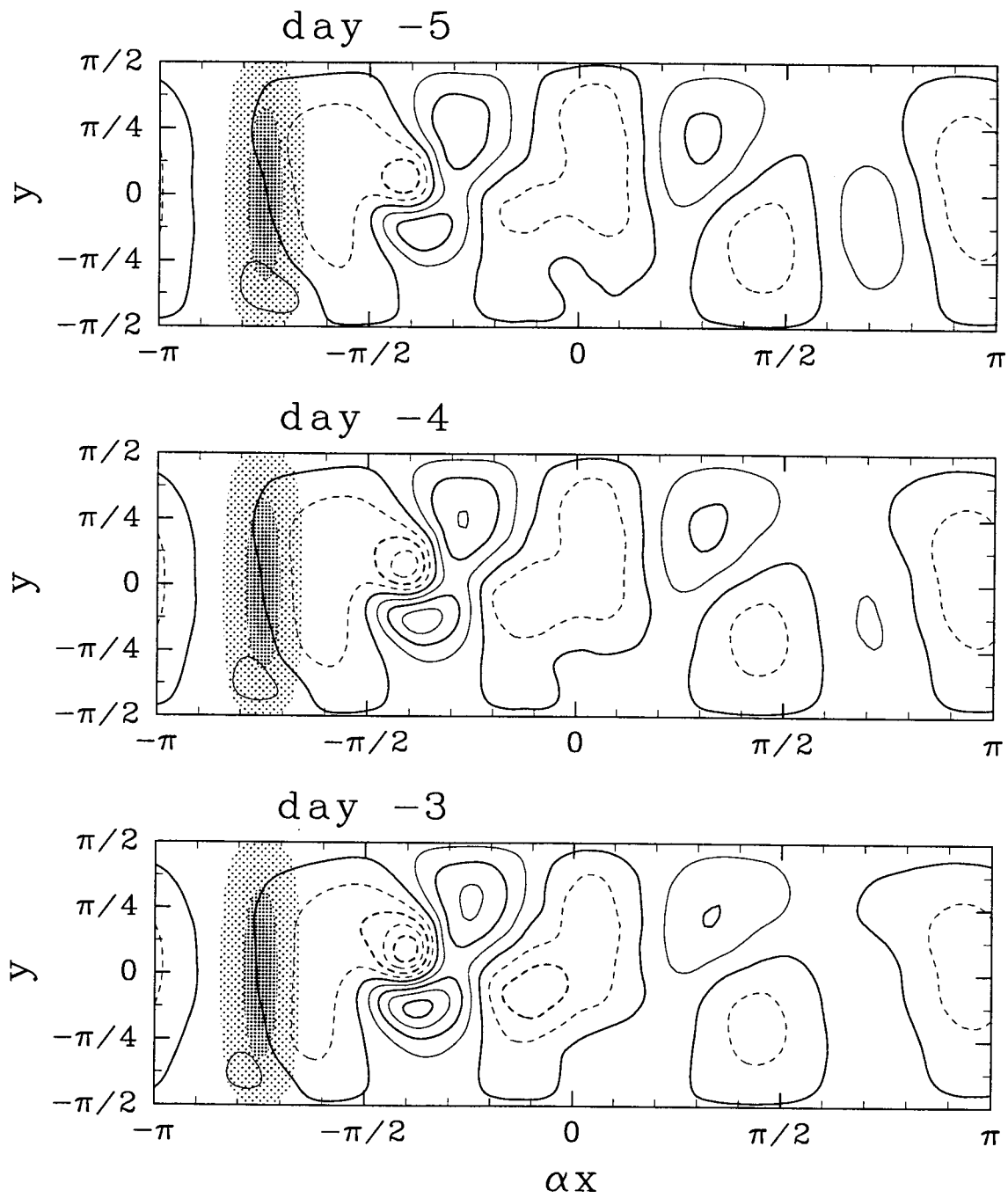


Figure 3.13: Time evolution of the composite low-pass filtered streamfunction  $\bar{\psi}^L$  from day -5 to day 0. Contour intervals are 0.005 and negative values are contoured by dashed lines.

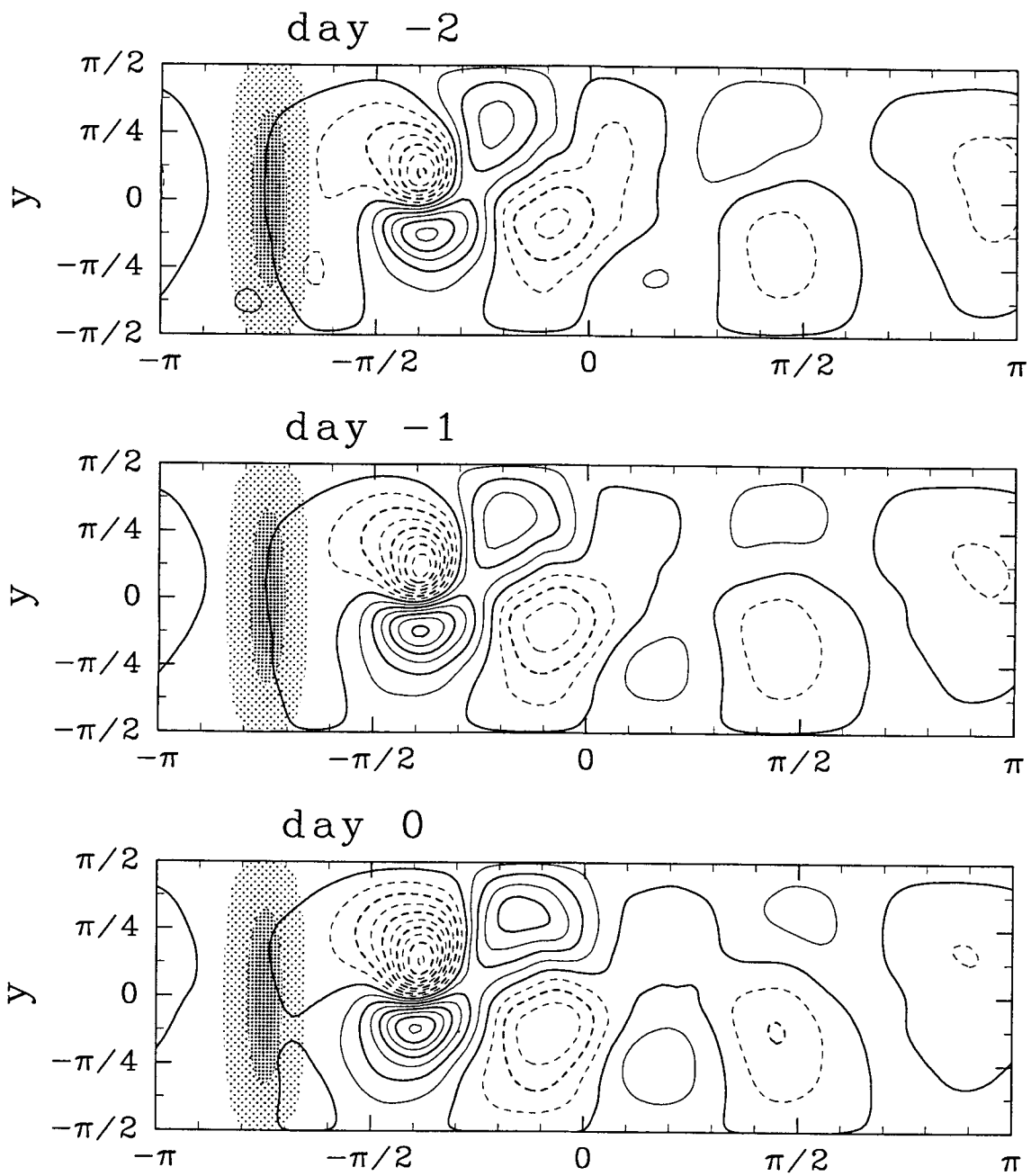


Figure 3.13: (Continued)

Figure 3.14

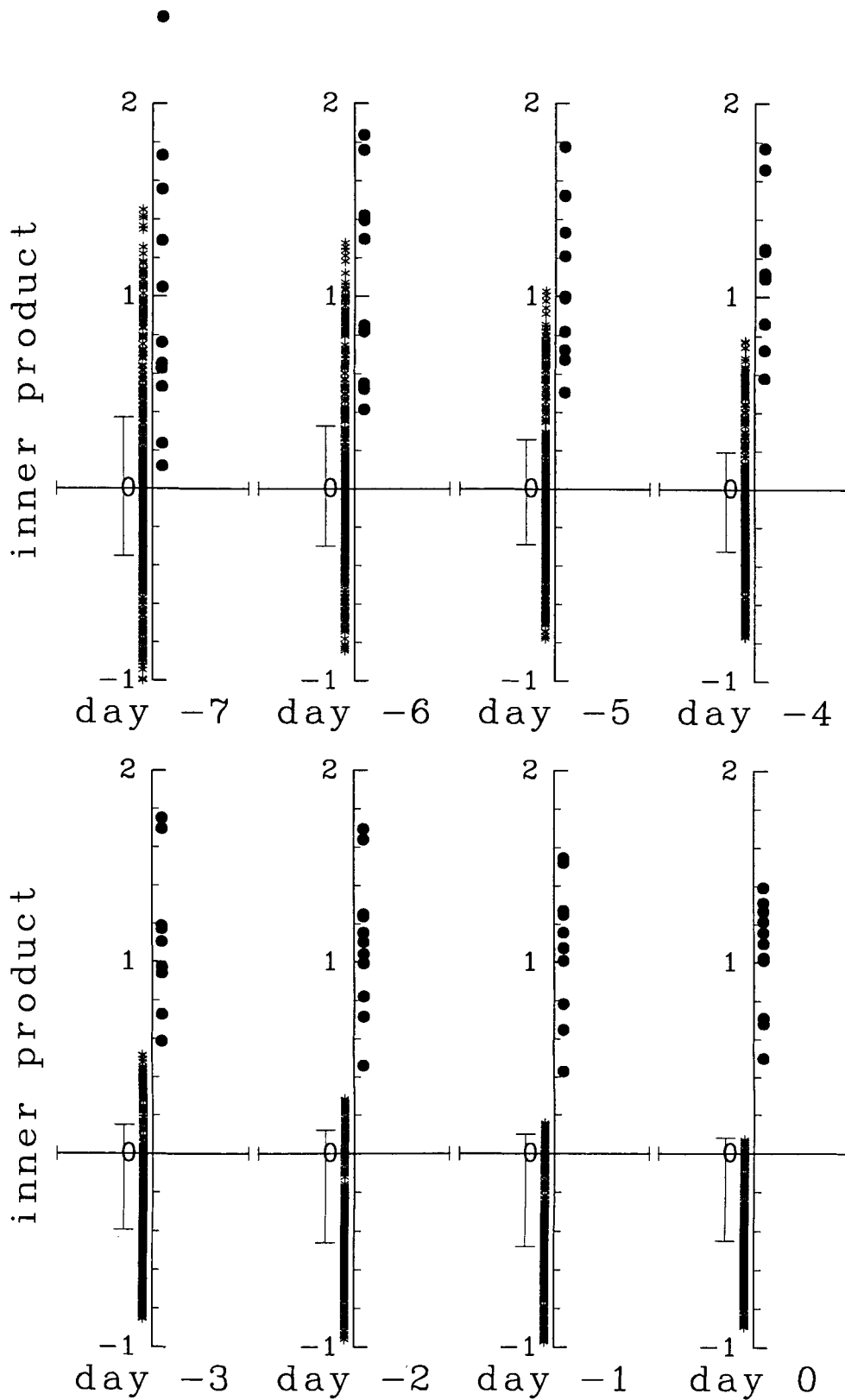


Figure 3.14: Inner-product of the low-pass filtered streamfunction in each blocking event from day -7 to day 0 and that of the composite value (closed circle). The inner product of that during non-blocking states are denoted by asterisks and its two standard deviation from the mean value is indicated by the vertical line.

Table 1

$U$	11	12	13	14	15	16	17
number	11	10	12	11	11	2	0
days	236	218	328	355	117	19	0

Table 1: Total number and days of blocking events during 2500 days for  $11 \text{ m/s} \leq U \leq 17 \text{ m/s}$ .